TUDelft

Delft University of Technology
Faculty of Electrical Engineering, Mathematics and Computer Science
Delft Institute of Applied Mathematics

Modeling an angiogenesis treatment after a myocardial infarction
- using the discontinuous Galerkin method -

A thesis submitted to the
Delft Institute of Applied Mathematics
in partial fulfillment of the requirements

for the degree

MASTER OF SCIENCE
in
APPLIED MATHEMATICS

by

L.Y.D. Crapts

Delft, the Netherlands
September 2012

MSc THESIS APPLIED MATHEMATICS

"Modeling an angiogenesis treatment after a myocardial infarction
- using the discontinuous Galerkin method -"

L.Y.D. Crapts

Delft University of Technology

Daily supervisor

Dr.ir. F.J. Vermolen
Dr. J.K. Ryan

Responsible professor

Prof.dr.ir. C. Vuik

Other thesis committee members

Dr. J.L.A. Dubbeldam

September 2012   Delft, the Netherlands

Preface

This report is the result of my Master of Science research project at the Delft University of Technology, the Netherlands. The project has been carried out at the faculty of Electrical Engineering, Mathematics and Computer Science, abbreviated as EEMCS, at the chair of numerical analysis.

I would like to thank my supervisor Fred Vermolen for his continuous support, good advice and the opportunity he gave me to do this project. Also I would like to thank my supervisor Jennifer Ryan for the support and advice with regard to the discontinuous Galerkin method.

Next to my supervisors I would like to thank my office mate Joost van Zwieten for his good advice, his help with the discontinuous Galerkin method and the nice chats, Dennis den Ouden for generating meshes for me in SEPRAN, Gemma, Dorien, Jacob, Frank, Michiel and André for the nice coffee and lunch breaks and Andreas for the emotional support.

I hope this report will be as informative for you as doing the project was for me.

Linda Crapts
Delft, September 2012

Contents

Nomenclature

Greek symbols

α	Coefficient for the increase of attractant due to the injected stem cells	$[\frac{1}{mm^3} \cdot \frac{1}{s}]$
α_0	Coefficient for the growth of tip density due to primary angiogenesis	$[\frac{mm^3}{mol} \cdot \frac{1}{s}]$
α_1	Coefficient for the growth of tip density due to secondary angiogenesis	$[\frac{mm^3}{mol} \cdot \frac{1}{s}]$
β_1	Coefficient for the decay of stem cells	$[s^{-1}]$
β_2	Coefficient for the decrease of capillary tips due to anastomoses	$[\frac{mm^3}{s}]$
χ_1	Chemotaxis coefficient	$[\frac{mm^2}{s} \cdot \frac{mm^3}{mol}]$
χ_2	Coefficient describing the influence of the number of tips due to a change in concentration TG-β	$[\frac{mm^3}{s} \cdot \frac{mm}{mol}]$
Δt	Time step size	[s]
Δx	Maximum element size	[mm]
δ	Radius of the wound	[mm]
Δ_j	Element size of element e_j	[mm]
δ_{ij}	Kronecker delta	[-]
ϵ	Diffusion coefficient of the vessel density	$[\frac{mm^2}{s}]$
γ	Coefficient for branching and forming loops	$[\frac{1}{s}]$
λ	Coefficient for the decrease of attractant due to other substances	$[\frac{1}{s}]$
λ_2	Coefficient for the influence of the attractant on the capillary tips	$[\frac{1}{s} \cdot \frac{mm^3}{mol} \cdot \frac{mm^3}{mol}]$
μ_1	Coefficient representing the influence of a change in the capillary tip density	$[\frac{mm}{s}]$
ν_n	nth eigenvalue of the Sturm-Liouville problem associated with the Bessel function	[-]
Ω	Our domain, so the total part of the heart, including the wound, that we observe	[-]
Ω_w	Damaged part of the heart	[-]
Φ	Space of all piecewise polynomials of degree (at most) K	[-]
ρ	Vessel density	$[\frac{1}{mm^3}]$

ρ_{eq}	Equilibrium value of the vessel density	$[\frac{1}{mm^3}]$
ρ_{ij}^k	Coefficient for element e_{ij} corresponding to the Legendre polynomial of order k for determining the vessel density	[-]
σ_j^k	Slope for the Van Leer limiter	[-]
τ	Time at which the front of the capillary tips enters the wound	[s]
$\tilde{\lambda}$	$\frac{\lambda}{D_1}$	$[\frac{1}{mm^2}]$
φ	Basis function	[-]

Latin symbols

$\bar{c}$	Total number of moles of TG-β	[mol]
$\bar{c}_0$	Initial concentration of TG-β	$[\frac{mol}{mm^3}]$
$\bar{t}$	Time at which the characteristics are close enough to the center of the wound	[s]
$\bar{u}_j^k$	Coefficients for u on element e_j for polynomial woth order k	[-]
$\hat{c}$	Threshold of attractant	$[\frac{mol}{mm^3}]$
$\mathbf{M}$	Mass matrix	[-]
$\mathbf{S}$	Stiffness matrix	[-]
$\mathbf{f}$	Source vector	[-]
c	Concentration TG-β	$[\frac{mol}{mm^3}]$
c_h	Homogeneous solution of the concentration TG-*beta*	$[\frac{mol}{mm^3}]$
c_{app}	Approximation using the discontinuous Galerkin method	$[\frac{mol}{mm^3}]$
c_{ij}^k	Coefficient for element e_{ij} corresponding to the Legendre polynomial of order k for determining the concentration TG$-\beta$	[-]
D_1	Diffusion coefficient of the concentration TG-β	$[\frac{mm^2}{s}]$
D_2	Diffusion coefficient of the capillary tips	$[\frac{mm^2}{s}]$
e_j	Element j	[-]
J_0	Bessel function of the first kind of zero-th order	[-]
K	Order of the polynomials	[-]
m	Number of stem cells	[-]
m_0	Initial injected number of stem cells in the wound	[-]
n	Capillary tip denisty	$[\frac{1}{mm^3}]$
n_{ij}^k	Coefficient for element e_{ij} corresponding to the Legendre polynomial of order k for determining the capillary tip density	[-]

P_n	Legendre polynomial of order n	[-]
q	Gradient of the concentration TG-β	$[\frac{1}{mm^3} \cdot \frac{1}{mm}]$
r	Coordinate on the $r-$ axis, when using polar coordinates	[-]
T	Time end	[s]
t	Time	$[s]$
u	Gradient of the vessel density	$[\frac{1}{mm^3} \cdot \frac{1}{mm}]$
w	Gradient of the capillary tip density	$[\frac{1}{mm^3} \cdot \frac{1}{mm}]$
x	Coordinate in the $x-$direction	[-]
x_0	Initial location of the front of the characteristics of the capillary tip density	[-]
y	Coordinate in the $y-$direction	[-]

List of Figures

List of Tables

Chapter 1

Introduction

A serious complication that patients face after a heart attack is the formation of scar tissue at the damaged part of the heart. This scar leads to stiffening of the damaging region, and thereby it requires more perfomance of the heart muscle, which leads to fatigue and hence to failure and thereby causing immediate death of the patient. To circumvent scar tissue formation, stem cells are injected which trigger the angiogenetic response, leading to fewer invading fibroblast which produce scar tissue in the form of an excess on extra cellular matrix.

The goal of this research is to learn more about the number of stem cells that has to be injected into the wound of the heart after a heart attack, aiming to avoid the formation of scar tissue. Therefore, the main question of this research reads as

> "How many stem cells should be injected when aiming at avoiding the formation of scar tissue?"

To better understand this question, we need to know more about the underlying biology and mathematics. Therefore, we give an introduction into the biological background and some mathematical approaches.

1.1 Biological background

1.1.1 Myocardial infarction

A myocardial infarction, or commonly called a 'heart attack', is often the result of a blockage in the coronary artery after the artery has been narrowed. In this chapter we treat events before and after the myocardial infarction and we start with the narrowing of the arteries.

The condition in which an artery wall thickens as a result of the accumulation of fatty acids and cholesterol is called atherosclerosis (the layer of these fatty acids and cholesterol is named plaque). Bad lifestyle habits like

- smoking,
- alcohol,
- obesity,
- lack of exercise,
- stress,

and genetic deficiencies like

- cardiovascular disease,

- diabetes,

- high blood pressure,

are risk factors for atherosclerosis. When atherosclerosis occurs, the passage of blood through the arteries will be smaller and the blood flowing to the heart muscle decreases. Even a small blood clot can become a blockage of the (coronary) artery and therefore cause a myocardial infarction. Such a blood clot can be formed near and due to a tear in the wall of a artery which is caused by the atherosclerosis. In Figure 1.1 atherosclerosis and clotting blood are shown.
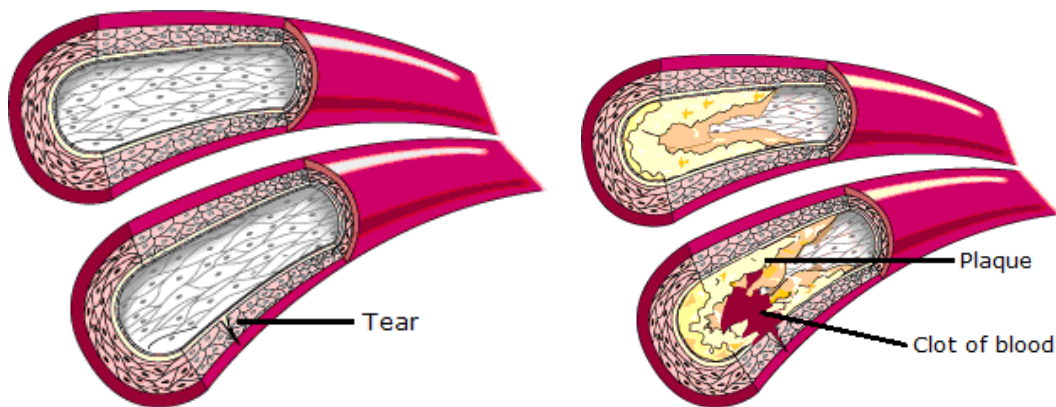
(a) Two arteries without atherosclerosis, where the lowest artery has a tear in the artery wall.

(b) Both arteries with atherosclerosis, where a clot of blood is formed near the tear.

Figure 1.1: *Atherosclerosis in the arteries*[1].

At the moment of such a blockage, the blood supply to the heart is poor and therefore the supply of oxygen and nutrients is insufficient. Due to the insufficient supply, a myocardial infarction occurs where the infarction represents the decease of myocardial tissue (death of heart cells in the heart muscle).

The dead cells in the affected heart region, cause fibroblasts to excessively secrete collagen, which results into scar tissue with stiff mechanical properties. These mechanical properties will result in a higher resistence of the pump function to be carried by the heart muscle. This higher resistence, which frustrates the pump function, will result in growth of the present myocyte cells as a natural reaction of all muscle cells to hard labor. As a result, the muscle cells will decease more rapidly than in circumstances without a heart attack, which eventually will result in heart failure, and hence in death of the patient.

1.1.2   Angiogenesis

In this section we give an introduction to angiogenesis [2]. In short, angiogenesis is the formation of new blood vessels from existing blood vessels. For example, angiogenesis is important in the process of wound healing and in the present application, angiogenesis is stimulated to reduce the amount of fibrosis at locations suffering from a myocardial infarction and hence to reduce the risk of heart failure after a myocardial infarction.

---

[1]`www.hartaanval.nl`

The formation of new blood vessels happens due to angiogenic factors, like hormones, which are secreted by neighboring cells. The angiogenic factors stimulate the growth, division and mobility of neighboring endothelial cells (EC), which constitute the walls of the blood vessels. By doing this, the endothelial cells will split at the tops of the capillaries such that the capillaries grow and branch off.
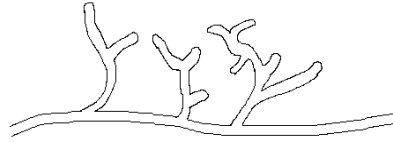
Figure 1.2: *Capillaries branching off.*

Cell-division is a complicated biological process. At the moment the angiogenic factors are stimulating the endothelial cells, these endothelial cells secrete enzymes which degrade their basal membrane/lamina (a thin acellular layer around a capillary which separates different types of tissue) and the extracellular matrix (ECM, acellular part that provides mechanical support to cells). After 'breaking down' the basale membrane and the extracellular matrix the endothelial cells have the possibility to branch off. After branching off, the endothelial cells will form a new basale membrane around themselves.

After forming new vessels and new capillary tips they do not necessarily branch off again. It is also possible that neighboring vessels fuse together and form a new loop. This process is called anastomosis. It is also possible that a tip of a capillary fuses together with another vessel.
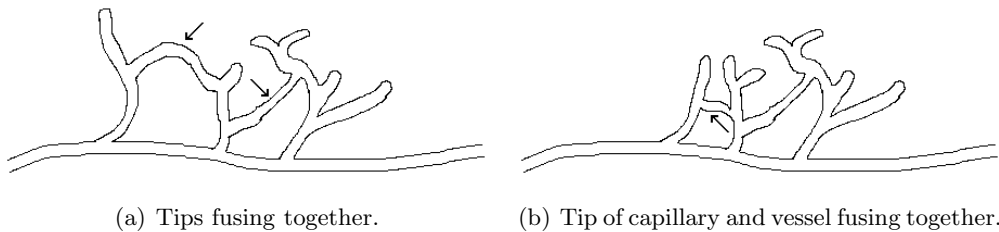
(a) Tips fusing together.

(b) Tip of capillary and vessel fusing together.

Figure 1.3: *Two modes of anastomosis.*

1.1.3   New treatment

In Chapter 1.1.1, we described the consequences and the events that occur after a myocardial infarction. In order to prevent the formation of scar tissue, and therewith to lower the possibility of heart failure, a new treatment is currently being investigated. With this treatment, stem cells are injected onto damaged regions of the heart (the so called wound). These stem cells will secrete, among many others, the growth factor $TG-\beta$, which enhances angiogenesis (see Chapter 1.1.2) in the sense that

- endothelial cells are provoked to move towards the 'wound' (chemotaxis);

- endothelial cells are provoked to divide, by which new arteries are formed and extended as a result of proliferation of endothelial cells.

After the enhanced angiogenesis, vessels have been formed in the damaged part of the heart aiming at avoiding the formation of scar tissue.

1.2   Mathematical approaches

The damaged part of the heart, which occurs after a myocardial infarction, can mathematically be seen as a wound. In literature different mathematical approaches are described in order to perform numerical simulations for the healing of different types of wounds.

Wound healing depends on many different biological processes like, among others, random walk, tensotaxis, chemotaxis, cell profileration and death, secretion and signaling of growth factors which will all be taken into account in the mathematical models. For these processes, the following mathematical approaches are used in literature, see references in [13]:

- Cellular automata models (involving a minimization of a virtual energy with a Monte-Carlo like scheme);

- Cell based models;

- Phenomenological models where the wound healing is modeled as a moving boundary problem where the boundary moves as a result of a growth factor and local curvature;

- Continuum-based partial differential equations involving transport (random walk, chemotaxis,...).

The last approach is used during this project. The partial differential equations that we use will be introduced in Chapter 2.

1.3   Numerical techniques

In order to find approximations to solutions of partial differential equations many numerical methods can be used. During this project we used three different numerical methods:

- finite difference method;

- finite element method;

- discontinuous Galerkin method.

In the literature study [4] done in the first few months of this project, we looked at numerical methods for the one dimensional problem. First the finite difference method was dealt with, followed by the finite element method. Both methods were used in combination with Euler Backward time integration.

A disadvantage of the finite difference method is that it cannot easily handle complicated geometries. Since the damaged part of the wound can have all kinds of geometries this method is not suitable. Therefore, we looked at the finite element method which we extended to the two dimensional model in this report. Despite that it can handle complicated geometries, it turns out that it cannot handle models with a relatively large influence of the convection term, which is biologically induced by chemotaxis. So if it appears that the influence of chemotaxis is too large, then the method fails. Moreover, the method cannot handle any discontinuities hence possible jumps in the approximation will be smeared out or induce spurious oscillations as a consequence of this method.

Therefore, we looked at the discontinuous Galerkin method. This method can handle complicated geometries, discontinuities and hopefully cases with a high influence of the convection terms.

1.4 Organisation of this thesis

First we introduce the mathematical model that we will use throughout this report. This is done in Chapter 2.

Subsequently, we determine some analytical solutions in Chapter 3 in order to give some clarity of how the biology of this model works, to have a benchmark for validation of the numerical solutions, and to draw some first conclusions.

Then the implementation of some numerical methods is described. We first implement the finite element method for the two dimensional model, followed by the implementation of the discontinuous Galerkin method for the one and for the two dimensional model. For the two dimensional model, we consider circular and rectangular wounds. For the circular wounds, we use an approximation based on polar coordinates. Furthermore, for the rectangular wounds we use discontunous Galerkin similar to how we used it for the one dimensional model but now in two directions, the $x-$ and the $y-$direction. All the numerical simulations are done in Chapter 4.

Some points of discussion and recommendation are treated in Chapter 6. The thesis is finalized by the conclusions-section.

Chapter 2

Mathematical Model

In this chapter we introduce two different mathematical models to describe angiogenesis. The first model we describe is based on a model for tumor angiogenesis from Byrne et al [2] and the second formalism is based on a model from Maggelakis [10] [11].

In order to work with these models we consider the damaged part of the heart, Ω_w, as well as the tissue around the wound to be symmetric and circulair. So we obtain

$$\Omega: \ x \in [-1, 1], \ y \in [-1, 1], \ \text{s.t. } x^2 + y^2 \leq 1.$$
$$\Omega_w: \ x \in [-\delta, \delta], \ y \in [-\delta, \delta], \ \text{s.t. } x^2 + y^2 \leq \delta^2.$$
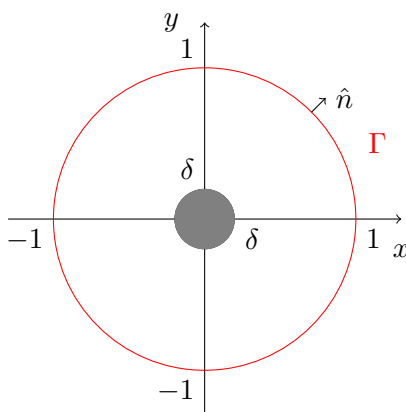
Figure 2.1: *The wound (gray) and some tissue around it.*

2.1 Tip-vessel model: based on the model from Byrne et al.

The model for tumor angiogenesis based on the model from Byrne et al. [2] takes into account an attractant, the change in capillary tip density and the change in the vessel density. Further, we have a partial differential equation for the stem cell density since the injected stem cells excrete the attractant TG$-\beta$.

2.1.1   Stem cell density

To stimulate angiogenesis around the specific area of the heart an number of stem cells is injected once. These stem cells secrete the attractant $TG-\beta$. Due to reactions the number of stem cells will decrease exponentially in time. Therefore the equation for the number of stem cells is given by

$$\frac{\partial m}{\partial t} = -\beta_1 m, \tag{2.1}$$

with coefficient β_1 and where we have the initial injected number of stem cells

$$m(x, y, 0) = \begin{cases} m_0 & x \in \Omega_w, \\ 0 & x \in \Omega \backslash \Omega_w. \end{cases} \tag{2.2}$$

The dimension of the coefficient β_1 is s^{-1}.

2.1.2   Concentration $TG-\beta$

As an addition to Eq. (2.1) for the concentration attractant in [2], we now have an injected source that secretes the attractant. The equation for the concentration $TG-\beta$ becomes

$$\frac{\partial c}{\partial t} - \underbrace{D_1 \nabla \cdot (\nabla c)}_{\text{random walk}} + \lambda c = \alpha m(x, y, t), \tag{2.3}$$

with diffusion coefficient D_1, coefficient λ for the decrease of attractant due to reactions with other substances [4] and coefficient α for the increase of attractant due to the injected stem cells. The initial condition of the concentration $TG-\beta$ is given by

$$c(x, y, 0) = 0, \tag{2.4}$$

while the Neumann boundary condition equals

$$\left. \frac{\partial c}{\partial \hat{n}} \right|_\Gamma = 0. \tag{2.5}$$

The dimensions of the coefficients are

- $\dim(D_1) = \left[\frac{mm^2}{s} \right]$,

- $\dim(\alpha) = \left[\frac{1}{mm^3} \cdot \frac{1}{s} \right]$,

- $\dim(\lambda) = \left[\frac{1}{s} \right]$.

2.1.3   Capillary tip density

Since the source of $TG-\beta$, a number of stem cells, has already been taken into account in the partial differential equation for the concentration $TG-\beta$, the number of stem cells plays only an indirect role in the density of the capillary tips. Therefore the partial differential equation from [2] is also applicable to our model. Hence the partial differential equation for the capillary tip density is given by

$$\frac{\partial n}{\partial t} + \underbrace{\chi_1 \nabla \cdot (n \nabla c)}_{\text{chemotaxis}} - \underbrace{D_2 \nabla \cdot (\nabla n)}_{\substack{\text{random} \\ \text{walk}}} = \underbrace{\alpha_0 \rho c}_{\substack{\text{bifur-} \\ \text{cation} \\ \text{at} \\ \text{vessels}}} + \underbrace{\alpha_1 H(c - \hat{c}) n c}_{\substack{\text{bifurcation} \\ \text{of tips}}} - \underbrace{\beta_2 n \rho}_{\substack{\text{anasto-} \\ \text{mosis}}}, \tag{2.6}$$

where χ_1 is the chemotaxis coefficient which models the influence of attractant TG$-\beta$ on the mobility of the capillary tips towards the gradient of TG$-\beta$, and D_2 the diffusion coefficient. Further, we have α_0 as a coefficient for the first type of angiogenesis, which is an increase of capillary tips because they branch of from blood vessels as a reaction to the attractant TG$-\beta$. The coefficient of the second type of angiogenesis is α_1 where exceeding a threshold of attractant, $\hat{c}$, causes capillary tips to branch off. Finally we have β_2 as the coefficient for the decrease of capillary tips because of the joining of tips-sprouts. This process is called anastomosis [4]. Note that $H(c - \hat{c})$ is the Heaviside term defined by

$$H(c - \hat{c}) = \begin{cases} 1, & c \geq \hat{c}, \\ 0, & c < \hat{c}. \end{cases} \tag{2.7}$$

Initially there are no capillary tips, so

$$n(x, y, 0) = 0, \tag{2.8}$$

and we have a no-flux condition on the boundary

$$\chi_1 n \frac{\partial c}{\partial \hat{n}} - D_2 \frac{\partial n}{\partial \hat{n}}\Big|_{\Gamma} = 0. \tag{2.9}$$

The dimensions of these coefficients are

- $\dim(\chi_1) = \left[\frac{mm^2}{s} \cdot \frac{mm^3}{mol} \right]$,

- $\dim(D_2) = \left[\frac{mm^2}{s} \right]$,

- $\dim(\alpha_0) = \left[\frac{mm^3}{mol} \cdot \frac{1}{s} \right]$,

- $\dim(\alpha_1) = \left[\frac{mm^3}{mol} \cdot \frac{1}{s} \right]$,

- $\dim(\beta_2) = \left[\frac{mm^3}{s} \right]$.

2.1.4 Vessel density

Since the vessel density, ρ modeled by the partial differential equation proposed in [2] tends to zero as the time goes to infinity, we need to change the partial differential equation for the vessel density a bit since we want to end with an equilibrium value, unequal to zero, for the vessel density. The new equation becomes

$$\frac{\partial \rho}{\partial t} - \underbrace{\epsilon \nabla \cdot (\nabla \rho)}_{\substack{\text{random} \\ \text{walk}}} + \gamma(\rho - \rho_{eq}) = \underbrace{(\mu_1 \nabla n - \chi_2 n \nabla c)}_{\text{snail trail}} \cdot \frac{\bar{x}}{\|\bar{x}\|}, \tag{2.10}$$

where $\bar{x} = \begin{pmatrix} x \\ y \end{pmatrix}$ such that the snail trail moves towards the center of the wound [6], which is located at $(0, 0)$ in this study. In Eq. (2.10) we have the diffusion coefficient ϵ and γ as coefficient for branching and forming loops. Further, we also have coefficient μ_1 which represents the influence of a change in the capillary tip density and coefficient χ_2 which describes the influence of the number of tips due to a change in the concentration TG$-\beta$.

Initially there are no viable vessels present in the damaged part of the heart and there is an

equilibrium vessel density around the wound. Far away from the wound the vessel density should have its equilibrium value, so we obtain

$$\rho(x, y, 0) = \begin{cases} 0, & x \in \Omega_w, \\ \rho_{eq}, & x \in \Omega \backslash \Omega_w, \end{cases} \tag{2.11}$$

$$\rho|_\Gamma = \rho_{eq}. \tag{2.12}$$

Where the dimensions of the coefficients are

- $\dim(\epsilon) = \left[\frac{mm^2}{s} \right]$,

- $\dim(\gamma) = \left[\frac{1}{s} \right]$,

- $\dim(\mu_1) = \left[\frac{mm}{s} \right]$,

- $\dim(\chi_2) = \left[\frac{mm^3}{s} \cdot \frac{mm}{mol} \right]$.

2.2 Endothelial cells model: based on the model from Maggelakis

The model just described is not the only available model we observe. We have a second, more compact, model. This model, based on a model of Maggelakis [10, 11], consists of the following three equations:

$$\frac{\partial m}{\partial t} = -\beta_1 m, \tag{2.13}$$

$$\frac{\partial c}{\partial t} - D_1 \nabla \cdot (\nabla c) + \lambda c = \alpha m(x, y, t), \tag{2.14}$$

$$\frac{\partial n}{\partial t} + \chi_1 \nabla \cdot (n \nabla c) = \lambda_2 c (1 - n) n, \tag{2.15}$$

where the initial and boundary conditions are given by

$$m(x, y, 0) = m_0, \tag{2.16}$$

$$c(x, y, 0) = 0, \tag{2.17}$$

$$n(x, y, 0) = \begin{cases} 0, & x \in \Omega_w, \\ n_{eq}, & x \in \Omega \backslash \Omega_w, \end{cases} \tag{2.18}$$

$$\left. \frac{\partial c}{\partial \hat{n}} \right|_\Gamma = 0, \tag{2.19}$$

$$\left. \frac{\partial n}{\partial \hat{n}} \right|_\Gamma = 0. \tag{2.20}$$

The equation, and therefore also the dimensions of the coefficients, for the stem cell density, see Eq. (2.13), is equal to the equation for the stem cell density in our first model, given by Eq. (2.1). This also applies to the equation for the concentration TG$-\beta$, see Eq. (2.14), which is equal to Eq. (2.3). And Eq. (2.15) denotes the density of the endothelial cells and the dimensions of the coefficients are therefore

- $\dim(\chi_1) = \left[\frac{mm^2}{s} \cdot \frac{mm^3}{mol} \right]$,

- $\dim(\lambda_2) = \left[\frac{1}{s} \cdot \frac{mm^3}{mol} \cdot \frac{mm^3}{mol} \right]$,

- $\dim(1) = \left[\frac{mol}{mm^3} \right]$.

Biologically, the compact model differs from the first model in the sense that no influence is included between the capillary tip density and the vessel density, since we look at the density for the endothelial cells in this model. This equation does not contain the snail trail term which is included in the equation for the vessel density in the other model. One may wonder whether this equation represents reality. An other significant difference is that there is no diffusion, random walk, for the tips included in this model.

Mathematically, the difference is that this method misses some relatively complicated terms, like the snail trail, which are included in the other model. This means that the challenge, when doing numerical computations, lies in the first model.

Combining the biological and mathematical differences we choose the first model based on Byrne et al. [2] since we believe that this model is biologically better and mathematically the bigger challenge.

Chapter 3

Analytical solutions

In this chapter we determine some analytical solutions for the one dimensional and for the two dimensional model. In order to do so, we will neglect terms with insignificant contributions. With help of the analytical solution for the capillary tip density, we find an equation which describes the location of the front of the capillary tips at all times. With this equation we can determine with which number of stem cells the front enters the wound, so when vessels are growing into the damaged part of the heart. However, first we determine the analytical solutions to the partial differential equations.

3.1 Tip-vessel model: based on the model from Byrne et al.

3.1.1 Number of stem cells

The exact solution to Eq. (2.1) is given by

$$m(x, y, t) = \begin{cases} m_0 e^{-\beta_1 t}, & x \in \Omega_w, \\ 0, & x \in \Omega \backslash \Omega_w. \end{cases} \tag{3.1}$$

The number of stem cells at different times t is now shown in Figure 3.1. This has been done for our one dimensional model so our domain equals $\Omega = [0, 1]$, where 0 is the center of the damaged part of the wound.

In Figure 3.1 we see the exact solution of the stem cell density in time. The figure illustrates how the density of stem cells is equal everywhere in the wound of the heart at a time t. Further we see that initially the density equals 2 million cells/mm^3 - which is probably not a realistic value, we use this for our mathematical purposes - and that it decreases exponentially in time, so after $t = 2$ the density is around the 0.75 million cells/ mm^3. After there are no stem cells left the 'production' of TG$-\beta$ ends and the angiogenesis trigger due to this attractant TG-beta comes to an end. This does not mean that the angiogenesis itself has come to an end.

3.1.2 Concentration TG$-\beta$

Eq. (2.3) reflects the evolution of the concentration TG$-\beta$. For this analytical solution we use the one dimensional domain $\Omega = [0, 1]$ where the damaged part of the heart is $\Omega_w = [0, \delta]$. Hence δ is the boundary of the damaged part of the wound.

Since the diffusion of TG$-\beta$ is a relatively fast process, we substitute $\frac{\partial}{\partial t} = 0$ into Eq. (2.3). Using the solution (3.1), our problem reduces to

$$-D_1 \frac{\partial^2 c}{\partial x^2} + \lambda c = \alpha m_0 e^{-\beta_1 t} \left(1 - H(x - \delta) \right) \tag{3.2}$$
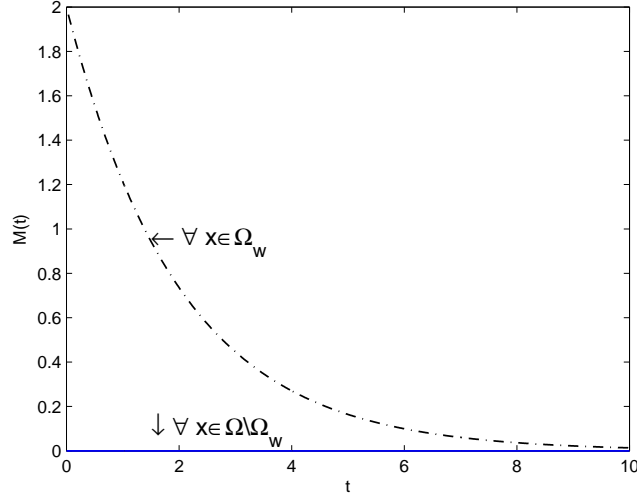
Figure 3.1: *The exact solution for the density of stem cells inside and outside the damaged part of the wound.*

with initial condition (2.4), boundary conditions (2.5) and where $H(x - \delta)$ is the Heaviside function

$$H(x - \delta) = \begin{cases} 0 & x < \delta, \\ 1 & x \geq \delta. \end{cases}$$

It can be proved that the solution to Eq. (2.3) can be approximated by the solution to Eq. (3.2). This has been done in Appendix A.

As we can see in Eq. (3.2) there is still a term depending on time t, while we substituted $\frac{\partial}{\partial t} = 0$. This is possible because we assume that we have a semi steady-state which means that we assume that at every time t a new equilibrium value for the concentration TG$-\beta$ sets in.

First we determine the homogeneous solution of Eq. (3.2) by substituting $c_h = e^{rx}$ into Eq. (3.2) and we determine the particular solution to our nonhomogeneous problem. Combining the homogeneous and the particular solution, we obtain the solution

$$c(x,t) = \begin{cases} \underbrace{\frac{\alpha m_0}{\lambda} e^{-\beta_1 t}}_{\text{particular solution}} + \underbrace{A_1 \cosh\left(\sqrt{\tilde{\lambda}} x\right) + A_2 \sinh\left(\sqrt{\tilde{\lambda}} x\right)}_{\text{homogeneous solution}}, & \forall x \in [0, \delta), \\ \underbrace{B_1 \cosh\left(\sqrt{\tilde{\lambda}} x\right) + B_2 \sinh\left(\sqrt{\tilde{\lambda}} x\right)}_{\text{homogeneous solution}}, & \forall x \in [\delta, 1], \end{cases} \quad (3.3)$$

with $\tilde{\lambda} = \frac{\lambda}{D_1}$ and where we only need to determine the coefficients. Using the boundary conditions (2.5) and since we require continuity on the boundary, $x = \delta$, for both $c(x,t)$ and the derivative $\frac{\partial c}{\partial x}$, the coefficients from our analytical solution are

$$A_1 = -\frac{\alpha m_0}{\lambda} e^{-\beta_1 t} \frac{\sinh\left(\sqrt{\tilde{\lambda}}(1-\delta)\right)}{\sinh\left(\sqrt{\tilde{\lambda}}\right)}, \qquad A_2 = 0, \tag{3.4}$$

$$B_1 = \frac{\alpha m_0}{\lambda} e^{-\beta_1 t} \frac{\sinh\left(\sqrt{\tilde{\lambda}}\delta\right)}{\tanh\left(\sqrt{\tilde{\lambda}}\right)}, \qquad B_2 = -\frac{\alpha m_0}{\lambda} e^{-\beta_1 t} \sinh\left(\sqrt{\tilde{\lambda}}\delta\right). \tag{3.5}$$

Where, after a very long time, when there are no stem cells left in the wound, the concentration TG$-\beta$ inside the wound goes to

$$t \to \infty \;\Rightarrow\; e^{-\beta_1 t} \to 0 \;\Rightarrow\; c(x,t) \to 0, \tag{3.6}$$

and outside the wound the concentration goes directly to

$$t \to \infty \;\Rightarrow\; c(x,t) \to 0. \tag{3.7}$$

3.1.3 Number of TG$-\beta$

In the previous chapter, we determined the concentration of TG$-\beta$ analytically. It is also possible to determine the total number of moles of TG$-\beta$ since the number of moles is the concentration integrated over the domain, i.e. $\bar{c}(t) = \int_\Omega c(x,y,t)\,d\Omega$. This has been done in Appendix B.

The number of moles TG-β is

$$\bar{c}(t) = \begin{cases} \bar{c}_0 e^{-\lambda t} + \frac{\alpha m_0}{\lambda - \beta_1}(e^{-\beta_1 t} - e^{-\lambda t})\frac{A(\Omega_w)}{A(\Omega)}, & \text{if } \lambda \neq \beta_1, \\ \bar{c}_0 e^{-\lambda t} + \alpha m_0 e^{-\lambda t}\frac{A(\Omega_w)}{A(\Omega)}, & \text{if } \lambda = \beta_1. \end{cases} \tag{3.8}$$

Initially we assume that there is no TG$-\beta$ present, so $\bar{c}_0 = 0$. The number of TG$-\beta$ will be different for the one and the two dimensional problem, since

$$\frac{A(\Omega_w)}{A(\Omega)} = \frac{\delta}{1} = \delta, \qquad\qquad \text{for the one dimensional problem,} \tag{3.9}$$

$$\frac{A(\Omega_w)}{A(\Omega)} = \frac{\pi\delta^2}{\pi} = \delta^2, \qquad\qquad \text{for the two dimensional problem.} \tag{3.10}$$

With $\delta = 0.2$ this means that the total amount of TG$-\beta$ will be five times smaller in the two dimensional problem than in the one dimensional problem. This can also be seen in Figure 3.2.

In Figure 3.2(a) the number of moles of TG$-\beta$ is shown for $t > 0$ for the one dimensional problem. Initially there are no TG-β molecules present and we know that the stem cells produce TG-β. In Figure 3.1 the number of stem cells is shown. In that figure we see that TG$-\beta$ is still being produced at $t = 10$, while we see in Figure 3.2 that the number of moles of TG$-\beta$ is decreasing at this time. This means that from a certain moment TG$-\beta$ reduces faster than it is being produced.

(a) For the one dimensional problem.

(b) For the two dimensional problem.
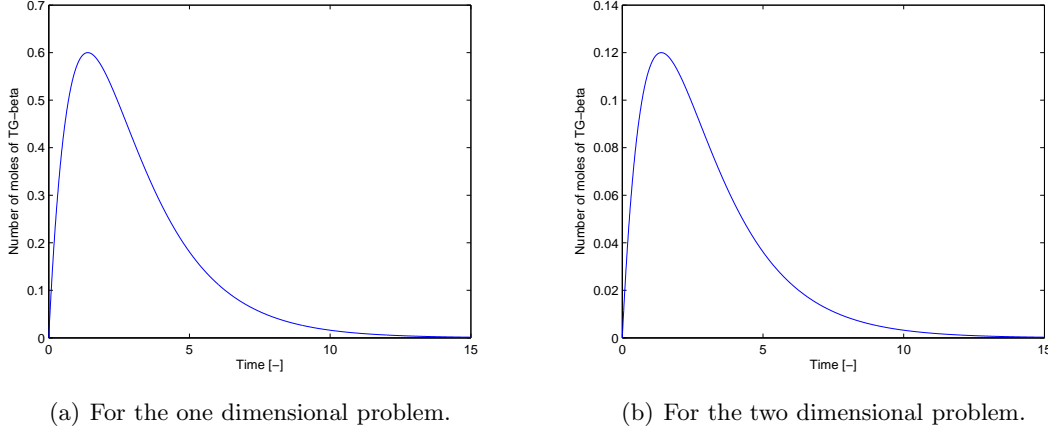
Figure 3.2: *Number of moles of TG*$-\beta$.

3.1.4 Characteristics of the capillary tip density

The analytical solution for the density of the capillary tips, given by Eq. (2.6) is difficult to find. First we simplify the problem to

$$\frac{\partial n}{\partial t} + \chi_1 \frac{\partial}{\partial x}\left(n\frac{\partial c}{\partial x}\right) = \alpha_0\rho c + \alpha_1 H(c-\hat{c})nc - \beta_2 n\rho, \qquad (3.11)$$

where we neglect the diffusion part since in reality the problem is dominated by convection. Application of the Product Rule for differentiation into (3.11), gives

$$\frac{dn}{dt} = -\chi_1 n\frac{\partial^2 c}{\partial x^2} + \alpha_0\rho c + \alpha_1 H(c-\hat{c})nc - \beta_2 n\rho = F(n,c), \qquad (3.12)$$

over a characteristic that travels at speed

$$\frac{dx}{dt} = \chi_1 \frac{\partial c}{\partial x}, \qquad (3.13)$$

where

$$\frac{dn}{dt} = \frac{\partial n}{\partial t} + \frac{\partial n}{\partial x}\frac{dx}{dt}.$$

For now we focus on the equation for the location of the front of the capillary tips, Eq. (3.13). We define $t = \tau$ as the time that the characteristic is on the boundary of the wound, i.e. $x(\tau) = \delta$. First we determine the location of the front as $x_0 < \delta$ and therefore $t > \tau$. In order to do this, we use (3.3) and (3.4). We obtain

$$\frac{dx}{dt} = -\frac{\alpha m_0}{\lambda}\chi_1\sqrt{\tilde{\lambda}}e^{-\beta_1 t}\frac{\sinh\left(\sqrt{\tilde{\lambda}}(1-\delta)\right)}{\sinh\left(\sqrt{\tilde{\lambda}}\right)}\sinh\left(\sqrt{\tilde{\lambda}}x\right).$$

The solution as obtained in Appendix C.3 is

$$x(t) = \frac{2}{\sqrt{\tilde{\lambda}}} \operatorname{arctanh}\left[\tanh\left(\frac{\sqrt{\tilde{\lambda}} x_0}{2}\right) \right.$$
$$\left. \cdot \exp\left(\frac{\alpha m_0}{\lambda \beta_1} \chi_1 \tilde{\lambda} \frac{\sinh\left(\sqrt{\tilde{\lambda}}(1-\delta)\right)}{\sinh\left(\sqrt{\tilde{\lambda}}\right)}\left(e^{-\beta_1 t} - e^{-\beta_1 \tau}\right)\right)\right], \qquad (3.14)$$

for $x_0 < \delta$, $t > \tau$.

We do the same for $x_0 \geq \delta$ and therefore $t \leq \tau$ when using (3.3) and (3.5) and obtain

$$\frac{dx}{dt} = -\frac{\alpha m_0}{\lambda} \chi_1 \sqrt{\tilde{\lambda}} \sinh\left(\sqrt{\tilde{\lambda}} \delta\right) e^{-\beta_1 t} \left[\cosh\left(\sqrt{\tilde{\lambda}} x\right) - \frac{\sinh\left(\sqrt{\tilde{\lambda}} x\right)}{\tanh\left(\sqrt{\tilde{\lambda}}\right)}\right],$$

where the solution as obtained in Appendix C.3 equals

$$x(t) = \frac{1}{\sqrt{\tilde{\lambda}}} \ln\left(\sqrt{\frac{A+B}{A-B}} \cdot \frac{1 + \psi_2(t)}{1 - \psi_2(t)}\right), \qquad (3.15)$$

for $x_0 \geq \delta$, $t \leq \tau$, where

$$\psi_2(t) = \exp\left[\ln\left(\frac{e^{\sqrt{\tilde{\lambda}} x_0} - \sqrt{\frac{A+B}{A-B}}}{e^{\sqrt{\tilde{\lambda}} x_0} + \sqrt{\frac{A+B}{A-B}}}\right) - \sqrt{\tilde{\lambda}}\sqrt{A^2 - B^2}\psi_1(t)\right], \qquad (3.16)$$

$$\psi_1(t) = \frac{\alpha m_0}{\lambda \beta_1} \chi_1 \sqrt{\tilde{\lambda}} \sinh\left(\sqrt{\tilde{\lambda}} \delta\right)\left(e^{-\beta_1 t} - 1\right). \qquad (3.17)$$

Note that if $x_0 < \delta$, the front has already passed the boundary of the wound and we immediately have $\tau = 0$. If $x_0 \geq \delta$, τ can be determined from Eq. (C.7) with substituting $x(\tau) = \delta$.

In Figure 3.3(a) the movement of the characteristics of the capillary tip density is shown for the situation that the characteristics already start in the wound of the heart. In this figure we see that the speed of the characteristics decreases as the characteristics move towards the center of the wound. Note that this is the conclusion in this situation with a certain choice for all the biological parameters, Table D.1.

In Figure 3.3(b) and in Figure 3.3(c) the movement is shown for the characteristics of the capillary tips when they are initially outside the wound. When the characteristics reach δ, here $\delta = 0.2$, the boundary of the wound, the characteristics follow Eq. (3.14) instead of Eq. (3.15). For the chosen values of our parameters we see that the characteristics do reach the boundary of the heart when starting at $x = 0.4$ but they do not reach it when they start at $x = 0.8$. The characteristics move through $\frac{dx}{dt} = \chi_1 \frac{\partial c}{\partial x}$, where χ_1 is a biological constant parameter. This means that $\frac{\partial c}{\partial x}$ goes to zero before the front, starting at $x = 0.4$, can reach the boundary of the wound. The only parameter that is not fixed by biology, is the number of injected stem cells. So from Figure 3.3(c) we conclude that not enough stem cells are injected in order to get the capillary tips, initially outside the wound, inside the wound.
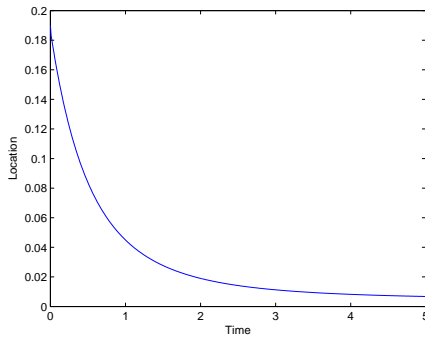
(a) Characteristics start inside the wound at $x = 0.19$
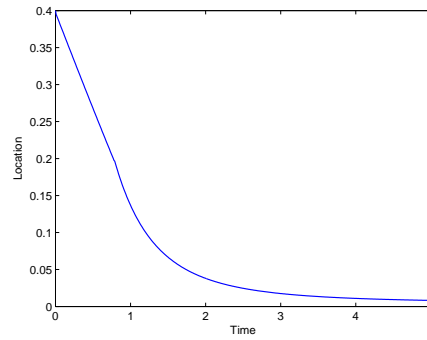
(b) Characteristics start outside the wound at $x = 0.4$
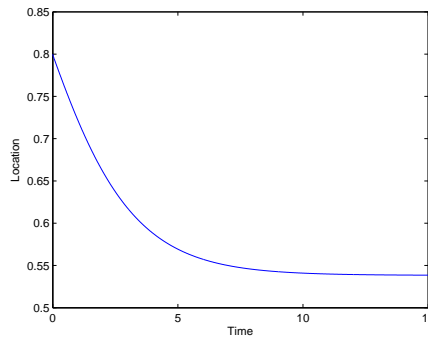
(c) Characteristics start outside the wound at $x = 0.8$

Figure 3.3: *The movement of the characteristics of the capillary tip density.*

More important are the characteristics that originate at the boundary of the damaged part of the heart. We want to know whether these characterstics reach the center of the wound to form a network of vessels inside the wound since then we have a sufficient number of capillaries all over the initially damaged part of the heart. Therefore we have taken different numbers of stem cells and in Figure 3.4 the movement of the characteristics for the different situations are shown.

In Figure 3.4 we see that when we inject a relatively small number of stem cells the characteristcs do not reach the center of the wound and when we inject a relatively large number of stem cells converge to it asymptotically.

The wound will have sufficient blood supply if there is a time t, given a number of stem cells, such that the characteristics are close enough to the center of the wound. If they get close enough we also want to know that value of t. We describe this as

$$\tilde{t} = \operatorname*{argmin}_{t \in (0,T]} \{t \in (0,T] : |x(t)| < \epsilon\}, \text{ if } \tilde{t} \text{ exists,} \tag{3.18}$$

where we take $\epsilon = 10^{-6}$.

It appears that when we consider $t \in (0,10]$ and $m_0 = 4$ no sufficiently dense capillary network will be established despite that it is suggested by Figure 3.4.

In Figure 3.5 the time is shown that the characteristics need to come from the boundary to the center of the wound.
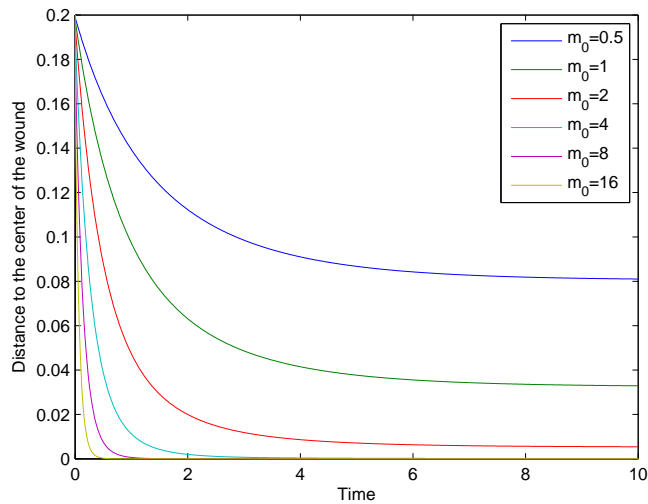
Figure 3.4: *The movement of the characteristics of the capillary tip density, starting at the boundary of the wound, where different numbers of stem cells are injected.*
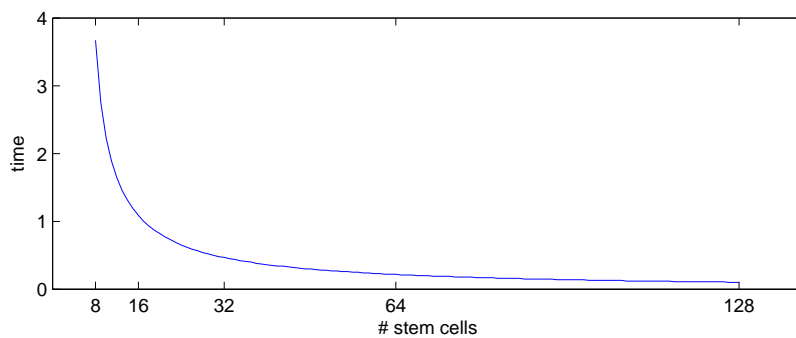
Figure 3.5: *Time that the characteristics need to come from the boundary to the center of the wound.*

Taking Figure 3.4 in mind we can conclude that enough stem cells should be injected in order to have an improvement of the density of capillary tips inside the heart. Combining this with the results that we observe in Figure 3.5 the importance of a fast recovery and the value of stem cells must be weighed in order to determine how many stem cells will be injected.

3.2 Endothelial cells model: based on the model from Maggelakis

The equations for the stem cell density and the concentration TG$-\beta$ are the same as in the tips-vessel model. Therefore, the exact solutions are given by Eq. (3.1) and Eq. (3.3). The amount of TG-β at each time t is also the same and is given by Eq. (3.8).

Rewriting Eq. (2.15) for the endothelial cells density equals

$$\frac{dn}{dt} = -\chi_1 \frac{\partial^2 c}{\partial x^2} n + \lambda_2 c(1-n)n \equiv F(n,c), \tag{3.19}$$

where $F(n,c)$ represents the characteristics and

$$\frac{dn}{dt} = \frac{\partial n}{\partial t} + \frac{\partial n}{\partial x}\frac{dx}{dt}, \text{ such that}$$

$$\frac{dx}{dt} = \chi_1 \frac{\partial c}{\partial x}, \tag{3.20}$$

which represents the speed of the characteristics.

In order to find the solution for $x(t)$, the characteristics of the capillary tips, we need to split the function into two: One if the characteristics are initially in the damaged part of the wound ($x_0 < \delta$) and one if the characteristics are initially outside the wound ($x_0 \geq \delta$). We assume that at time $t = \tau$ the front of the capillary tips enters the wound, so $x(\tau) = \delta$.

The solutions to $x(t)$ are now the same as in our previous model since $c(x,t)$ has the same solution for both models and therefore $\frac{\partial c}{\partial x}$ has the same solution for both models. Therefore the solutions are given by Eq. (3.14) and Eq. (3.15).

3.3 Analytical solutions using Bessel functions

In a later chapter we want to validate results we obtain from writing Eq. (3.2) into polar coordinates and where we approximate the solution using the discontinuous Galerkin method. In order to do the validation, we apply discontinuous Galerkin to a simplified version of Eq. (3.2) (a test problem) and compare it to the analytical solution that we determine here.

We consider the following test problem

$$\frac{\partial c}{\partial t} = \frac{\partial^2 c}{\partial r^2} + \frac{1}{2}\frac{\partial c}{\partial r} + -c, \ t > 0, \ 0 < r < 1, \tag{3.21}$$

$$c(r,0) = \frac{\sqrt{2}J_0(\nu_1 r)}{J_1(\nu)}, \ \nu_1 = 2.4048, \tag{3.22}$$

$$c(1,t) = 0. \tag{3.23}$$

where

$$J_0(x) = \sum_{k=0}^{\infty} \frac{(-1)^k}{(k!)^2}\left(\frac{x}{2}\right)^{2k}, \tag{3.24}$$

is the Bessel Function of the first kind of zeroth order, and ν_1 represents the first eigenvalue to the associated Sturm-Liouville problem. The eigenvalues ν_n satisfy

$$\nu_n \in \mathbb{R}: \ J_0(\nu_n) = 0,$$

where $\nu_1 = 2.4048$. The exact solution to the problem (3.21)-(3.23) is given by

$$c(r,t) = e^{-(1+\nu_1^2)t}\frac{\sqrt{2}J_0(\nu_1 r)}{J_1(\nu_1)},$$

$$J_0(\nu_1) = 0, \text{ hence } \nu_1 = 2.4048.$$

To evaluate $J_0(x)$ in Matlab, we type

BesselJ(0,x).

For cartesian coordinates, similar analytic solutions can be constructed. We will not treat this issue.

Chapter 4

Numerical methods

4.1 Finite element method for the two dimensional problem

To determine the solution for our model we approximate all equations, except the one for the stem cell density, using numerical methods. For the stem cell density we use the results obtained in Chapter 3.1.1.

In this chapter we use the finite element method to the two dimensional model. The one dimensional results can be found in [5]. Since the finite element method, as described in [9], can handle complicated geometries as well as conserving fluxes, this method can probably give us a good approximation to the solution of the two dimensional problem. Therefore we now observe the results using the finite element method for our one dimensional problem.

In order to do so we partition the scaled domain as shown in Figure 2.1 into triangular elements, see Figure 4.1. As our basisfunctions we use piecewise linear functions given by
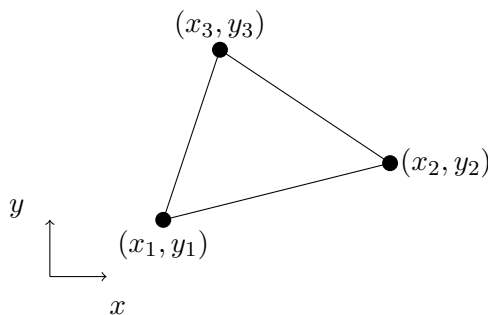
Figure 4.1: *Triangular elements.*

$$\varphi_i^{e_j}(\mathbf{x}) = \alpha_i^{e_j} + \beta_i^{e_j} x + \gamma_i^{e_j} y, \tag{4.1}$$

on element e_j where

$$\varphi_i(x_j) = \delta_{ij},$$

with δ_{ij} the Kronecker delta and with $i \in [l, m]$ and we use k for the current time step.

The first step in the finite element method is to determine the weak formulation. This is done by multiplying the equation by a test function $\varphi \in \Sigma$ where

$$\Sigma = \mathrm{H}^1(\Omega) = \{\varphi \in \mathrm{L}^2(\Omega) \,|\, \frac{\partial \varphi}{\partial x}, \frac{\partial \varphi}{\partial y} \in \mathrm{L}^2(\Omega)\}, \tag{4.2}$$

and integrating this over the whole domain Ω.

After finding the weak formulation we need to use Galerkin's method in order to find a approximation for the unknown, for example the concentration TG-beta. Therefore we need to approximate the solution by a linear combination of basisfunctions, $\varphi_l(\mathbf{x}) \in \Sigma$,

$$c(\mathbf{x}) \approx \sum_{l=1}^{N} c_l(t)\varphi_l(\mathbf{x}), \tag{4.3}$$

and replace the test function φ by each of the basic functions separately. The Galerkin method gives a formula for entries of the mass matrix, the stiffness matrix and of the right handside vector for internal elements.

Note that for an element e_j only the basisfunctions that have their influence are the nonzero ones.

The last step is to also find the element matrix and the element vector for boundary elements (the mass matrix is the same for internal and boundary elements). After finding these quantities for all elements, we need to combine everything into a final mass matrix, stiffness matrix source vector.

Concentration TG$-\beta$

In this section we follow the described steps for the finite element method on Eq. (2.3) in order to find a numerical approximation for our two dimensional problem.

Multiplying Eq. (2.3) with a testfunction φ and integrating over the domain gives us

$$c \in \mathrm{L}^2([0,T]; \mathrm{H}^2(\Omega)) :$$
$$\int_{\Omega} \frac{\partial c}{\partial t}\varphi - D_1 \nabla \cdot (\nabla c)\varphi + \lambda c\varphi \, d\Omega = \int_{\Omega} \alpha m(x,y,t)\varphi \, d\Omega, \ \forall \varphi \in \mathrm{L}^2(\Omega).$$

Using Integration by Parts and substituting the boundary condition (2.5),

$$\int_{\Omega} -D_1 \nabla \cdot (\nabla c)\varphi \, d\Omega = -D_1 \underbrace{\int_{\partial\Omega} \frac{\partial c}{\partial \hat{n}}\varphi \, d\Gamma}_{=0} + D_1 \int_{\Omega} \nabla c \cdot \nabla \varphi \, d\Omega,$$

we obtain the weak formulation

$$c \in \mathrm{L}^2([0,T]; \Sigma) : \ \int_{\Omega} \frac{\partial c}{\partial t}\varphi + D_1 \nabla c \cdot \nabla \varphi + \lambda c\varphi \, d\Omega = \int_{\Omega} \alpha m\varphi \, d\Omega, \ \forall \varphi \in \Sigma. \tag{4.4}$$

Now we insert the approximation with piecewise linear basisfunctions

$$c(\mathbf{x},t) \approx \sum_{l=1}^{N} c_l(t)\varphi_l(\mathbf{x}),$$

into the weak formulation (4.4). The weak formulation becomes

$$\sum_{l=1}^{N} \frac{dc_l}{dt} \underbrace{\int_{\Omega} \varphi_l\varphi_m \, d\Omega}_{\mathbf{M}_{ml}} + \sum_{l=1}^{N} c_l \underbrace{\int_{\Omega} D_1 \nabla\varphi_l \cdot \nabla\varphi_m + \lambda\varphi_l\varphi_m \, d\Omega}_{\mathbf{S}_{ml}} = \underbrace{\int_{\Omega} \alpha m\varphi_m \, d\Omega}_{\mathbf{f}_m}. \tag{4.5}$$

With Eq. (4.5), we can determine the mass matrix, the stiffness matrix and the source vector, since

$$\mathbf{M}_{ml} = \sum_{j=1}^{N_{el}} \mathbf{M}_{ml}^{e_j}, \qquad \mathbf{S}_{ml} = \sum_{j=1}^{N_{el}} \mathbf{S}_{ml}^{e_j}, \qquad \mathbf{f}_m = \sum_{j=1}^{N_{el}} \mathbf{f}_m^{e_j}. \tag{4.6}$$

Using Newton Côtes numerical integration, the element matrices and vector are

$$\mathbf{M}_{ml}^{e_j} = \int_{e_j} \varphi_l \varphi_m \, d\Omega \stackrel{NC}{\approx} \frac{|\Delta|}{6} \sum_{p=1}^{3} \varphi_l(x_p, y_p)\varphi_m(x_p, y_p)$$

$$= \frac{|\Delta|}{6}\delta_{ml}, \tag{4.7}$$

$$\mathbf{S}_{ml}^{e_j} = \int_{e_j} D_1 \nabla\varphi_l \cdot \nabla\varphi_m + \lambda\varphi_l\varphi_m \, d\Omega$$

$$\stackrel{NC}{\approx} \frac{|\Delta|}{2}D_1(\beta_m\beta_l + \gamma_m\gamma_l) + \lambda\frac{|\Delta|}{6} \sum_{p=1}^{3} \varphi_l(x_p, y_p)\varphi_m(x_p, y_p).$$

$$= \frac{|\Delta|}{2}D_1(\beta_m\beta_l + \gamma_m\gamma_l) + \lambda\frac{|\Delta|}{6}\delta_{ml}, \tag{4.8}$$

$$\mathbf{f}_m^{e_j} = \int_{e_j} \alpha m \varphi_m \, d\Omega \stackrel{NC}{\approx} \alpha\frac{|\Delta|}{6} \sum_{p=1}^{3} m(x_p, y_p)\varphi_m(x_p, y_p)$$

$$= \alpha\frac{|\Delta|}{6}m(x_m, y_m). \tag{4.9}$$

Using the implicit Backward Euler time integration, the solution to Eq. (2.3) can be approximated by

$$\mathbf{M}\mathbf{c}^{k+1} = \mathbf{M}\mathbf{c}^k + \Delta t \left(-\mathbf{S}\mathbf{c}^{k+1} + \mathbf{f}^{k+1} \right).$$

Capillary tip density

The same as what we did in the previous chapter can be done for Eq. (2.6). Multiplying by a testfunction and integrating over its domain gives us

$n \in \mathrm{L}^2([0,T]; H^2(\Omega)) :$

$$\int_\Omega \frac{\partial n}{\partial t}\varphi + \chi_1 \nabla \cdot (n\nabla c)\varphi - D_2 \nabla \cdot (\nabla n)\varphi \, d\Omega = \int_\Omega \alpha_0 \rho c \varphi + \alpha_1 H(c - \hat{c})nc\varphi - \beta_2 n\rho\varphi \, d\Omega,$$

$\forall \varphi \in \mathrm{L}^2(\Omega).$

Using the boundary condition (2.9) we have

$$\int_\Omega \chi_1 \nabla \cdot (n\nabla c)\varphi - D_2 \nabla \cdot (\nabla n)\varphi \, d\Omega$$

$$= \underbrace{\int_{\partial\Omega} \left(\chi_1 n\frac{\partial c}{\partial \hat{n}} - D_2\frac{\partial n}{\partial \hat{n}} \right) \varphi \, d\Gamma}_{=0} + \int_\Omega -\chi_1 n\nabla c \cdot \nabla\varphi + D_2\nabla n \cdot \nabla\varphi \, d\Omega,$$

which results in our weak formulation

$n \in \mathrm{L}^2([0,T]; \Sigma) :$

$$\int_\Omega \frac{\partial n}{\partial t}\varphi - \chi_1 n\nabla c \cdot \nabla\varphi + D_2\nabla n \cdot \nabla\varphi \, d\Omega = \int_\Omega \alpha_0 \rho c \varphi + \alpha_1 H(c - \hat{c})nc\varphi - \beta_2 n\rho\varphi \, d\Omega,$$

$\forall \varphi \in \Sigma.$

$$\tag{4.10}$$

Substituting our approximations by a linear combination of piecewise linear polynomials,

$$n(\mathbf{x}, t) \approx \sum_{l=1}^{N} n_l(t)\varphi_l(\mathbf{x}),$$

the weak formulation (4.10) becomes

$$\sum_{l=1}^{N} \frac{dn_l}{dt} \underbrace{\int_{\Omega} \varphi_l \varphi_m \, d\Omega}_{M_{ml}}$$

$$+ \sum_{l=1}^{N} n_l \underbrace{\int_{\Omega} -\chi_1 \varphi_l \nabla c \cdot \nabla \varphi_m + D_2 \nabla \varphi_l \cdot \nabla \varphi_m - \alpha_1 H(c - \hat{c})c\varphi_l\varphi_m + \beta_2 \varphi_l \varphi_m \rho \, d\Omega}_{S_{ml}}$$

$$= \underbrace{\int_{\Omega} \alpha_0 \rho c \varphi_m \, d\Omega}_{f_m}. \qquad (4.11)$$

From Eq. (4.11) we can determine the mass matrix, stiffness matrix and the source vector. As we can see in Eq. (4.6) these are determined by the element matrice and vector. The element mass matrix is equal to the relation given in (4.7). For the stiffness matrix and the source vector, the element contributions are

$$\mathbf{S}_{ml}^{e_j} = \int_{e_j} -\chi_1 \varphi_l \nabla c \cdot \nabla \varphi_m + D_2 \nabla \varphi_l \cdot \nabla \varphi_m - \alpha_1 H(c - \hat{c})c\varphi_l\varphi_m + \beta_2 \varphi_l \varphi_m \rho \, d\Omega$$

$$\overset{NC}{\approx} -\chi_1 \frac{|\Delta|}{6} \sum_{p=1}^{3} \varphi_l(x_p, y_p) \left(\frac{\partial c}{\partial x}(x_p, y_p)\beta_m + \frac{\partial c}{\partial y}(x_p, y_p)\gamma_m \right) + D_2 \frac{|\Delta|}{2}(\beta_m \beta_l + \gamma_m \gamma_l)$$

$$- \alpha_1 \frac{|\Delta|}{6} \sum_{p=1}^{3} H(c(x_p, y_p) - \hat{c})c(x_p, y_p)\varphi_l(x_p, y_p)\varphi_m(x_p, y_p)$$

$$+ \beta_2 \frac{|\Delta|}{6} \sum_{p=1}^{3} \rho(x_p, y_p)\varphi_l(x_p, y_p)\varphi_m(x_p, y_p), \qquad (4.12)$$

$$\mathbf{f}_m^{e_j} = \int_{e_j} \alpha_0 \rho c \varphi_m \, d\Omega$$

$$\overset{NC}{\approx} \alpha_0 \frac{|\Delta|}{6} \sum_{p=1}^{3} \rho(x_p, y_p)c(x_p, y_p)\varphi_m(x_p, y_p). \qquad (4.13)$$

where

$$\frac{\partial c}{\partial x} = \sum_{p} c(x_p, y_p, t)\frac{\partial \varphi_p}{\partial x} = \sum_{p} c(x_p, y_p, t)\beta_p, \qquad (4.14)$$

$$\frac{\partial c}{\partial y} = \sum_{p} c(x_p, y_p, t)\frac{\partial \varphi_p}{\partial y} = \sum_{p} c(x_p, y_p, t)\gamma_p. \qquad (4.15)$$

The approximation to Eq. (2.6) can now be determined by

$$\mathbf{M}\mathbf{n}^{k+1} = \mathbf{M}\mathbf{n}^k + \Delta t \left(\mathbf{S}\mathbf{n}^{k+1} + \mathbf{f}(\mathbf{c}^{k+1}, \rho^k) \right),$$

where we use the IMEX method, a combination of Backward Euler and Forward Euler time integration.

Vessel density

And as last we determine the approximation for Eq. (2.10). Multiplying the equation by a testfunction $\varphi \in \Sigma_0$ where

$$\Sigma_0 = \{\mathrm{H}^1(\Omega), \varphi(1) = 0\} = \{\varphi \in \mathrm{L}^2(\Omega) \,|\, \frac{\partial \varphi}{\partial x}, \frac{\partial \varphi}{\partial y} \in \mathrm{L}^2(\Omega), \varphi(1) = 0\}, \tag{4.16}$$

and integrating over its domain, we obtain

$$\rho \in \mathrm{L}^2([0, T]; \mathrm{H}^2(\Omega)) :$$
$$\int_\Omega \frac{\partial \rho}{\partial t} \varphi - \epsilon \nabla \cdot (\nabla \rho)\varphi + \gamma(\rho - \rho_{eq})\varphi \, d\Omega = \int_\Omega (\mu_1 \nabla n - \chi_2 n \nabla c) \cdot \frac{\mathbf{x}}{|\mathbf{x}|} \varphi \, d\Omega, \ \varphi \in \mathrm{L}^2(\Omega).$$

Using Integration by Parts and the boundary condition (2.12) we get

$$-\epsilon \int_\Omega \nabla \cdot (\nabla \rho)\varphi \, d\Omega = \underbrace{-\epsilon \int_{\partial\Omega} \frac{\partial \rho}{\partial \hat{n}} \varphi \, d\Gamma}_{=0} + \epsilon \int_\Omega \nabla \rho \cdot \nabla \varphi \, d\Omega,$$

since $\varphi \in \Sigma_0$, (4.2), due to the Dirichlet boundary condition. Using this we find our weak formulation

$$\rho \in \mathrm{L}^2([0, T]; \Sigma)$$
$$\int_\Omega \frac{\partial \rho}{\partial t} \varphi + \epsilon \nabla \rho \cdot \nabla \varphi + \gamma(\rho - \rho_{eq})\varphi \, d\Omega = \int_\Omega (\mu_1 \nabla n - \chi_2 n \nabla c) \cdot \frac{\mathbf{x}}{|\mathbf{x}|} \varphi \, d\Omega, \ \forall \varphi \in \Sigma. \tag{4.17}$$

Substituting the approximation using piecewise linear polynomials,

$$\rho(\mathbf{x}, t) \approx \sum_{l=1}^{N_{in}} \rho_l(t)\varphi_l(\mathbf{x}) + \sum_{l=N_{in}+1}^{N} \rho_{eq}\varphi_l(\mathbf{x}),$$

where we separated the internal elements and boundary elements due to our Dirichlet boundary condition (2.12), the weak formulation (4.17) becomes

$$\sum_{l=1}^{N_{in}} \frac{d\rho_l}{dt} \underbrace{\int_\Omega \varphi_l \varphi_m \, d\Omega}_{M_{ml}} + \sum_{l=1}^{N_{in}} \rho_l \underbrace{\int_\Omega \epsilon \nabla \varphi_l \cdot \nabla \varphi_m + \gamma \varphi_l \varphi_m \, d\Omega}_{\mathbf{S}_{ml}}$$
$$+ \sum_{l=N_{in}+1}^{N} \rho_{eq} \underbrace{\int_\Omega \epsilon \nabla \varphi_l \cdot \nabla \varphi_m + \gamma \varphi_l \varphi_m \, d\Omega}_{\mathbf{S}_{ml}}$$
$$= \underbrace{\int_\Omega (\mu_1 \nabla n - \chi_2 n \nabla c) \cdot \frac{\mathbf{x}}{|\mathbf{x}|} \varphi_m + \gamma \rho_{eq}\varphi_m \, d\Omega}_{\mathbf{f}_m}. \tag{4.18}$$

In the same way as before we determine our element matrices and vector using Newton Côtes numerical integration. Again the mass matrix is equal to the formulatioon given in Eq. (4.7).

$$\mathbf{S}_{ml}^{e_j} = \int_{e_j} \epsilon \nabla \varphi_l \cdot \nabla \varphi_m + \gamma \varphi_l \varphi_m \, d\Omega$$

$$\overset{NC}{\approx} \epsilon \frac{|\Delta|}{2} (\beta_m \beta_l + \gamma_m \gamma_l) + \gamma \frac{|\Delta|}{6} \sum_{p=1}^{3} \varphi_l(x_p, y_p) \varphi_m(x_p, y_p), \tag{4.19}$$

$$\mathbf{f}_m^{e_j} = \int_{\Omega} (\mu_1 \nabla n - \chi_2 n \nabla c) \cdot \frac{\mathbf{x}}{|\mathbf{x}|} \varphi_m \, d\Omega - \sum_{l=N_{in}+1}^{N} \rho_{eq} S_{ml}^{eq}$$

$$\overset{NC}{\approx} \mu_1 \frac{|\Delta|}{6} \sum_{p=1}^{3} \frac{\frac{\partial n}{\partial x}(x_p, y_p, t) \cdot x_p + \frac{\partial n}{\partial y}(x_p, y_p, t) \cdot y_p}{|\sqrt{x_p^2 + y_p^2}|} \varphi_m(x_p, y_p)$$

$$- \chi_2 \frac{|\Delta|}{6} \sum_{p=1}^{3} n(x_p, y_p, t) \frac{\frac{\partial c}{\partial x}(x_p, y_p, t) \cdot x_p + \frac{\partial c}{\partial y}(x_p, y_p, t) \cdot y_p}{|\sqrt{x_p^2 + y_p^2}|} \varphi_m(x_p, y_p)$$

$$+ \gamma \frac{|\Delta|}{6} \rho_{eq} \sum_{p=1}^{3} \varphi_m(x_p, y_p) - \sum_{l=N_{in}+1}^{N} \rho_{eq} S_{ml}^{eq}, \tag{4.20}$$

with the relations given in Eq. (4.14) and Eq. (4.15) and

$$\frac{\partial n}{\partial x} = \sum_{p=1}^{3} n(x_p, y_p, t) \frac{\partial \varphi_p}{\partial x} = \sum_{p=1}^{3} n(x_p, y_p, t) \beta_p, \tag{4.21}$$

$$\frac{\partial n}{\partial y} = \sum_{p=1}^{3} n(x_p, y_p, t) \frac{\partial \varphi_p}{\partial y} = \sum_{p=1}^{3} n(x_p, y_p, t) \gamma_p. \tag{4.22}$$

Using the obtained element matrix and element vector, the approximation for Eq. (2.10) using Backward Euler time integration, is given by

$$\mathbf{M}\rho^{k+1} = \mathbf{M}\rho^k + \Delta t \left(\mathbf{S}\rho^{k+1} + \mathbf{f}^k \right),$$

4.1.1   Numerical simulations

As mentioned in the beginning of the chapter, we partitioned the scaled domain as shown in Figure 2.1 into triangular elements. The accuracy of the finite element method increases with decreasing element size. This is partly due to the fact that we approximate a circle using a polygon built by linear triangular elements.

For the following simulations, which are after $t = 8$, we used the parameter values from Table D.2 and a triangular grid with 9408 elements. In this grid there are relatively more triangles around the boundary of the damaged part of the heart with respect to the outer part. A similar grid is shown in Figure 4.2 using only 576 elements, illustrating the spatial variations in the grid resolution.

As mentioned earlier, the stem cells injected in the damaged part of the heart secrete the attractant TG-β. This is still visible in Figure 4.3 where the attractant is relatively well spread with the highest concentration inside the wound.

The simulations are after $t = 8$ which is a relatively long period after the injection of the stem cells. The concentration TG-β in Figure 4.3 is already relative low. This also applies to the
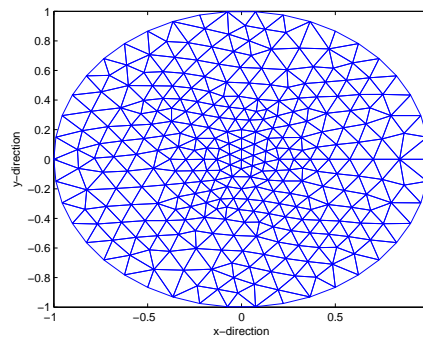
Figure 4.2: *A coarse triangular grid using* 576 *triangles.*
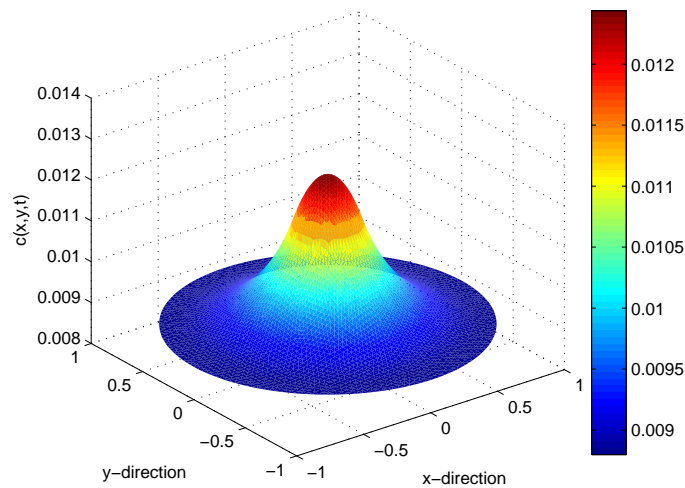
Figure 4.3: *Concentration TG-β after t = 8 with time step Δt = 0.1.*

capillary tip density shown in Figure 4.4 and the vessel density in Figure 4.5. The different concentration and densities are therefore going to their limits which is already visible in these figures.

Outside the wound the capillary tip density is almost back to zero, which is the initial and equilibrium value. This also applies to the outer part of the wound. Inside the wound a relatively large amount of TG-β is still present so tips are still branching and looping.

This can also be seen in Figure 4.5 where we see that the vessels are now present both outside and inside the wound. Together with the vessel density outside the wound, the vessel density inside the wound converges to the equilibrium value if enough stem cells were injected at the beginning.
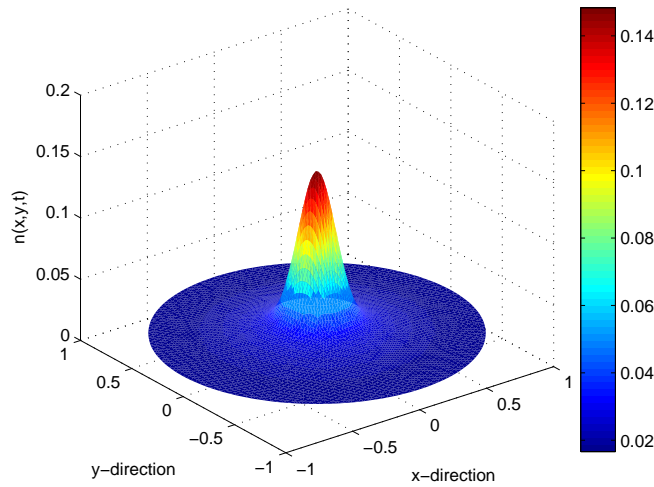
Figure 4.4: *Capillary tip density after $t = 8$ with time step $\Delta t = 0.1$.*

(a) View 1   (b) View 2
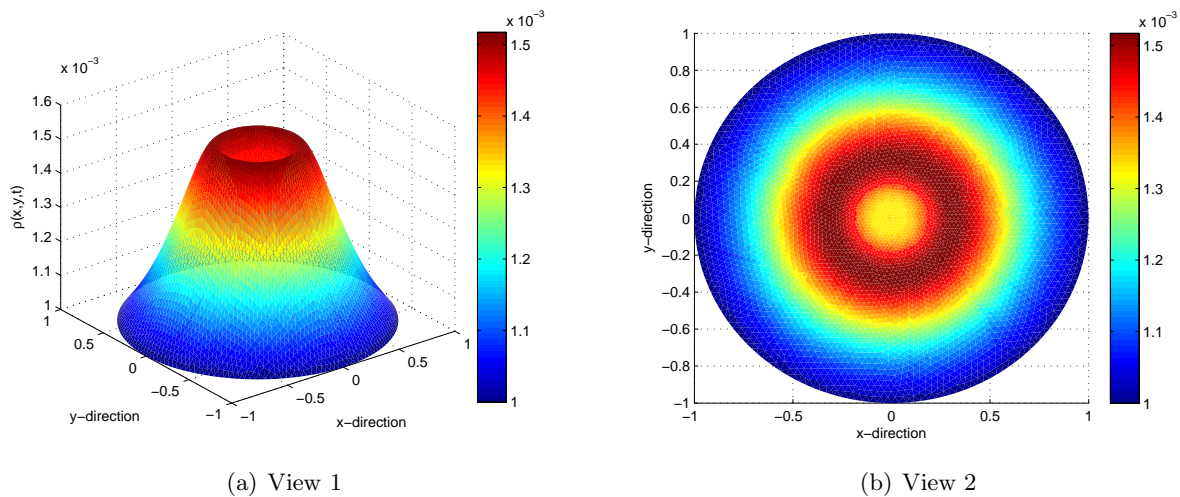
Figure 4.5: *Vessel density after $t = 8$ with time step $\Delta t = 0.1$.*

4.1.2   Convergence

In the previous section we have seen some simulations using a grid partitioned into 9408 elements. These simulations of course represent approximations to the exact solution and contain errors. First, a grid partitioned into triangles has a polygon shape and not a round shape as our domain has. With these triangles we already lose some data at the edge of our domain. And secondly, the finite element method with piecewise linear basis functions makes us lose accuracy by the size of the elements. These errors give us an accuracy of $\mathcal{O}(h^2)$ when using linear elements. The more triangles we use in our partition, the smaller the triangles are and the more accurate our approximation will be.

What we would like to know is if the approximation converges to the exact solution by reducing the size of the elements and thereby increasing the number of elements. On page 405 (Eq.

(10.4.4)) and on page 407 (Eq. (10.4.10) of Corollary 10.4.4) in [1] it is proved that the finite element method does converge:

$$\|u - u_h\|_{\mathrm{L}^2(\Omega)} \leq Ch^2 |u|_{2,\Omega},$$

with linear elements for a poisson problem, where $|u|_{2,\Omega}$ is a semi-norm.

Hence the more triangles that are used for the partitioning the more accurate the approximation is.

4.2   Motivation for a different numerical method

In the previous section we have seen some simulations for among others the capillary tip density. This has been done using the parameter values as described in Table D.2.

If it turns out that the chemotaxis term has more influence then is included in the parameter values from Table D.2, the hyperbolicity of the problem will increase, and the finite element method will no longer be attractive. This is illustrated in Figure 4.6. As an alternative we use the discontinuous Galerkin method.

(a) FEM 1D   (b) DG 1D
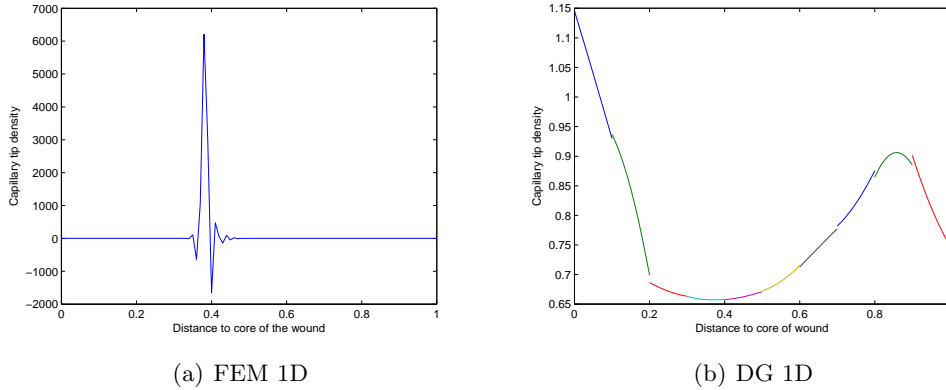
Figure 4.6: *Simulations for the capillary tip density using the parameter values from Table D.2 with the changes and additions from Table D.3.*

Despite that this method will be introduced in the next chapter we already show some simulations in Figure 4.6 in order to compare both methods both for the one dimensional problem. We used the same values for the various model parameters in both simulations, where the convection term has been made larger by assigning a higher value for the chemotaxis constant χ_1. From this figure we see that the finite element method is not suitable anymore while the discontinuous Galerkin method is.

4.3 Discontinuous Galerkin method for the one dimensional problem

The discontinuous Galerkin method has many similarities with the finite element method as dividing the domain into elements and introducing the testfunction and basis functions. The main difference and also advantage of the discontinuous Galerkin method is that the method determines a local solution for each element which results in a discontinuous global solution while the finite element method determines a continuous global solution where no jumps can occur.

Before we will apply the discontinuous Galerkin method [7] to our model as defined in Chapter 2 but then in the one dimensional case, we apply the method to the advection equation in order to practice the method.

For the discontinuous Galerkin method for one dimensional problems, we need to divide our domain into N elements. Each element is denoted as $e_j = [x_{j-1/2}, x_{j+1/2}]$ with $1 \leq j \leq N$ and element size Δ_j. The maximum element size is given by $\Delta x = \max_{1 \leq j \leq N} \Delta_j$.

In order to derive the weak formulation we need to use test functions φ from the finite dimensional space

$$\Phi = \left\{ \varphi \in \mathrm{L}^1(0,1) : \varphi|_{e_j} \in P^K(e_j), \ 1 \leq j \leq N \right\}, \tag{4.23}$$

where Φ is the space of all piecewise polynomials of degree (at most) K on element e_j.

As our basisfunctions we choose the Legendre polynomials since their L^2-orthogonality comes in a convenient manner for the treatment of our mass matrix. The nth Legendre polynomial is of order n and is given by

$$P_n(x) = \frac{1}{2^n n!} \frac{d^n}{dx^n} \left[\left(x^2 - 1 \right)^n \right]. \tag{4.24}$$

The first five Legendre polynomials are plotted in Figure 4.7.
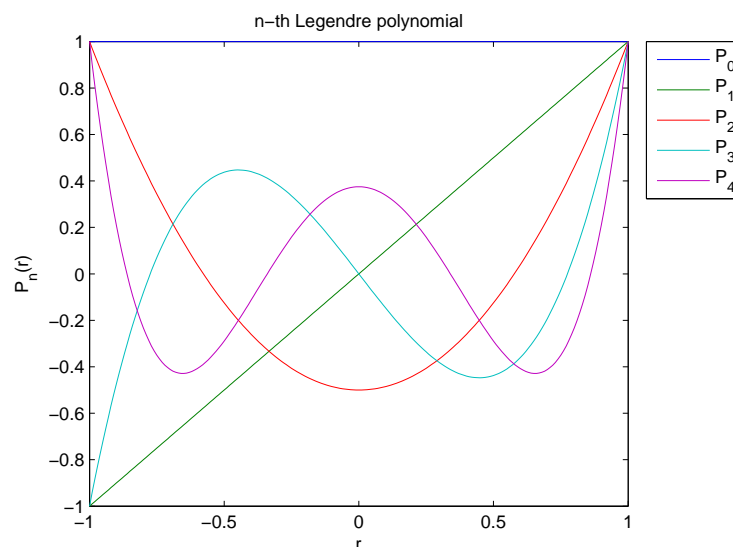
Figure 4.7: *The first five Legendre polynomials.*

In order to use these Legendre polynomials, we redefine our weak formulation to a weak formulation on the scaled interval $[-1, 1]$ instead on our element interval $e_j = [x_{j-1/2}, x_{j+1/2}]$, this is often done by substituting $r = \frac{2(x-x_j)}{\Delta x}$.

With the discontinuous Galerkin method we get two (possibly) different solutions on the boundaries of all elements. One solution by the element left from the inter-element boundary and one solution by the element right from the inter-element boundary. Therefore we need to define a link between these two results. This can be done in different ways, for example we can use the central or the upwind flux.

4.3.1   Advection equation

We introduced the space of our test functions and the basis functions we use for each element e_j. Now we can approximate the solution to the advection equation. The advection equation with periodic boundary conditions is given by

$$\frac{\partial u}{\partial t} + \frac{\partial u}{\partial x} = 0, \ \forall x \in [0, 1], \forall t \in [0, T], \tag{4.25}$$

$$u(x, 0) = g(x), \ \forall x \in [0, 1], \tag{4.26}$$

$$u(0, t) = u(1, t) = 0, \ \forall t \in [0, T]. \tag{4.27}$$

The solution in element e_j is approximated by

$$u_h(x, t) = \sum_{l=0}^{K} u_j^l(t) \varphi_j^l(x), \tag{4.28}$$

where $\varphi^l(x) = P_l\left(\frac{2(x-x_j)}{\Delta x}\right)$ is the Legendre polynomial of lth order and $u_j^l(t)$ is the corresponding time-dependent coefficient.

Initial coefficients

First we need to determine the initial coefficients such that initial condition (4.26) applies. Therefore we multiply the initial condition by the test function $\varphi_j^m(x) \in \Phi$ and integrate it over the element e_j. By inserting Eq. (4.28), we obtain

$$\int_{e_j} u_h(x, 0) P_m\left(\frac{2(x-x_j)}{\Delta x}\right) \, dx = \int_{e_j} \sum_{l=0}^{K} u_j^l(0) P_l\left(\frac{2(x-x_j)}{\Delta x}\right) P_m\left(\frac{2(x-x_j)}{\Delta x}\right) \, dx,$$

$$m \in \{0, \ldots, K\},$$

where we subsitute Eq. (4.28) and $r = \frac{2(x-x_j)}{\Delta x}$ to obtain

$$\frac{\Delta x}{2} \int_{-1}^{1} u_h\left(\frac{\Delta x}{2}r + x_j, 0\right) P_m(r) \, dr = \frac{\Delta x}{2} \sum_{l=0}^{K} u_j^l(0) \int_{-1}^{1} P_l(r) P_m(r) \, dr$$

$$= \frac{\Delta x}{2} \frac{2}{2m+1} u_j^m(0), \ m \in \{0, \ldots, K\}.$$

Therefore the initial coefficients are given by

$$u_j^m(0) = \frac{2m+1}{2} \int_{-1}^{1} u_0\left(\frac{\Delta x}{2}r + x_j\right) P_m(r) \, dr, \ m \in \{0, \ldots, K\}. \tag{4.29}$$

The initial coefficients given by Eq. (4.31) can be determined numerically using the Gauss-Legendre quadrature which read as

$$\int_{-1}^{1} f(x) \ dx \approx \sum_{i=1}^{p} w_i f(\hat{x}_i). \tag{4.30}$$

Here p denotes the number of points (and therefore also the number of weights) in which we need to evaluate the integrand. A $p-$point Gauss-Legendre quadrature is used to find the exact result to a polynomial of order $2p - 1$ or less by a suitable choice of points and their weights. We choose to approximate the integral using six points as this will be enough when we use polynomials up to order three. The points and weights we use are listed in Table 4.1.

Points	Weights
$\pm$ 0.23861918	0.46791393
$\pm$ 0.66120939	0.36076157
$\pm$ 0.93246951	0.17132449

Table 4.1: *Six points and their weights for the Gauss-Legendre quadrature*[1]

By substituting the points and their weights from Table 4.1 into Equation (4.29), we obtain

$$u_j^m(0) = \frac{2m + 1}{2} \int_{-1}^{1} u_0 \left(\frac{\Delta x}{2} r + x_j, 0 \right) P_m(r) \ dr$$

$$\approx \frac{2m + 1}{2} \sum_{i=1}^{6} u_0 \left(\frac{\Delta x}{2} r_i + x_j \right) P_m(r_i) w_i. \tag{4.31}$$

[1]`http://pathfinder.scar.utoronto.ca/~dyer/csca57/book_P/node44.html`

Weak formulation

Once the initial coefficients are known, we determine the weak formulation for Eq. (4.25). This is done by multiplying it by the testfunction $\varphi_j \in \Phi$ and integrating it over element e_j. We obtain

$$\int_{e_j} \frac{\partial u}{\partial t}\varphi_j + \frac{\partial u}{\partial x}\varphi_j \; dx = 0,$$

which becomes after Integration by Parts

$$\int_{e_j} \frac{\partial u}{\partial t}\varphi_j - u\frac{d\varphi_j}{dx} \; dx + u\varphi_j|_{x_{j-1/2}}^{x_{j+1/2}} = 0.$$

Subsequently, we substitute Eq. (4.28) into the above equation, and we set $\varphi_j = \varphi_j^m$ to obtain

$$\sum_{l=0}^{K} \frac{du_j^l}{dt} \underbrace{\int_{e_j} \varphi_j^l \varphi_j^m \; dx}_{\mathbf{M}_{ml}} - \sum_{l=0}^{K} u_j^l \underbrace{\int_{e_j} \varphi_j^l \frac{d\varphi_j^m}{dx} \; dx}_{\mathbf{S}_{ml}} + u^\star \varphi_j|_{x_{j-1/2}}^{x_{j+1/2}} = 0. \tag{4.32}$$

In order to determine the fluxes we can choose from different schemes. We consider two choices:

- Upwind flux: $u^\star(x_{j+1/2}) = u(x_{j+1/2}^-)$,

- Central flux: $u^\star(x_{j+1/2}) = \frac{1}{2}\left(u(x_{j+1/2}^-) + u(x_{j+1/2}^+)\right)$.

Mass matrix, element matrix and flux

Before we determine the mass matrix $\mathbf{M}_{ml}$, the element matrix $\mathbf{S}_{ml}$ and the values on the boundaries we choose the number of Legendre polynomials we use. In this section we determine the matrices using two Legendre polynomials, so $K = 1$.

From the weak formulation (4.32), we know that the mass matrix $\mathbf{M}_{ml}$ equals

$$\mathbf{M}_{ml} = \int_{e_j} \varphi_j^l(x)\varphi_j^m(x) \; dx = \frac{\Delta x}{2} \int_{-1}^{1} P_l(r)P_m(r) \; dr$$

$$= \frac{\Delta x}{2}\frac{2}{2m+1}\delta_{ml},$$

where δ_{ml} is the Kronecker delta. Hence

$$\mathbf{M} = \Delta x \begin{pmatrix} 1 & 0 \\ 0 & \frac{1}{3} \end{pmatrix}. \tag{4.33}$$

The element matrix is given by

$$\mathbf{S}_{ml} = \int_{e_j} \varphi_j^l(x)\frac{d\varphi_j^m}{dx}(x) \; dx = \int_{-1}^{1} P_l(r)\frac{dP_m}{dr}(r) \; dr.$$

Hence

$$\mathbf{S} = \Delta x \begin{pmatrix} 0 & 0 \\ 2 & 0 \end{pmatrix}. \tag{4.34}$$

For the flux term we use an upwind scheme and we insert Eq. (4.28) into relation (4.32). Furthermore, we know that $\varphi_j^m(x_{j+1/2}) = P_m(1) = 1$ and $\varphi_j^m(x_{j-1/2}) = P_m(-1) = (-1)^m$, $m \in \{0, 1\}$. Therefore the boundary values are determined by

$$u_h(x_{j+1/2}, t)\varphi_j^m(x_{j+1/2}) - u_h(x_{j-1/2}, t)\varphi_j^m(x_{j-1/2})$$
$$= \sum_{l=0}^{1} u_j^l(t)\varphi_j^l(x_{j+1/2}) - (-1)^m \sum_{l=0}^{1} u_{j-1}^l(t)\varphi_j^l(x_{j-1/2}), \quad m \in \{0, 1\}.$$

For the flux of the current cell and the flux of the previous cell we have two matrices, A and B, such that we have

$$\mathbf{A}\mathbf{u}_j + \mathbf{B}\mathbf{u}_{j-1},$$

with

$$\mathbf{A} = \begin{pmatrix} 1 & 1 \\ 1 & 1 \end{pmatrix}, \ \mathbf{B} = -\begin{pmatrix} 1 & 1 \\ -1 & -1 \end{pmatrix} = \begin{pmatrix} -1 & -1 \\ 1 & 1 \end{pmatrix}, \ \text{and} \ \mathbf{u}_j = \begin{pmatrix} u_j^0 \\ u_j^1 \end{pmatrix}. \tag{4.35}$$

With Eq. (4.33)-(4.35) we rewrite the weak formulation (4.32) into the following equation

$$\mathbf{M}\frac{d\mathbf{u}_j}{dt} - \mathbf{S}\mathbf{u}_j + \mathbf{A}\mathbf{u}_j + \mathbf{B}\mathbf{u}_{j-1} = 0.$$

Since we apply discontinuous Galerkin on the advection equation only as a practice, and therefore we do not focus on the accuracy, we use the most simple and cheapest method, Forward Euler. Using the Forward Euler time integration we need to solve

$$\mathbf{M}\mathbf{u}_j^{k+1} = (\mathbf{M} + \Delta t\mathbf{S} - \Delta t\mathbf{A})\mathbf{u}_j^k - \Delta t\mathbf{B}\mathbf{u}_{j-1}^k, \tag{4.36}$$

where k denotes the time index at time t^k.

In order to determine the coefficients for the first element, e_1, we created a ghost cell on the left which is an exact copy of the most right element, element e_N. This can be done since we have periodic boundary conditions.

Numerical simulations

We have the following exact solution to the initial boundary value problem defined in Eq. (4.25)-(4.27) with $g(x) = \sin(2\pi x)$:

$$u(x, t) = \sin(2\pi(x - t)). \tag{4.37}$$

For comparison the exact solution is also shown in the figures where we show our approximations using the discontiuous Galerkin method. This is done by determining the exact solution for 10001 points with $\Delta x = 0.0001$ between the points.

In Figures 4.8 and 4.9 we respectively show the approximation using five and ten elements.

Concentrating on Figure 4.8 it is clear that if we use three Legendre polynomials per element instead of two, the approximation gets more accurate. This can be explained since the third Legendre polynomial, the polynomial of order 2, is the first polynomial that is curved. So the third polynomial gives a significant contribution to the approximation of the curved exact solution given in Eq. (4.37).

(a) Two Legendre polynomials   (b) Three Legendre polynomials
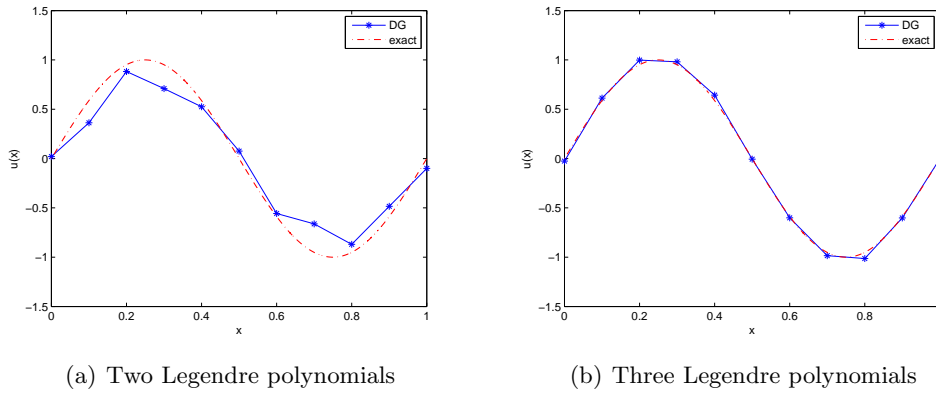
Figure 4.8: *Results (two points per element) for the advection equation after $t = 2$ with five elements ($\Delta x = 0.2$) and $\Delta t = 0.001$.*

(a) Two Legendre polynomials   (b) Three Legendre polynomials
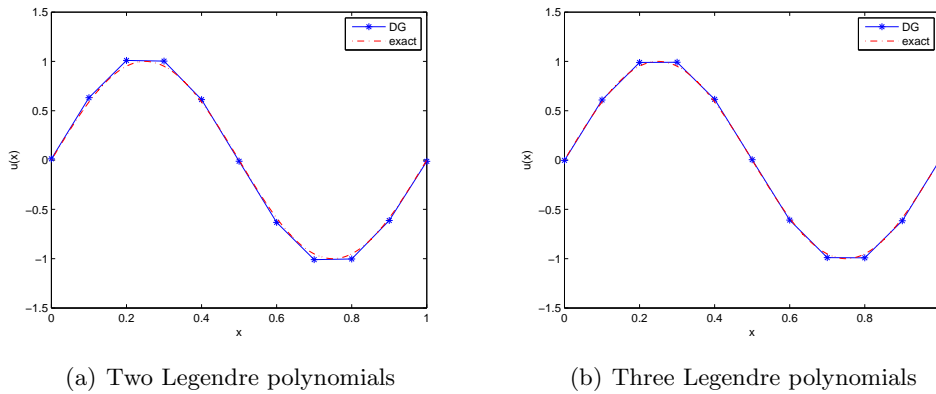
Figure 4.9: *Results (one point per element) for the advection equation after $t = 2$ with ten elements ($\Delta x = 0.1$) and $\Delta t = 0.001$.*

If we consider more elements, with smaller size, the exact solution will more and more look like a straight line on each element. Therefore, if we have a small enough element size, it is sufficient to just use two Legendre polynomials to get a good approximation. Figure 4.9 demonstrates this convergence since the solutions using two and three Legendre polynomials are very muck alike.

We also consider the approximation for a discontinuous initial condition. So we have our initial boundary value problem defined in Eq. (4.25)-(4.27) with

$$g(x) = \begin{cases} 5 & x \leq 0.5, \\ 0 & \text{elsewhere.} \end{cases} \tag{4.38}$$

The exact solution is given by

$$u(x,t) = 5H\left((0.5 + t) - x\right). \tag{4.39}$$

In Figure 4.10 the approximations are shown for different choices of number of elements and the time step Δt. For these approximations we have always used only one Legendre polynomial, so we have basisfunctions of order zero. In Figure 4.10(a) we see that the solution with one
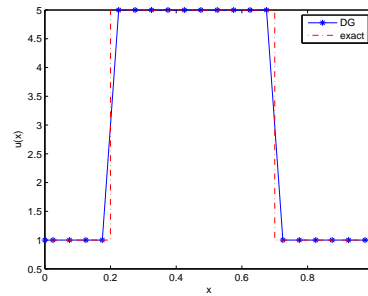
(a) With $\Delta x = 0.1$, $\Delta t = 0.1$ after $t = 0.25$
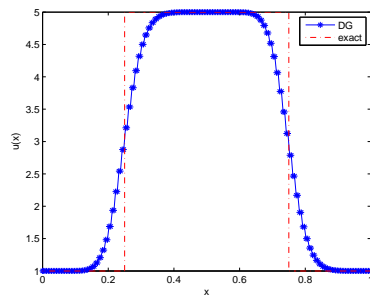
(b) With $\Delta x = 0.01$, $\Delta t = 0.001$ after $t = 0.25$
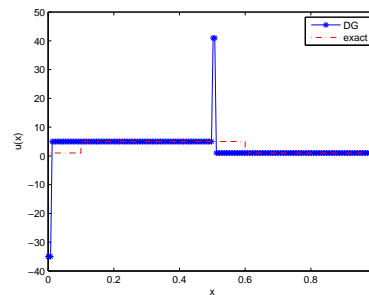
(c) With $\Delta x = 0.01$, $\Delta t = 0.1$ after $t = 0.1$

Figure 4.10: *Results (two points per element) using one Legendre polynomial for the advection equation with discontinuous initial condition.*

Legendre polynomial is a good approximation to our exact solution. Here we have used a time step that is equal to the size of our elements. This means that the new solution of a cell e_j is exactly the old solution of the neighbouring cell e_{j-1}.

In Figure 4.10(b) we use a time step that is smaller than the size of our elements such that it satisfies the CFL condition. This means that after one time step, only a part of the solution of element e_{j-1} is shifted into element e_j. Therefore the new solution of element e_j will be a weighted average of the old solution of e_{j-1} and e_j. This also happens at the location of the discontinuity. Hence with $\Delta t < \Delta x$ numerical diffusion will occur.

The last situation is that the time step is larger than the size of our elements. In our case, where we have our speed equal to one, this means that the CFL condition is not satisfied. After one time step, the solution of element e_{j-1} is then multiple shifted to element e_j and wiggles will occur. This is shown in Figure 4.10(c).

We can also approximate the solution with higher order Legendre polynomials. This is done in Figure 4.11. Using a higher order approximation, in order to get stability, $\Delta t / \Delta x$ should be smaller than a certain value that depends on the order of the approximation and the order of the time integration method that is used. We used the Forward Euler time integration method (order one) and Legendre polynomials of order four. This means that $\Delta t / \Delta x$ should be smaller than zero, hence the approximation will never be stable.

In Figure 4.11(a) we have $\Delta t / \Delta x = 0.01$ and some wiggles occur in the approximation. We can use a limiter to improve the approximation. In Figure 4.11(b) we have $\Delta t / \Delta x = 0.1$ which gives
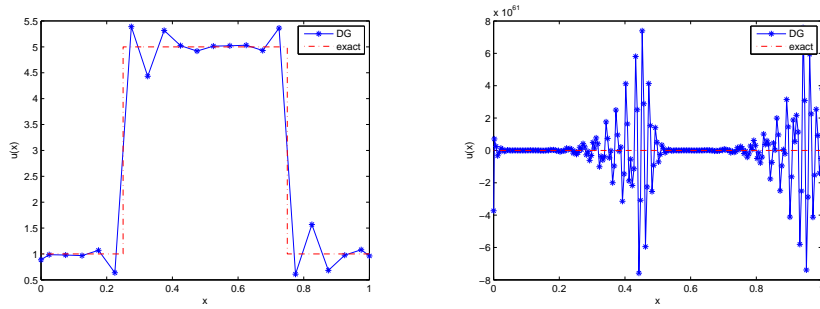
(a) With $\Delta x = 0.1$, $\Delta t = 0.001$ after $t = 0.25$

(b) With $\Delta x = 0.01$, $\Delta t = 0.001$ after $t = 0.25$

Figure 4.11: *Results (two points per element) using five Legendre polynomials for the advection equation with discontinuous initial condition.*

larger wiggles such that the approximation is clearly unstable. So we should choose the Δx and Δt carefully.

Limiting

When using Legendre polynomials of higher order, limiting can be needed. In this chapter we apply limiting to the advection equation with discontinuous initial condition.

Minmod limiter

The minmod limiter is a limiter that is applied to the whole domain and it can be used for a polynomial basis P_0 or P_0, P_1, a basis of order 0 or 1. When we use a polynomial basis of a higher order we can still use the minmod limiter, but only where limiting is needed. In those elements the approximation will be reduced to order 1, while in the other elements the approximation is still of the higher order. To determine in which elements limiting is needed we should use some kind of detection. For now, we focus on a polynomial basis of order 1 so we can use the minmod limiter on the whole domain.

For the minmod limiter we need the minmod function which is given by

$$m(a, b, c) = \begin{cases} \text{sgn}(a) \cdot \min\{|a|, |b|, |c|\} & \text{if } \text{sgn}(a) = \text{sgn}(b) = \text{sgn}(c), \\ 0 & \text{elsewhere.} \end{cases} \qquad (4.40)$$

For example, the minmod function is used in the monotonized central-difference limiter (van Leer [8]). We will use this limiter to improve the approximation to the advection equation. With this limiter the approximation $u_h(x, t^k)$ of the solution to element e_j, $j = 1 \ldots N$, at t^k is given by

$$u_h(x, t^k) = \bar{u}_j^k + \sigma_j^k (x - x_j), \qquad (4.41)$$

where $\bar{u}_j^k$ denotes the averaged approximation over element e_j. For $\bar{u}_j^k$ we obtain

$$\bar{u}_j^k = \frac{1}{\Delta x} \int_{x_{j-\frac{1}{2}}}^{x_{j+\frac{1}{2}}} u_h(x, t^k) \, dx,$$

$$= \frac{1}{\Delta x} \int_{x_{j-\frac{1}{2}}}^{x_{j+\frac{1}{2}}} \sum_{l=0}^{K} u_j^{(l)}(t^n) P_l \frac{2}{\Delta x}(x - x_j) \, dx$$

$$= \frac{1}{\Delta x} \sum_{l=0}^{K} u_j^{(l)}(t^k) \cdot \frac{\Delta x}{2} \int_{-1}^{1} P_l(\xi) \, d\xi$$

$$= u_j^{(0)}(t^k), \qquad (4.42)$$

since

$$\int_{-1}^{1} P_l(\xi) \, d\xi = \int_{-1}^{1} P_l(\xi) P_0(\xi) \, d\xi = \left\{ \begin{array}{ll} 2 & l = 0, \\ 0 & l \neq 0. \end{array} \right.$$

The slope σ_j^k for the Van Leer limiter is determined by

$$\sigma_j^k = m \left(\frac{\bar{u}_{j+1}^k - \bar{u}_{j-1}^k}{2\Delta x}, 2\frac{\bar{u}_j^k - \bar{u}_{j-1}^k}{\Delta x}, 2\frac{\bar{u}_{j+1}^k - \bar{u}_j^k}{\Delta x} \right). \qquad (4.43)$$

For the advection equation (4.25) with discontinuous initial condition (4.26) defined in (4.38) we use a polynomial basis of order 1. Hence our solution after limiting is given by

$$u_h(x, t^k) = \sum_{l=0}^{1} u_j^{(l)}(t^k) P_l(\xi)$$

$$= u_j^{(0)} + u_j^{(1)} \frac{2}{\Delta x}(x - x_j)$$

$$= u_j^{(0)} + \sigma_j^k(x - x_j). \qquad (4.44)$$

Therefore, when we use limiting, the renewed value equals

$$u_j^{(1)}(t^k) = \sigma_j^k \frac{\Delta x}{2}.$$

The algorithm that we applied for limiting the advection equation is as following:

Algorithm 1 Determine limited u^{k+1} with u^k

---

u^0 initial coefficients
$\bar{u}_{-1}^{(l)}(t^0) = \bar{u}_N^{(l)}(t^0)$;
$\bar{u}_{N+1}^{(l)}(t^0) = \bar{u}_0^{(l)}(t^0)$;
for $k = 1..Nt - 1$ **do**
  for $j = 1..N$ **do**
    $in1 = (\bar{u}_{j+1}^{(l)}(t^k) - \bar{u}_{j-1}^{(l)}(t^k))/(2\Delta x)$;
    $in2 = 2 * (\bar{u}_j^{(l)}(t^k) - \bar{u}_{j-1}^{(l)}(t^k))/\Delta x$;
    $in3 = 2 * (\bar{u}_{j+1}^{(l)}(t^k) - \bar{u}_j^{(l)}(t^k))/\Delta x$;
    $\sigma = minmod(|in1|, |in2|, |in3|)$;
    $\bar{u}_j^{(1)}(t^k) = \sigma * \Delta x/2$;   %Limited coefficient
  end for
  $\bar{u}_{-1}^{(l)}(t^k) = \bar{u}_N^{(l)}(t^k)$;
  $\bar{u}_{N+1}^{(l)}(t^k) = \bar{u}_0^{(l)}(t^k)$;
  Determine $\bar{u}^{(l)}(t^{k+1})$ with Euler Forward
  $\bar{u}_{-1}^{(l)}(t^{k+1}) = \bar{u}_N^{(l)}(t^{k+1})$;
  $\bar{u}_{N+1}^{(l)}(t^{k+1}) = \bar{u}_0^{(l)}(t^{k+1})$;
  Determine solution $u_h(x, t^k)$ with limited coefficients
end for

Numerical simulations

In Figure 4.12 the results are shown for the advection equation with discontinuous initial condition using only ten elements and a polynomial basis of order 1. The same is shown in Figure 4.13 with 100 elements. Both with a different time step in order to satisfy the CFL condition. In both figures the results without limiting are bad. Wiggles start to occur, especially when we have 100 elements. When using the limiter described before, the wiggles seem to be gone and the approximations are more accurate. Especially when we use 100 elements.

(a) Without limiting

(b) With limiting
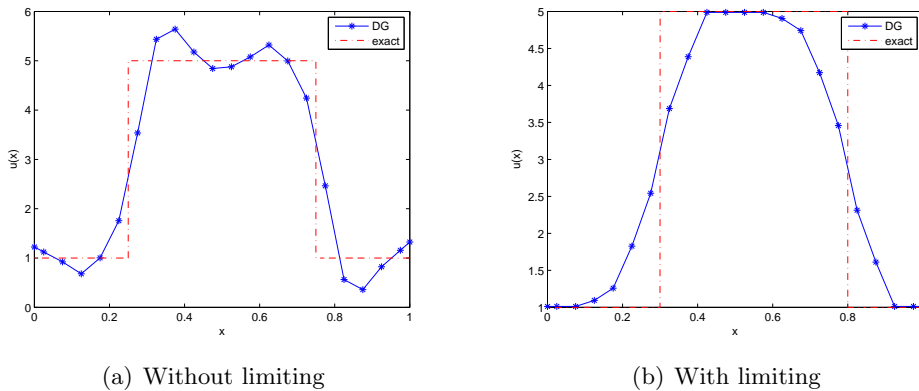
Figure 4.12: *Results (two points per element) using two Legendre polynomials (up to order $K = 1$) for the advection equation with discontinuous initial condition, using $\Delta x = 0.1$, $\Delta t = 0.01$ and $t = 0.25$.*

(a) Without limiting   (b) With limiting
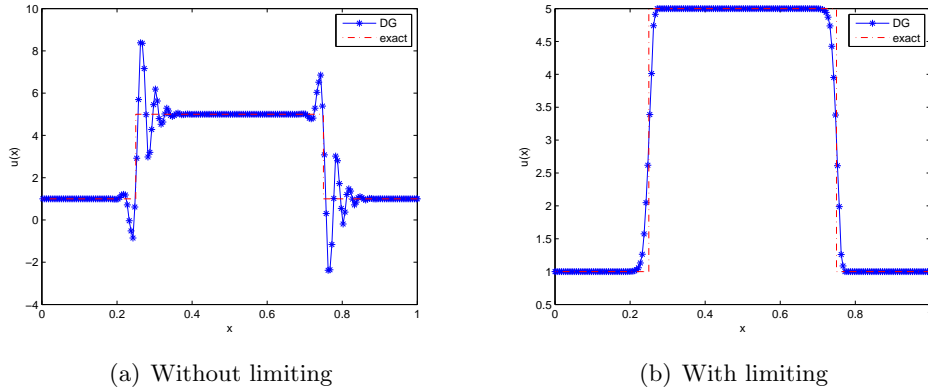
Figure 4.13: *Results (two points per element) using two Legendre polynomials (up to order $K = 1$) for the advection equation with discontinuous initial condition, using $\Delta x = 0.01$, $\Delta t = 0.001$ and $t = 0.25$.*

4.3.2   Tip-vessel model

In this section we use the discontinuous Galerking method to the full model as described in Chapter 2 but then for the one dimensional case. In order to deal with the diffusion terms in all equations we split each equation into a system of two equations, [7, 3].

Concentration TG$-\beta$

First we work with the one dimensional form of Eq. (2.3) which describes the concentration TG$-\beta$. Splitting this equation we obtain

$$\frac{\partial c}{\partial t} = D_1 \frac{\partial q}{\partial x} - \lambda c + \alpha m,$$
$$q = \frac{\partial c}{\partial x},$$

where the one dimensional initial and Neumann boundary conditions are given by

$$c(x,0) = 0, \ \frac{\partial c}{\partial x}(0,t) = \frac{\partial c}{\partial x}(1,t) = 0.$$

The solution will be approximated as in Eq. (4.28) where c_j^m are coefficients.

With this initial condition we know by Eq. (4.31) that

$$c_j^m(0) = 0, \ \forall m,$$

which means that initially all the coefficients are zero.

In order to determine the weak formulation we multiply the system of two equations by the testfunction $\varphi_j \in \Phi$, see Eq. (), and integrate it over element e_j. After applying Integration by Parts we obtain

$$\int_{e_j} \frac{\partial c}{\partial t} \varphi_j \ dx = -D_1 \int_{e_j} q \frac{d\varphi_j}{dx} \ dx - \int_{e_j} \lambda c \varphi_j \ dx + \int_{e_j} \alpha m \varphi_j \ dx + D_1 q \varphi_j \big|_{e_j}, \tag{4.45}$$

$$\int_{e_j} q \varphi_j \ dx = - \int_{e_j} c \frac{d\varphi_j}{dx} \ dx + c \varphi_j \big|_{e_j}. \tag{4.46}$$

Subsequently, we substitute (4.28) and we set $\varphi_j = \varphi_j^m$ to obtain

$$\sum_{l=0}^{K} \frac{\partial c_j^l}{\partial t} \int_{e_j} \varphi_j^l \varphi_j^m \, dx = -\sum_{l=0}^{K} q_j^l \int_{e_j} D_1 \varphi_j^l \frac{d\varphi_j^m}{dx} \, dx - \sum_{l=0}^{K} c_j^l \int_{e_j} \lambda \varphi_j^l \varphi_j^m \, dx$$

$$+ \int_{e_j} \alpha m \varphi_j^m \, dx + D_1 q^\star \varphi_j^m \big|_{e_j} \tag{4.47}$$

$$\sum_{l=0}^{K} q_j^l \int_{e_j} \varphi_j^l \varphi_j^m \, dx = -\sum_{l=0}^{K} c_j^l \int_{e_j} \varphi_j^l \frac{d\varphi_j^m}{dx} \, dx + c^\star \varphi_j^m \big|_{e_j} , \tag{4.48}$$

where we use the central flux such that

$$q^\star = \left\{ \left\{ \sum_{l=0}^{K} q_j^l \varphi_j^l \right\} \right\} = \frac{1}{2} \left(\sum_{l=0}^{K} q_j^l \varphi_j^l + \sum_{l=0}^{K} q_{j+1}^l \varphi_{j+1}^l \right) - \frac{1}{2} \left(\sum_{l=0}^{K} q_{j-1}^l \varphi_{j-1}^l + \sum_{l=0}^{K} q_j^l \varphi_j^l \right), \tag{4.49}$$

$$c^\star = \left\{ \left\{ \sum_{l=0}^{K} c_j^l \varphi_j^l \right\} \right\} .$$

For our basis functions and our testfunction we choose to use the Legenre polynomials as defined in Eq. 4.24. We substitute $r = \frac{2(x-x_j)}{\Delta x}$ and $\varphi_j^l(x_j + \frac{\Delta x}{2} r) = P_l(r)$ and we use four Legendre polynomials, so polynomials up to order 3, to obtain:

$$\mathbf{M}_{ml} = \frac{\Delta x}{2} \int_{-1}^{1} P_l P_m dr = \frac{\Delta x}{2m+1} \delta_{ml}, \Rightarrow \mathbf{M} = \Delta x \begin{pmatrix} 1 & 0 & 0 & 0 \\ 0 & \frac{1}{3} & 0 & 0 \\ 0 & 0 & \frac{1}{5} & 0 \\ 0 & 0 & 0 & \frac{1}{7} \end{pmatrix} \tag{4.50}$$

where δ_{ml} is the Kronecker delta, and

$$\mathbf{S}_{ml} = \int_{-1}^{1} -P_l \frac{dP_m}{dr} dr, \Rightarrow \mathbf{S} = \begin{pmatrix} 0 & 0 & 0 & 0 \\ 2 & 0 & 0 & 0 \\ 0 & 2 & 0 & 0 \\ 2 & 0 & 2 & 0 \end{pmatrix}, \tag{4.51}$$

$$\mathbf{f}_{j,m} = \frac{\Delta x}{2} \alpha \int_{-1}^{1} m(x_j + \frac{\Delta x}{2} r, t) P_m dr = \frac{\Delta x}{2} \alpha m(x_j, t) \int_{-1}^{1} P_m dr,$$

$$\Rightarrow \mathbf{f}_j = \frac{\Delta x}{2} \alpha m(x_j, t) \begin{pmatrix} 2 \\ 0 \\ 0 \\ 0 \end{pmatrix}, \tag{4.52}$$

where we use the fact that $m(x,t)$ has a constant value inside an element and j denotes the element number.

Finally, in order to determine the approximation using discontinuous Galerkin, we need to write out the central flux term. So for example

$$\left\{ \left\{ \sum_{l=0}^{K} c_j^l \varphi_j^l \right\} \right\} \varphi_j^m \bigg|_{e_j} = \frac{1}{2} \sum_{l=0}^{K} \left(c_j^l \varphi_j^l(x_{j+1/2}) + c_{j+1}^l \varphi_{j+1}^l(x_{j+1/2}) \right) \varphi_j^m(x_{j+1/2})$$

$$- \frac{1}{2} \sum_{l=0}^{K} \left(c_j^l \varphi_j^l(x_{j-1/2}) + c_{j-1}^l \varphi_{j-1}^l(x_{j-1/2}) \right) \varphi_j^m(x_{j-1/2}). \tag{4.53}$$

Eq. (4.53) can be written as

$$\left\{\left\{\sum_{l=0}^{K} c_j^l \varphi_j^l\right\}\right\} \varphi_j^m \Bigg|_{e_j} = \mathbf{A}\mathbf{c_j} - \mathbf{B}\mathbf{c}_{j-1} + \mathbf{C}\mathbf{c}_{j+1}, \tag{4.54}$$

where, after substituting $r = \frac{2(x-x_j)}{\Delta x}$,

$$\mathbf{A} = \frac{1}{2}\underbrace{\begin{pmatrix} 1 & 1 & 1 & 1 \\ 1 & 1 & 1 & 1 \\ 1 & 1 & 1 & 1 \\ 1 & 1 & 1 & 1 \end{pmatrix}}_{\mathbf{A_1}} - \frac{1}{2}\underbrace{\begin{pmatrix} 1 & -1 & 1 & -1 \\ -1 & 1 & -1 & 1 \\ 1 & -1 & 1 & -1 \\ -1 & 1 & -1 & 1 \end{pmatrix}}_{\mathbf{A_2}}, \tag{4.55}$$

$$\mathbf{B} = \frac{1}{2}\begin{pmatrix} 1 & 1 & 1 & 1 \\ -1 & -1 & -1 & -1 \\ 1 & 1 & 1 & 1 \\ -1 & -1 & -1 & -1 \end{pmatrix}, \quad \mathbf{C} = \frac{1}{2}\begin{pmatrix} 1 & -1 & 1 & -1 \\ 1 & -1 & 1 & -1 \\ 1 & -1 & 1 & -1 \\ 1 & -1 & 1 & -1 \end{pmatrix}. \tag{4.56}$$

With Eq. (4.50)-(4.52) and Eq. (4.55)-(4.56), the approximation for the coeffcients for Eq. (4.47) and Eq. (4.48) using discontinuous Galerkin can now be written as

$$\mathbf{M}\frac{\partial \mathbf{c}_j}{\partial t} = D_1(\mathbf{A} - \mathbf{S})\mathbf{q}_j - D_1\mathbf{B}\mathbf{q}_{j-1} + D_1\mathbf{C}\mathbf{q}_{j+1} - \lambda\mathbf{M}\mathbf{c}_j + \mathbf{f}_j, \tag{4.57}$$

$$\mathbf{M}\mathbf{q}_j = (\mathbf{A} - \mathbf{S})\mathbf{c}_j - \mathbf{B}\mathbf{c}_{j-1} + \mathbf{C}\mathbf{c}_{j+1}, \tag{4.58}$$

where we integrate in time by the third order version of a total variation diminishing (TVD) Runge-Kutta method [14]. For a semidiscrete schema, written as

$$\frac{\partial u}{\partial t} = L(u),$$

this scheme is given by

$$u^{(1)} = u^n + \Delta t L(u^n),$$
$$u^{(2)} = \frac{3}{4}u^n + \frac{1}{4}u^{(1)} + \frac{1}{4}\Delta t L(u^{(1)}),$$
$$u^{n+1} = \frac{1}{3}u^n + \frac{2}{3}u^{(2)} + \frac{2}{3}\Delta t L(u^{(2)}). \tag{4.59}$$

Discretizing in space using discontinuous Galerkin has the advantage that it can handle complicated geometries and arbitrary triangulations. Using a TVD scheme like RK3-TVD has the advantage that it can compute approximations, which are either smooth or have weak shocks and other discontinuities, without further modification. Hence discontinuities may become smeared in future time steps but cannot become oscillatory. If however, the discontinuities are to strong, oscillations and even nonlinear instability can occur. To avoid these both, a slope limiter, like the minmod-limiter described in Eq. (4.44), can be used.

Capillary tip density

Now we determine the approximation to the one dimensional form of Eq. (2.6) which describes the capillary tip density. Splitting this equation we obtain

$$\frac{\partial n}{\partial t} = -\chi_1\frac{\partial}{\partial x}(nq) + D_2\frac{\partial w}{\partial x} + \alpha_0\rho c + \alpha_1 H(c - \hat{c})nc - \beta_2 n\rho,$$
$$w = \frac{\partial n}{\partial x},$$

where the one dimensional initial and Neumann boundary conditions are given by

$$n(x,0) = 0, \ \frac{\partial n}{\partial x}(0,t) = \frac{\partial n}{\partial x}(1,t) = 0.$$

With this inital condition we know by Eq. (4.31) that

$$u_j^m(0) = 0, \ \forall m,$$

which means that initially all the coefficients are zero.

Just as before, we multiply the system of two equations by the testfunction $\varphi_j \in \Phi$ and integrate it over element e_j. We use Integration by Parts to get our weak formulation

$$\int_{e_j} \frac{\partial n}{\partial t} \varphi_j \, dx = \int_{e_j} \chi_1 n q \frac{\varphi_j}{dx} \, dx - \int_{e_j} D_2 w \frac{d\varphi_j}{dx} \, dx + \int_{e_j} \alpha_0 \rho c \varphi_j \, dx$$
$$+ \int_{e_j} \alpha_1 H(c - \hat{c}) n c \varphi_j - \beta_2 n \rho \varphi_j \, dx - \chi_1 n q \varphi_j |_{e_j} + D_2 w \varphi_j |_{e_j}, \quad (4.60)$$

$$\int_{e_j} w \varphi_j \, dx = - \int_{e_j} n \frac{d\varphi_j}{dx} \, dx + n \varphi_j |_{e_j}. \quad (4.61)$$

As last, we substitute $n(\mathbf{x},t) = \sum_{l=0}^{K} n_j^l(t) \varphi_j^l(\mathbf{x})$ and we set $\varphi_j = \varphi_j^m$ to obtain

$$\sum_{l=0}^{K} \frac{\partial n_j^l}{\partial t} \int_{e_j} \varphi_j^l \varphi_j^m \, dx = \sum_{l=0}^{K} n_j^l \int_{e_j} \chi_1 q_j \varphi_j^l \frac{\varphi_j^m}{dx} \, dx - \sum_{l=0}^{K} w_j^l \int_{e_j} D_2 \varphi_j^l \frac{d\varphi_j^m}{dx} \, dx$$
$$+ \int_{e_j} \alpha_0 \rho_j c_j \varphi_j^m \, dx + \sum_{l=0}^{K} n_j^l \int_{e_j} \alpha_1 H(c_j - \hat{c}) c_j^l \varphi_j^l \varphi_j^m - \beta_2 \rho_j \varphi_j^l \varphi_j^m \, dx$$
$$- \chi_1 (nq)^\star \varphi_j^m \big|_{e_j} + D_2 w^\star \varphi_j^m \big|_{e_j}, \quad (4.62)$$

$$\sum_{l=0}^{K} w_j^l \int_{e_j} \varphi_j^l \varphi_j^m \, dx = - \sum_{l=0}^{K} n_j^l \int_{e_j} \varphi_j^l \frac{d\varphi_j^m}{dx} \, dx + n^\star \varphi_j^m \big|_{e_j}, \quad (4.63)$$

where we use central fluxes and for the flux of the convection term the local Lax-Friedrich flux [7] (central flux with an additional stabilisation term). We obtain

$$w^\star = \left\{ \left\{ \sum_{l=0}^{K} w_j^l \varphi_j^l \right\} \right\}, \ n^\star = \left\{ \left\{ \sum_{l=0}^{K} n_j^l \varphi_j^l \right\} \right\}, \quad (4.64)$$

$$(nq)^\star = \left\{ \left\{ \sum_{l=0}^{K} n_j^l \varphi_j^l \right\} \right\} q - \frac{z}{2} [[n]], \quad (4.65)$$

with

$$\begin{aligned}
[[n(x_{j-1/2})]] &= n_j(x_{j-1/2}) - n_{j-1}(x_{j-1/2}), \\
[[n(x_{j+1/2})]] &= n_j(x_{j+1/2}) - n_{j+1}(x_{j-1/2}), \\
z(x_{j-1/2}) &= \max\{|q_j(x_{j-1/2})\varphi_j^m(x_{j-1/2})|, |q_{j-1}(x_{j-1/2})\varphi_j^m(x_{j-1/2})|\}, \\
z(x_{j+1/2}) &= \max\{|q_j(x_{j+1/2})\varphi_j^m(x_{j+1/2})|, |q_{j+1}(x_{j+1/2})\varphi_j^m(x_{j+1/2})|\}.
\end{aligned} \quad (4.66)$$

Substituting $r = \frac{2(x - x_j)}{\Delta x}$, using Legendre polynomials and with the use of Gauss-Legendre quadrature we define

$$\mathbf{V_1}_{j,ml} \approx \sum_{i=1}^{6} \chi_1 q\left(x_j + \frac{\Delta x}{2} r_i\right) P_l(r_i) \frac{dP_m(r_i)}{dr} w_i, \tag{4.67}$$

$$\mathbf{V_2}_{j,ml} \approx \sum_{i=1}^{6} \frac{\Delta x}{2} P_l(r_i) P_m(r_i) \left[\alpha_1 H\left(c\left(x_j + \frac{\Delta x}{2} r_i\right) - \hat{c}\right) c\left(x_j + \frac{\Delta x}{2} r_i\right)\right.$$
$$\left. - \beta_2 \rho\left(x_j + \frac{\Delta x}{2} r_i\right)\right] w_i, \tag{4.68}$$

$$\mathbf{V_3}_{j,m} \approx \sum_{i=1}^{6} \frac{\Delta x}{2} \alpha_0 \rho\left(x_j + \frac{\Delta x}{2} r_i\right) c\left(x_j + \frac{\Delta x}{2} r_i\right) P_m(r_i) w_i, \tag{4.69}$$

$$\left\{\left\{\sum_{l=0}^{K} n_j^l \varphi_j^l q_j\right\}\right\} \varphi_j^m \bigg|_{e_j} = \left((\mathbf{C}\mathbf{n}_{j+1} + \mathbf{A_1}\mathbf{n_j}) \sum_{l=0}^{K} q_j^l P_l(1)\right.$$
$$\left. - (\mathbf{A_2}\mathbf{n_j} + \mathbf{B}\mathbf{n_{j-1}}) \sum_{l=0}^{K} q_j^l P_l(-1)\right), \tag{4.70}$$

where we used the points and weights from Table 4.1.

The numerical approximation for the coefficients using discontinuous Galerkin for the one dimensional form of Eq. (2.6) can be obtained by using Eq. (4.50)-(4.51), Eq. (4.54)-(4.56) and Eq. (4.67)-(4.70). These approximations are given by

$$\mathbf{M}\frac{\partial \mathbf{n_j}}{\partial t} = D_2(\mathbf{A} - \mathbf{S})\mathbf{w}_j + \mathbf{q}_j - D_2\mathbf{B}\mathbf{w}_{j-1} + D_2\mathbf{C}\mathbf{w}_{j+1} + (\mathbf{V_1}_j + \mathbf{V_2}_j)\mathbf{n}_j + \mathbf{V_3}_j,$$
$$- \chi_1\left((\mathbf{C}\mathbf{n}_{j+1} + \mathbf{A_1}\mathbf{n_j}) \sum_{l=0}^{3} q_j^l P_l(1) - (\mathbf{A_2}\mathbf{n_j} + \mathbf{B}\mathbf{n_{j-1}}) \sum_{l=0}^{3} q_j^l P_l(-1)\right), \tag{4.71}$$
$$\mathbf{M}\mathbf{w}_j = (\mathbf{A} - \mathbf{S})\mathbf{n}_j - \mathbf{B}\mathbf{n}_{j-1} + \mathbf{C}\mathbf{n}_{j+1}. \tag{4.72}$$

Here we also integrate in time by the third order version of the total variation diminishing Runge-Kutta method described in (4.59).

Vessel density

The last equation we apply the discontinuous Galerkin method to is the one dimensional form of Eq. (2.10) for the vessel density. Writing this equation as a system of two equations gives us

$$\frac{\partial \rho}{\partial t} = \epsilon \frac{\partial u}{\partial x} - \gamma(\rho - \rho_{eq}) + \mu_1 w - \chi_2 nq,$$
$$u = \frac{\partial \rho}{\partial x},$$

where the one dimensional initial and boundary conditions are given by

$$\rho(x, 0) = \begin{cases} 0, & x \in \Omega_w, \\ \rho_{eq}, & x \in \Omega \backslash \Omega_w, \end{cases}$$
$$\frac{\partial \rho}{\partial x}(0, t) = 0, \quad \rho(1, t) = \rho_{eq},$$

with the one dimensional domains Ω and Ω_w. With this inital condition we know the initial coefficients by applying Eq. (4.31).

In order to determine the weak formulation we multiply the system of two equations by the testfunction $\varphi_j \in \Phi$ and integrate it over element e_j. After applying Integration by Parts, the weak formulation is given by

$$\int_{e_j} \frac{\partial \rho}{\partial t} \varphi_j \; dx = \int_{e_j} -\epsilon u \frac{\varphi_j}{dx} \; dx + \epsilon u \varphi_j|_{e_j} - \int_{e_j} \gamma \left(\rho - \rho_{eq} \right) \varphi_j \; dx$$

$$+ \int_{e_j} \mu_1 w \varphi_j \; dx - \int_{e_j} \chi_2 n q \varphi_j \; dx, \tag{4.73}$$

$$\int_{e_j} u \varphi_j \; dx = - \int_{e_j} \rho \frac{d\varphi_j}{dx} \; dx + \rho \varphi_j|_{e_j} . \tag{4.74}$$

Substitute $\rho(x,t) = \sum_{l=0}^{K} \rho_j^l(t) \varphi_j^l(x)$ and set $\varphi_j = \varphi_j^m$ to obtain

$$\sum_{l=0}^{K} \frac{\partial \rho_j^l}{\partial t} \int_{e_j} \varphi_j^l \varphi_j^m \; dx = - \sum_{l=0}^{K} u_j^l \int_{e_j} \epsilon \varphi_j^l \frac{\varphi_j^m}{dx} \; dx + \epsilon u^\star \varphi_j^m|_{e_j}$$

$$- \sum_{l=0}^{K} \rho_j^l \int_{e_j} \gamma \varphi_j^l \varphi_j^m \; dx + \int_{e_j} \left(\gamma \rho_{eq} + \mu_1 w - \chi_2 n q \right) \varphi_j^m \; dx \tag{4.75}$$

$$\sum_{l=0}^{K} u_j^l \int_{e_j} \varphi_j^l \varphi_j^m \; dx = - \sum_{l=0}^{K} \rho_j^l \int_{e_j} \varphi_j^l \frac{d\varphi_j^m}{dx} \; dx + \rho^\star \varphi_j^m|_{e_j} , \tag{4.76}$$

where we use central fluxes such that

$$u^\star = \left\{ \left\{ \sum_{l=0}^{K} u_j^l \varphi_j^l \right\} \right\}, \; \rho^\star = \left\{ \left\{ \sum_{l=0}^{K} \rho_j^l \varphi_j^l \right\} \right\} . \tag{4.77}$$

Substituting $r = \frac{2(x - x_j)}{\Delta x}$, using Legendre polynomials and using Gauss-Legendre quadrature, we define

$$\mathbf{g1}_{j,m} = \frac{\Delta x}{2} \int_{-1}^{1} \gamma \rho_{eq} P_m(r) dr,$$

$$\rightarrow \mathbf{g1}_j = \frac{\Delta x}{2} \gamma \rho_{eq} \begin{pmatrix} 2 \\ 0 \\ 0 \\ 0 \end{pmatrix}, \tag{4.78}$$

$$\mathbf{g2}_{j,m} \approx \mu_1 \frac{\Delta x}{2} \sum_{i=1}^{6} w \left(x_j + \frac{\Delta x}{2} r_i \right) P_m(r_i) w_i, \tag{4.79}$$

$$\mathbf{g3}_{j,m} \approx \chi_2 \frac{\Delta x}{2} \sum_{i=1}^{6} n \left(x_j + \frac{\Delta x}{2} r_i \right) q \left(x_j + \frac{\Delta x}{2} r_i \right) P_m(r_i) w_i, \tag{4.80}$$

where j denotes the element number and where we used four Legendre polynomials, so up to order three, and the points and weights from Table 4.1 such that

$$\mathbf{g}_j = \mathbf{g1}_j + \mathbf{g2}_j - \mathbf{g3}_j. \tag{4.81}$$

The numerical approximation for the coefficients using discontinuous Galerkin for the one dimensional form of Eq. (2.10) can be obtained by using Eq. (4.50)-(4.51), Eq. (4.54)-(4.56) and Eq. (4.78)-(4.80). These approximations are given by

$$\mathbf{M}\frac{\partial \rho_j}{\partial t} = \epsilon(\mathbf{A} - \mathbf{S})\mathbf{u}_j - \epsilon\mathbf{B}\mathbf{u}_{j-1} + \epsilon\mathbf{C}\mathbf{u}_{j+1} - \gamma\mathbf{M}\rho_j + \mathbf{g}_j, \tag{4.82}$$

$$\mathbf{M}\mathbf{u}_j = (\mathbf{A} - \mathbf{S})\rho_j - \mathbf{B}\rho_{j-1} + \mathbf{C}\rho_{j+1}. \tag{4.83}$$

And for this numerical approximation we also integrate in time by the third order version of the total variation diminishing Runge-Kutta method described in Eq. (4.59).

Numerical simulations

Before we look at the approximations for the two dimensional model with discontinuous Galerkin we show some simulations for the one dimensional model using the discontinuous Galerkin method. The values for the different coefficients that we use are given in Table D.2.
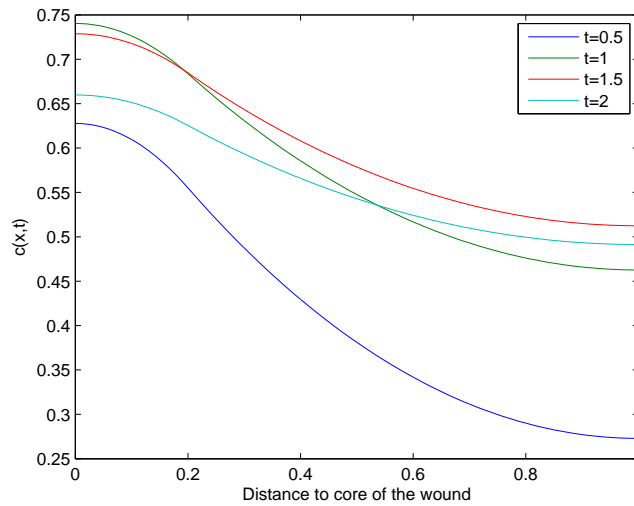
Figure 4.14: *Concentration TG*$-\beta$ *with element size* $\Delta x = 0.1$ *and time step* $\Delta t = 10^{-4}$.

In Figure 4.14, the concentration TG$-\beta$ is shown for different times t. Initially there is no TG$-\beta$ present. When the stem cells are injected, they 'release' some TG$-\beta$. Since the stem cells are injected in the wound of the heart, Ω_w, the 'production' of TG$-\beta$ takes place there. From there the attractant TG$-\beta$ will spread towards outside Ω_w. Hence at the beginning the most attractant is in Ω_w. After a while the attractant is more spread around the wound. Since the stem cells decrease exponentially, the production of TG$-\beta$ will come to an end. This can be seen in Figure 4.14 where the concentration attractant is already decreasing in the core of the wound at $t = 1$.

In Figure 4.15 we see the capillary tip density for different time t. Initially there are no tips. The first tips are formed at the boundary of the wound since that is the first location in time where the attractant meets the vessels. Vessels are constantly branching of and forming new
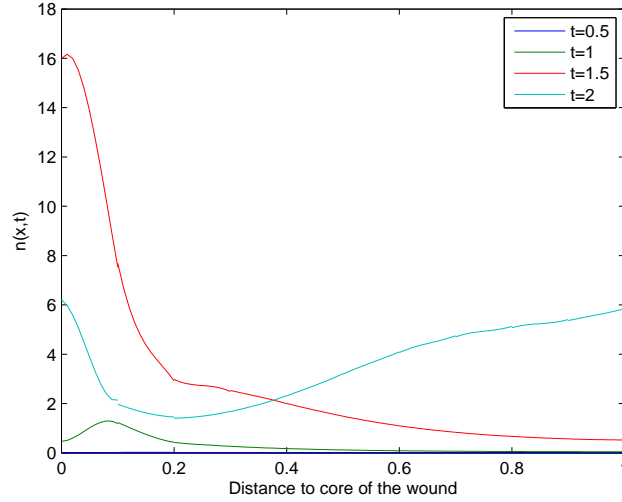
Figure 4.15: *Capillary tip density with element size $\Delta x = 0.1$ and time step $\Delta t = 10^{-4}$.*

loops such that the tip density increases and decreases. After a while, when the attractant has spread, vessels outside the heart wound also branch of and more tips are formed.

At the moment the number of stem cells has decreased enormously and no more TG$-\beta$ is being produced inside the wound, no more vessels will branch of near the wound and since vessels keep forming new loops, the density of capillary tips will decrease in and near the wound. As long as some TG$-\beta$ is still present far away from the wound the tip density keeps increasing there for a while. So there is a time interval during which the density of capillary tips is decreasing inside and near the wound and at the same time, it is increasing further away from the wound. This can be seen in Figure 4.15 at $t = 2$.

Combined with the change in the capillary tip density, the vessel density changes since both densities are influenced by each other. Initially the vessel density has an equilibrium value, $\rho_{eq} = 0.001$, outside the wound and was zero inside the wound. This can still be deduced from Figure 4.16 at $t = 0.5$. Due to the increasing concentration TG$-\beta$ a few vessels are grown into the wound of the heart after a short time. The growth of the vessel density is maximal around the wound since the concentration TG$-\beta$ is much higher there than far away from the wound. This is shown in Figure 4.16 at $t = 1$. Further, since initially there were no vessels in the wound, however there were vessels at the surface of the wound, we see at all times that the vessel density is highest around the surface of the wound. Further, as we can see in all figures, there is always just a little bit of attractant present far away from the wound such that there is not much branching over there.

These results for the one dimensional problem using discontinuous Galerkin are in accordance with the results obtained using the finite difference method and the finite element method in [5].

4.3.3   Convergence

In order to determine the quality of the approximations of the solutions to the partial differential equations in the model, we integrated in time using RK3-TVD as given in Eq. (4.59), which is
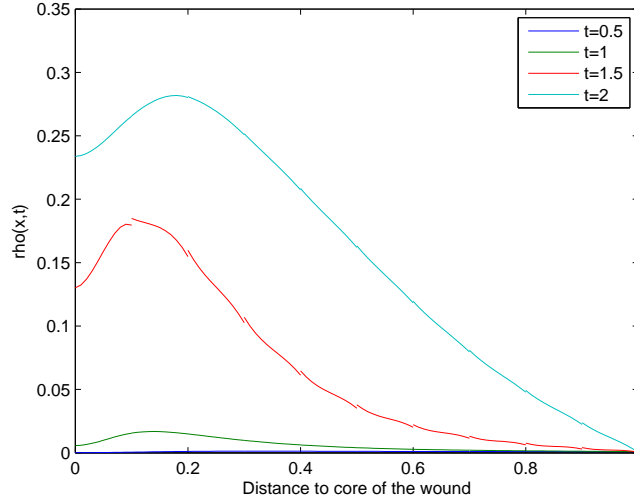
Figure 4.16: *Vessel density with element size $\Delta x = 0.1$ and time step $\Delta t = 10^{-4}$.*

a third order method. In this subsection we will determine the order of the convergence for this method combined with the discontinuous Galerkin method. We will do this by considering the advection equation. This is motivated in Chapter 6.

The advection equation is given by Eq. (4.25) with initial condition (4.26) and boundary condition (4.27), where $g(x) = \sin(2\pi x)$.

We will determine the order of this method as follows: First we need to know the norm of an approximation

$$||u_{ex} - u_{app}||_{\mathrm{L}^2(\Omega)} = \sqrt{\int_\Omega (u_{ex} - u_{app})^2 \; dx},$$

$$(4.84)$$

where u_{app} corresponds to the approximation and u_{ex} to the exact solution given by

$$u(x,t) = \sin(2\pi(x - t)).$$

Further we know

$$\int_\Omega (u_{ex} - u_{app})^2 \; dx = \sum_{j=1}^N \int_{\Omega_j} (u_{ex} - u_{app})^2 \; dx,$$

where Ω_j denotes the element with index j. Further,

$$u_{app} = \sum_{l=0}^k \hat{u}_j^l(t)\varphi_j^l(x) = \sum_{l=0}^k \hat{u}_j^l P_l(r),$$

and

$$\int_{-1}^1 f(r) \; dr \approx \sum_{i=1}^6 f(r_i)w_i,$$

using the Gauss-Legendre quadrature with the points and weights from Table 4.1.

$$(4.85)$$

Inserting these equalities, we find the norm

$$||u_{ex} - u_{app}||_{\mathrm{L}^2(\Omega)} = \sqrt{\frac{\Delta x}{2} \sum_{j=1}^{N} \sum_{i=1}^{6} \left(u_{ex}(x_j + \frac{\Delta x}{2} r_i) - \sum_{l=0}^{k} \hat{u}_j^l P_l(r_i) \right)^2 dr}.$$

Then, after determining how to calculate the norm, we should do this for several different element sizes. Plotting the log of the norms with the log of the element sizes gives us a graph which slope corresponds to the order of the approximation.

In Figure 4.17 we plot the log of the norms corresponding to the log of the element sizes. Here we have used the element sizes $\Delta x = 0.2$, $\Delta x = 0.1$, $\Delta x = 0.05$, $\Delta x = 0.025$ and $\Delta x = 0.0125$.
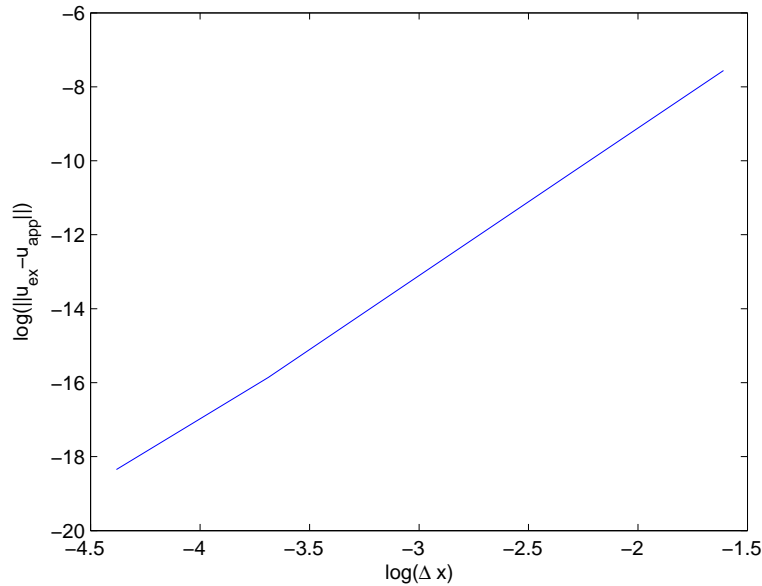
Figure 4.17: *A log plot of the error of the discontinuous Galerkin method for the advection equation.*

Calculating the slope of this graph gives us the order $p = 3.9096$, hence we have an approximation with almost order 4. This result is in line with theory [7], that states that the expected order equals $p = k + 1$, where k is the highest degree of the used polynomials, in our case $k = 3$.

4.4 Discontinuous Galerkin method for the two dimensional problem

4.4.1 Radial symmetric wound using polar coordinates

Our model as defined in Chapter 2 has the property of radial symmetry ($\frac{\partial}{\partial \theta} = 0$). This has the advantage that we can write the two dimensional model into polar coordinates which translates to an one dimensional problem with the radius as our variable.

The exact solution of the stem cell density in polar coodinates is

$$m(r,t) = \begin{cases} m_0 e^{-\beta_1 t}, & r \leq \delta, \\ 0, & r > \delta, \end{cases} \tag{4.86}$$

where δ denotes the boundary of the damaged part of the wound.

The rest of the model from Chapter 2 including the initial and boundary conditions rewritten in polar coordinates becomes:

Concentration TG-β:

$$r\frac{\partial c}{\partial t} = D_1 \frac{\partial}{\partial r}(r\tilde{q}) - r\lambda c + r\alpha m(r,t), \tag{4.87}$$

$$\tilde{q} = \frac{\partial c}{\partial r}, \tag{4.88}$$

$$c(r,0) = 0, \tag{4.89}$$

$$\frac{\partial c}{\partial r}(1,t) = 0. \tag{4.90}$$

Capillary tip density:

$$r\frac{\partial n}{\partial t} = -\chi_1 \frac{\partial}{\partial r}(rn\tilde{q}) + D_2 \frac{\partial}{\partial r}(r\tilde{w}) + r\alpha_0 \rho c + r\alpha_1 H(c - \hat{c})nc - r\beta_2 n\rho, \tag{4.91}$$

$$\tilde{w} = \frac{\partial n}{\partial r}, \tag{4.92}$$

$$n(r,0) = 0, \tag{4.93}$$

$$\frac{\partial n}{\partial r}(1,t) = 0. \tag{4.94}$$

Vessel density:

$$r\frac{\partial \rho}{\partial t} = \epsilon \frac{\partial}{\partial r}(r\tilde{u}) - r\gamma\rho + r\gamma\rho_{eq} + r(\mu_1 \tilde{w} - \chi_2 n\tilde{q}), \tag{4.95}$$

$$\tilde{u} = \frac{\partial \rho}{\partial r}, \tag{4.96}$$

$$\rho(r,0) = \begin{cases} 0, & \rho \leq \delta, \\ \rho_{eq}, & \rho > \delta, \end{cases} \tag{4.97}$$

$$\rho(1,t) = \rho_{eq}. \tag{4.98}$$

Eq. (4.87), Eq. (4.91) and Eq. (4.95) have all been multiplied by r in order to avoid dividing by zero. Further we have already introduced the variables $\tilde{q}$, $\tilde{w}$ and $\tilde{u}$ as a preparation to the implementation of the discontinuous Galerkin method.

Applying the discontinuous Galerkin method

Determining the weak formulations using the discontinuous Galerkin method is analogous to the derivations in Chapter 4.3. Therefore, we will not treat them.

The variables $\tilde{q}$, $\tilde{w}$ and $\tilde{u}$ are respectively determined as in Eq. (4.58), Eq. (4.72) and Eq. (4.83). The solutions to the concentration TG-β, the capillary tip density and the vessel density itself are now given by

$$\mathbf{M_r}\frac{\partial \mathbf{c}_j}{\partial t} = D_1(\mathbf{A_r} - \mathbf{S_r})\mathbf{q}_j - D_1\mathbf{B_r}\mathbf{q}_{j-1} + D_1\mathbf{C_r}\mathbf{q}_{j+1} - \lambda\mathbf{M_r}\mathbf{c}_j + \mathbf{f_r}, \tag{4.99}$$

$$\mathbf{M_r}\frac{\partial \mathbf{n}_j}{\partial t} = D_2(\mathbf{A_r} - \mathbf{S_r})\mathbf{w}_j + \mathbf{q}_j - D_2\mathbf{B_r}\mathbf{w}_{j-1} + D_2\mathbf{C_r}\mathbf{w}_{j+1} + (\mathbf{V_{r1}} + \mathbf{V_{r2}})\mathbf{n}_j + \mathbf{V_{r3}},$$

$$- \chi_1\left((\mathbf{C_r}\mathbf{n}_{j+1} + \mathbf{A_{1r}}\mathbf{n}_j)\sum_{l=0}^{3} q_j^l P_l(1) - (\mathbf{A_{2r}}\mathbf{n}_j + \mathbf{B_r}\mathbf{n_{j-1}})\sum_{l=0}^{3} q_j^l P_l(-1)\right), \tag{4.100}$$

$$\mathbf{M_r}\frac{\partial \rho_j}{\partial t} = \epsilon(\mathbf{A_r} - \mathbf{S_r})\mathbf{u}_j - \epsilon\mathbf{B_r}\mathbf{u}_{j-1} + \epsilon\mathbf{C_r}\mathbf{u}_{j+1} - \gamma\mathbf{M_r}\rho_j + \mathbf{g_r}. \tag{4.101}$$

The matrices and vectors used now depend on r. Therefore, the three solutions on element e_j using Gauss-Legendre quadrature with the points and weights from Table 4.1 are given by:

$$\mathbf{M}_{\mathbf{r}j,ml} = \frac{\Delta r}{2}\int_{-1}^{1}\left(r_j + \frac{\Delta r}{2}s\right)P_l P_m \, ds$$

$$\approx \frac{\Delta r}{2}\sum_{i=1}^{6}\left(r_j + \frac{\Delta r}{2}s_i\right)P_l(s_i)P_m(s_i)w_i, \tag{4.102}$$

$$\mathbf{S}_{\mathbf{r}j,ml} = \frac{\Delta r}{2}\int_{-1}^{1}\left(r_j + \frac{\Delta r}{2}s\right)P_l\frac{dP_m}{ds} \, ds$$

$$\approx \frac{\Delta r}{2}\sum_{i=1}^{6}\left(r_j + \frac{\Delta r}{2}s_i\right)P_l(s_i)\frac{dP_m(s_i)}{ds}w_i, \tag{4.103}$$

$$\mathbf{A_{r1}}_{j,ml} = \frac{1}{2}\left(r_j + \frac{\Delta r}{2}\right), \tag{4.104}$$

$$\mathbf{A_{r2}}_{j,ml} = \frac{1}{2}(-1)^l(-1)^m\left(r_j - \frac{\Delta r}{2}\right), \tag{4.105}$$

$$\mathbf{B}_{\mathbf{r}j,ml} = \frac{1}{2}(-1)^l\left(r_j + \frac{\Delta r}{2}\right), \tag{4.106}$$

$$\mathbf{C}_{\mathbf{r}j,ml} = \frac{1}{2}(-1)^m\left(r_j - \frac{\Delta r}{2}\right), \tag{4.107}$$

where $\mathbf{A_r} = \mathbf{A_{r1}} + \mathbf{A_{r2}}$. Further we use for the concentration TG-β

$$\mathbf{f}_{\mathbf{r}j} = \frac{\Delta r}{2}\int_{-1}^{1}\alpha\left(r_j + \frac{\Delta r}{2}s\right)P_l\frac{dP_m}{ds} \, ds$$

$$\approx \frac{\Delta r}{2}\alpha m\left(r_j, t\right)\sum_{i=1}^{6}\left(r_j + \frac{\Delta r}{2}s_i\right)P_m(s_i)w_i, \tag{4.108}$$

for the capillary tip density

$$\mathbf{V_{r1}}_{j,ml} \approx \sum_{i=1}^{6} \chi_1 \left(r_j + \frac{\Delta r}{2} s_i \right) \tilde{q} \left(r_j + \frac{\Delta r}{2} s_i \right) P_l(s_i) \frac{dP_m(s_i)}{dr} w_i, \tag{4.109}$$

$$\mathbf{V_{r2}}_{j,ml} \approx \frac{\Delta x}{2} \sum_{i=1}^{6} \left(r_j + \frac{\Delta r}{2} s_i \right) P_l(s_i) P_m(s_i) \left[\alpha_1 H \left(c \left(r_j + \frac{\Delta r}{2} s_i \right) - \hat{c} \right) c \left(r_j + \frac{\Delta r}{2} s_i \right) \right.$$
$$\left. - \beta_2 \rho \left(r_j + \frac{\Delta r}{2} s_i \right) \right] w_i, \tag{4.110}$$

$$\mathbf{V_{r3}}_{j,m} \approx \frac{\Delta r}{2} \sum_{i=1}^{6} \left(r_j + \frac{\Delta r}{2} s_i \right) \alpha_0 \rho \left(r_j + \frac{\Delta r}{2} s_i \right) c \left(r_j + \frac{\Delta r}{2} s_i \right) P_m(s_i) w_i, \tag{4.111}$$

and for the vessel density

$$\mathbf{g_{r1}}_{j,m} \approx \frac{\Delta r}{2} \sum_{i=1}^{6} \left(r_j + \frac{\Delta r}{2} s_i \right) \gamma \rho_{eq} P_m(s_i) w_i, \tag{4.112}$$

$$\mathbf{g_{r2}}_{j,m} \approx \mu_1 \frac{\Delta r}{2} \sum_{i=1}^{6} \left(r_j + \frac{\Delta r}{2} s_i \right) \tilde{w} \left(r_j + \frac{\Delta r}{2} s_i \right) P_m(s_i) w_i, \tag{4.113}$$

$$\mathbf{g_{r3}}_{j,m} \approx \chi_2 \frac{\Delta r}{2} \sum_{i=1}^{6} \left(r_j + \frac{\Delta r}{2} s_i \right) n \left(r_j + \frac{\Delta r}{2} s_i \right) \tilde{q} \left(r_j + \frac{\Delta r}{2} s_i \right) P_m(s_i) w_i, \tag{4.114}$$

where $\mathbf{g_r} = \mathbf{g_{r1}} + \mathbf{g_{r2}} - \mathbf{g_{r3}}$.

Numerical simulations

For our numerical simulations we use the parameters from Table D.2 with the changes from Table D.4.
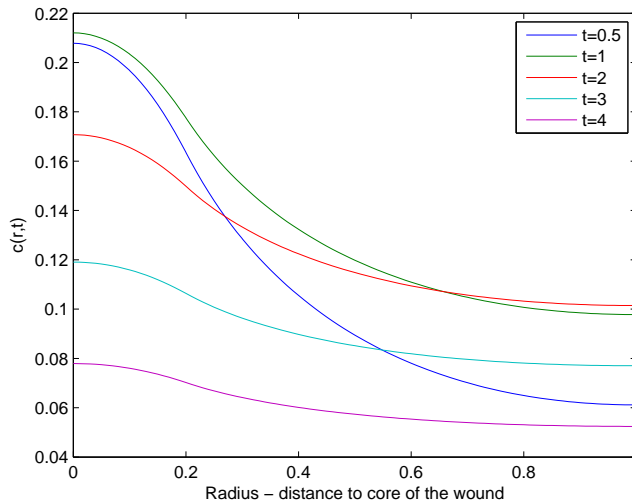
Figure 4.18: *Concentration TG$-\beta$ with element size $\Delta x = 0.1$ and time step $\Delta t = 10^{-4}$.*

In all simulations, the discontinuous Galerkin method is implemented using four basisfunctions per element, which should give up to third order accuracy.

In Figure 4.18 the concentration TG-β is shown at consecutive times for the two dimensional problem. We can see more clearly than in Figure 4.14 that the concentration TG-β arises from the damaged part of the wound where the attractant is produced by the injected stem cells. After a while, $t = 8$, only a few stem cells or none are left and the concentration TG-β drops back to zero everywhere.
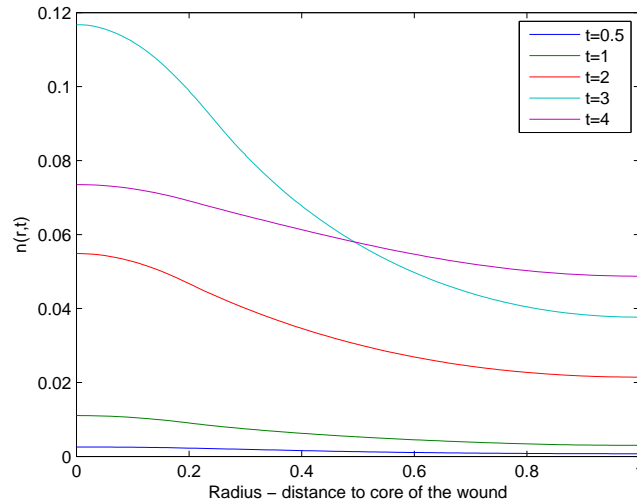
Figure 4.19: *Capillary tip density with element size $\Delta x = 0.1$ and time step $\Delta t = 10^{-4}$.*

In the simulation for the capillary tip density we set the influence of the diffusion significantly larger than in the results in Figure 4.15 for the one dimensional problem. Hence no direct comparison can be made. However, Figure 4.19 does make clear that the capillary tip density increases mostly around the damaged part of the wound, since there is the highest concentration of TG-β at the times plotted. Further, by the relatively large influence of the diffusion, the capillary tip density becomes, after a relative long time, spread throughout the tissue around the wound. After a while, when the concentration TG-β drops back to zero, the capillary tip density also goes back to zero.

In Figure 4.20 we do not yet see a decrease in the vessel density but we notice that the vessel density increases mostly on the edge of the damaged part of the wound. This first phenomenon is observed again, because the vessels and tips come into contact with the attractant TG-β.

As mentioned earlier these simulations were done for the two dimensional model written in polar coordinates. This means that these simulations are only valid in case of a circular wound within circular tissue where everything is axially symmetric. Of course it is not realistic that a wound of any kind is a perfect circle. Therefore, these simulations will not be used in real-world cases. However, they can give us good insight since this method delivers a very low relative error, according to the next subsection.
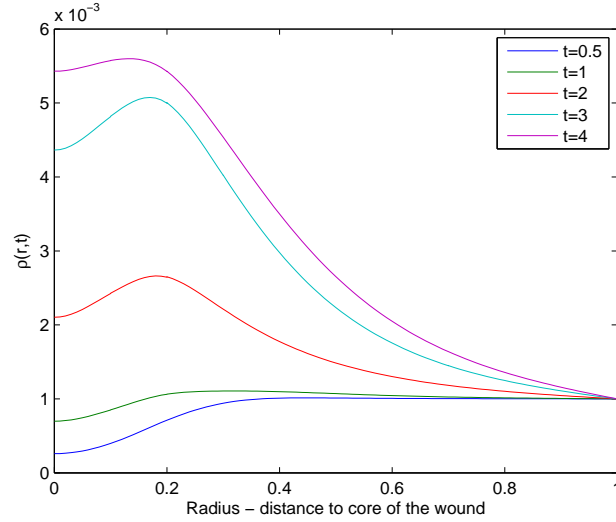
Figure 4.20: *Vessel density with element size* $\Delta x = 0.1$ *and time step* $\Delta t = 10^{-4}$.

4.4.2 Relative error of a test problem

As mentioned briefly in Section 3.3 we have a test case in order to validate results obtained using the discontinuous Galerkin method. This test equation is given in Eq. (3.21) with initial condition (3.22) and boundary condition (3.23). The relative errors using different time steps are shown in Table 4.2.

Time	$\dfrac{\|\mathbf{c}_{\mathrm{ex}} - \mathbf{c}_{\mathrm{app}}\|}{\|\mathbf{c}_{\mathrm{ex}}\|}$
$t = 0.25$	$1.0730 \cdot 10^{-5}$
$t = 0.50$	$4.6088 \cdot 10^{-5}$
$t = 0.75$	$7.3597 \cdot 10^{-5}$
$t = 1.00$	$1.0294 \cdot 10^{-4}$

Table 4.2: *Relative errors of our test problem where* c_{ex} *is the exact solution using Bessel functions and* c_{app} *is the approximation using the disonctinuous Galerkin method.*

In Table 4.2 we see that the relative errors are always very small. Contrary to the finite element method, where we should take very small element size Δx for the approximation to converge to the exact solution, we see that the discontinous Galerkin method already gives a very good approximation to the exact solution with relative large elements.

4.4.3   Rectangular wound using rectangular elements

It is desirable to do the simulations from Chapter 2 for many different wound geometries. In the previous chapter we have done this for circular wounds and in this chapter we will describe the simulation approach for wounds with a rectangular shape.

In order to do so we have partitioned our domain into rectangular elements, N in the $x-$direction and M in the $y-$direction. These elements are denoted by e_{ij}, $i = 1 \ldots N$, $j = 1 \ldots M$. On each element we define basis functions, the Legendre polynomials, up to order k. Since we need the basisfunctions in both the $x-$ and the $y-$directions, using basis functions up to order k means that we use the basisfunctions from the set $\mathbb{P}^k$, where

$$\varphi \in \mathbb{P}^k = \{P_0 P_0, P_0 P_1, P_1 P_0, P_1 P_1, P_2 P_0, \cdots, P_k P_k\}. \tag{4.115}$$

Applying the discontinuous Galerkin method

Applying the discontinuous Galerkin method for a two dimensional problem is very similar to what we have done in Chapter 4.3. Again, we split our equations to deal with the diffusion terms.

Concentration TG-β

Splitting Eq. (2.3) we obtain

$$\frac{\partial c}{\partial t} = D_1 \nabla \cdot q - \lambda c + \alpha m(x, y, t),$$
$$q = \nabla c,$$

where we have initial condition (2.4) and boundary conditions (2.5). The solution in element e_{ij} will be approximated by

$$c_h(x, y, t) = \sum_{l_x=0}^{k} \sum_{l_y=0}^{k} c_{ij}^{(l_x, l_y)} \varphi_i^{(l_x)}(x) \varphi_j^{(l_y)}(y), \tag{4.116}$$

where $c_{ij}^{(l_x, l_y)}$ are coefficients.

With this initial condition we know by Eq. (4.31) that

$$c_{ij}^{(l_x, l_y)}(0) = 0, \ \forall l_x, l_y,$$

which means that initially the coefficients for all the elements are zero.

The weak formulation is determined by multiplying the two equations by a testfunction φ and integrating it over element e_{ij}. After applying Integration by parts we obtain

$$\iint_{e_{ij}} \frac{\partial c}{\partial t} \varphi_{ij} \, dxdy = -D_1 \iint_{e_{ij}} q \nabla \varphi_{ij} \, dxdy + D_1 \int_{e_{ij}} q_1 \, \varphi_{ij}|_{x_{i-1/2}}^{x_{i+1/2}} \, dy$$

$$+ D_1 \int_{e_{ij}} q_2 \, \varphi_{ij}|_{y_{i-1/2}}^{y_{i+1/2}} \, dx - \iint_{e_{ij}} \lambda c \varphi_{ij} \, dxdy + \iint_{e_{ij}} \alpha m \varphi_{ij} \, dxdy,$$

$$\iint_{e_{ij}} q_1 \varphi_{ij} \, dxdy = -\iint_{e_{ij}} c \frac{\partial \varphi_{ij}}{\partial x} \, dxdy + \int_{e_{ij}} c \, \varphi_{ij}|_{x_{i+1/2}}^{x_{i-1/2}} \, dy,$$

$$\iint_{e_{ij}} q_2 \varphi_{ij} \, dxdy = -\iint_{e_{ij}} c \frac{\partial \varphi_{ij}}{\partial y} \, dxdy + \int_{e_{ij}} c \, \varphi_{ij}|_{y_{i+1/2}}^{y_{i-1/2}} \, dx,$$

subsequently, we substitute

$$c(x, y, t) \approx \sum_{l_x=0}^{k} \sum_{l_y=0}^{k} c_{ij}^{(l_x, l_y)} \varphi_i^{(l_x)}(x) \varphi_j^{(l_y)}(y), \tag{4.117}$$

over element e_{ij} and we set $\varphi_{ij} = \varphi_i^{(m_x)} \varphi_j^{(m_y)}$ to obtain the weak formulations

$$\sum_{l_x=0}^{k} \sum_{l_y=0}^{k} \frac{dc_{ij}}{dt} \iint_{e_{ij}} \varphi_i^{(l_x)} \varphi_j^{(l_y)} \varphi_i^{(m_x)} \varphi_j^{(m_y)} \, dxdy =$$

$$- D_1 \sum_{l_x=0}^{k} \sum_{l_y=0}^{k} q_{1_{ij}}^{(l_x, l_y)} \iint_{e_{ij}} \varphi_i^{(l_x)} \varphi_j^{(l_y)} \frac{d\varphi_i^{(m_x)}}{dx} \varphi_j^{(m_y)} \, dxdy + \int_{e_{ij}} q_1^{\star} \varphi_i^{(m_x)} \varphi_j^{(m_y)} \Big|_{x_{i-1/2}}^{x_{i+1/2}} dy$$

$$- D_1 \sum_{l_x=0}^{k} \sum_{l_y=0}^{k} q_{2_{ij}}^{(l_x, l_y)} \iint_{e_{ij}} \varphi_i^{(l_x)} \varphi_j^{(l_y)} \varphi_i^{(m_x)} \frac{d\varphi_j^{(m_y)}}{dy} \, dxdy + \int_{e_{ij}} q_2^{\star} \varphi_i^{(m_x)} \varphi_j^{(m_y)} \Big|_{y_{j-1/2}}^{y_{j+1/2}} dx$$

$$- \sum_{l_x=0}^{k} \sum_{l_y=0}^{k} c_{ij}^{(l_x, l_y)} \lambda \iint_{e_{ij}} \varphi_i^{(l_x)} \varphi_j^{(l_y)} \varphi_i^{(m_x)} \varphi_j^{(m_y)} \, dxdy + \alpha \iint_{e_{ij}} m(x, y, t) \varphi_i^{(m_x)} \varphi_j^{(m_y)} \, dxdy, \tag{4.118}$$

$$\forall (m_x, m_y) \in \{0, ..., k\} \times \{0, ..., k\},$$

and

$$\sum_{l_x=0}^{k} \sum_{l_y=0}^{k} q_{1_{ij}}^{(l_x, l_y)} \iint_{e_{ij}} \varphi_i^{(l_x)} \varphi_j^{(l_y)} \varphi_i^{(m_x)} \varphi_j^{(m_y)} \, dxdy$$

$$- \sum_{l_x=0}^{k} \sum_{l_y=0}^{k} c_{ij}^{(l_x, l_y)} \iint_{e_{ij}} \varphi_i^{(l_x)} \varphi_j^{(l_y)} \frac{d\varphi_i^{(m_x)}}{dx} \varphi_j^{(m_y)} \, dxdy, \tag{4.119}$$

$$\sum_{l_x=0}^{k} \sum_{l_y=0}^{k} q_{2_{ij}}^{(l_x, l_y)} \iint_{e_{ij}} \varphi_i^{(l_x)} \varphi_j^{(l_y)} \varphi_i^{(m_x)} \varphi_j^{(m_y)} \, dxdy$$

$$- \sum_{l_x=0}^{k} \sum_{l_y=0}^{k} c_{ij}^{(l_x, l_y)} \iint_{e_{ij}} \varphi_i^{(l_x)} \varphi_j^{(l_y)} \varphi_i^{(m_x)} \frac{d\varphi_j^{(m_y)}}{dy} \, dxdy, \tag{4.120}$$

where we use the central flux in both the $x-$ and the $y-$direction.

For our basis functions and testfunctions we choose to use the Legendre polynomials as defined in the set (4.115). We substitute $r = \frac{2(x-x_i)}{\Delta x}$, $s = \frac{2(y-y_j)}{\Delta y}$, $\varphi_i^{l_x}(x_i + \frac{\Delta x}{2}r) = P_{l_x}(r)$ and $\varphi_j^{l_y}(y_j + \frac{\Delta y}{2}s) = P_{l_y}(s)$.

Using these straightforward linear coordinate transformations, the mass matrix and stiffness

matrices for the two dimensional problem are given by

$$\mathbf{M}_{ml} = \frac{\Delta x}{2}\frac{\Delta y}{2}\int_{-1}^{1}\int_{-1}^{1} P_{l_x}P_{l_y}P_{m_x}P_{m_y}\ drds = \frac{\Delta x}{2\cdot l_x+1}\delta_{m_x,l_x}\frac{\Delta y}{2\cdot l_y+1}\delta_{m_y,l_y}, \qquad (4.121)$$

$$\mathbf{S}_{\mathbf{x}ml} = \frac{\Delta y}{2}\int_{-1}^{1}\int_{-1}^{1} P_{l_x}P_{l_y}\frac{dP_{m_x}}{dr}P_{m_y}\ drds = \frac{\Delta y}{2\cdot l_y+1}\delta_{m_y,l_y}\underbrace{\int_{-1}^{1} P_{l_x}\frac{dP_{m_x}}{dr}\ dr}_{\mathbf{S_{xx}}}, \qquad (4.122)$$

$$\mathbf{S}_{\mathbf{y}ml} = \frac{\Delta x}{2}\int_{-1}^{1}\int_{-1}^{1} P_{l_x}P_{l_y}P_{m_x}\frac{dP_{m_y}}{ds}\ drds = \frac{\Delta x}{2\cdot l_x+1}\delta_{m_x,l_x}\underbrace{\int_{-1}^{1} P_{l_y}\frac{dP_{m_y}}{ds}\ ds}_{\mathbf{S_{yy}}}, \qquad (4.123)$$

where ml denotes the order of the polynomials, so m_x, m_y, l_x and l_y and where

$$\mathbf{S_{xx}} = \begin{pmatrix} 0 & 0 & 0 & 0 & 0 & 0 & 0 & 0 & 0 \\ 2 & 0 & 2 & 0 & 0 & 2 & 0 & 0 & 0 \\ 0 & 0 & 0 & 0 & 0 & 0 & 0 & 0 & 0 \\ 2 & 0 & 2 & 0 & 0 & 2 & 0 & 0 & 0 \\ 0 & 2 & 0 & 2 & 0 & 0 & 0 & 2 & 0 \\ 0 & 0 & 0 & 0 & 0 & 0 & 0 & 0 & 0 \\ 0 & 2 & 0 & 2 & 0 & 0 & 0 & 2 & 0 \\ 2 & 0 & 2 & 0 & 0 & 2 & 0 & 0 & 0 \\ 0 & 2 & 0 & 2 & 0 & 0 & 0 & 2 & 0 \end{pmatrix},\ \mathbf{S_{yy}} = \begin{pmatrix} 0 & 0 & 0 & 0 & 0 & 0 & 0 & 0 & 0 \\ 0 & 0 & 0 & 0 & 0 & 0 & 0 & 0 & 0 \\ 2 & 2 & 0 & 0 & 2 & 0 & 0 & 0 & 0 \\ 2 & 2 & 0 & 0 & 2 & 0 & 0 & 0 & 0 \\ 0 & 0 & 0 & 0 & 0 & 0 & 0 & 0 & 0 \\ 0 & 0 & 2 & 2 & 0 & 0 & 2 & 0 & 0 \\ 2 & 2 & 0 & 0 & 2 & 0 & 0 & 0 & 0 \\ 0 & 0 & 2 & 2 & 0 & 0 & 2 & 0 & 0 \\ 0 & 0 & 2 & 2 & 0 & 0 & 2 & 0 & 0 \end{pmatrix} \qquad (4.124)$$

The source vector, $\mathbf{f}_{ij}$, for our two dimensional problem becomes

$$\mathbf{f}_{ij,m} = \frac{\Delta x}{2}\frac{\Delta y}{2}\alpha\int_{-1}^{1}\int_{-1}^{1} m\left(x_i+\frac{\Delta x}{2}r, y_j+\frac{\Delta y}{2}s, t\right)P_{m_x}P_{m_y}\ drds,$$

$$\rightarrow\ \mathbf{f}_{ij} = \frac{\Delta x}{2}\frac{\Delta y}{2}\alpha m(x_i,y_j,t)\begin{pmatrix} 4 \\ 0 \\ \vdots \\ 0 \end{pmatrix}, \qquad (4.125)$$

where ij denotes the element and where we use the fact that $m(x,y,t)$ has a constant value inside an element and m denotes the order of the polynomials m_x and m_y.

finally, we need to write out the flux terms, hence for instance

$$\int_{e_{ij}} c^{\star}\varphi_i^{(m_x)}\varphi_j^{(m_y)}\Big|_{x_{i-1/2}}^{x_{i+1/2}}\ dy = \int_{e_{ij}}\left(c^{\star}(x_{i+1/2}) - c^{\star}(x_{i-1/2})\right)\varphi_i^{(m_x)}\varphi_j^{(m_y)}\ dy$$

$$= \frac{1}{2}\sum_{l_x=0}^{k}\sum_{l_y=0}^{k} c_{ij}^{(l_x,l_y)}\int_{e_{ij}}\varphi_j^{(l_y)}\varphi_j^{(m_y)}\ dy$$

$$+ \frac{1}{2}\sum_{l_x=0}^{k}\sum_{l_y=0}^{k} c_{i+1,j}^{(l_x,l_y)}\int_{e_{ij}}\varphi_j^{(l_y)}\varphi_j^{(m_y)}\ dy\cdot(-1)^{l_x}$$

$$- \frac{1}{2}\sum_{l_x=0}^{k}\sum_{l_y=0}^{k} c_{ij}^{(l_x,l_y)}\int_{e_{ij}}\varphi_j^{(l_y)}\varphi_j^{(m_y)}\ dy\cdot(-1)^{l_x}(-1)^{m_x}$$

$$- \frac{1}{2}\sum_{l_x=0}^{k}\sum_{l_y=0}^{k} c_{i-1,j}^{(l_x,l_y)}\underbrace{\int_{e_{ij}}\varphi_j^{(l_y)}\varphi_j^{(m_y)}\ dy}_{=\frac{\Delta y}{2\cdot l_y+1}}\cdot(-1)^{m_x},$$

which is represented in vector-form by

$$\mathbf{A_{1y}}\mathbf{c}_{ij} + \mathbf{B_y}\mathbf{c}_{i,j+1} - \mathbf{A_{2y}}\mathbf{c}_{ij} - \mathbf{C_y}\mathbf{c}_{i,j-1}. \tag{4.126}$$

For the flux in the other direction we can do the exact same such that

$$\int_{e_{ij}} c^{\star} \varphi_i^{(m_x)} \varphi_j^{(m_y)} \Big|_{y_{j-1/2}}^{y_{j+1/2}} \, dx$$

can be rewritten as

$$\mathbf{A_{1x}}\mathbf{c}_{ij} + \mathbf{B_x}\mathbf{c}_{i+1,j} - \mathbf{A_{2x}}\mathbf{c}_{ij} - \mathbf{C_x}\mathbf{c}_{i-1,j}. \tag{4.127}$$

With Eq. (4.121)-(4.127), the approximation for the coefficients for (4.118)-(4.120), using discontinuous Galerkin, is written as

$$\mathbf{M}\frac{\partial \mathbf{c}_{ij}}{\partial t} = D_1(\mathbf{A_x} - \mathbf{S_x})\mathbf{q_1}_{ij} + D_1\mathbf{B_x}\mathbf{q_1}_{i+1,j} - D_1\mathbf{C_x}\mathbf{q_1}_{i-1,j}$$
$$+ D_1(\mathbf{A_y} - \mathbf{S_y})\mathbf{q_2}_{ij} + D_1\mathbf{B_y}\mathbf{q_2}_{i,j+1} - D_1\mathbf{C_y}\mathbf{q_2}_{i,j-1} - \lambda\mathbf{M}\mathbf{c}_{ij} + \mathbf{f}_{ij}, \tag{4.128}$$
$$\mathbf{M}\mathbf{q_1}_{ij} = (\mathbf{A_x} - \mathbf{S_x})\mathbf{c}_{ij} + \mathbf{B_x}\mathbf{c}_{i+1,j} - \mathbf{C_x}\mathbf{c}_{i-1,j}, \tag{4.129}$$
$$\mathbf{M}\mathbf{q_2}_{ij} = (\mathbf{A_y} - \mathbf{S_y})\mathbf{c}_{ij} + \mathbf{B_y}\mathbf{c}_{i,j+1} - \mathbf{C_y}\mathbf{c}_{i,j-1}, \tag{4.130}$$

where we integrate in time by the third order version of a total variation dimishing (TVD) Runga-Kutta method as given in Eq. (4.59).

Capillary tip density

Splitting Eq. (2.6) using $\mathbf{w} = \nabla n$, gives

$$\frac{\partial n}{\partial t} = -\chi_1 \nabla \cdot (nq) + D_2 \nabla \cdot w + \alpha_0 \rho c + \alpha_1 H(c - \hat{c})nc - \beta_2 n\rho,$$
$$w = \nabla n,$$

where we have initial condition (2.8) and boundary conditions (2.9). The solution is approximated as in Eq. (4.116) where $n_{ij}^{(l_x, l_y)}$ are coefficients.

With this initial condition we know by Eq. (4.31) that

$$n_{ij}^{(l_x, l_y)}(0) = 0, \ \forall l_x, l_y,$$

which means that initially the coefficients for all elements are zero.

As before we determine the weak formulation. We have done this many times before with the derivation of the weak formulation for the concentration TG-β in the two dimensional case using rectangular elements in the previous subsection. Therefore, we will not show the weak formulation for the capillary tip density and its derivation. The difference is the flux term that originates from the chemotaxis term. As in Eq. (4.65), we use a central flux with an additional

stabilisation term. Hence we obtain

$$\int_{e_{ij}} n^\star q_1 \varphi_i^{(m_x)} \varphi_j^{(m_y)} \Big|_{x_{i-1/2}}^{x_{i+1/2}} \, dy$$

$$= \int_{e_{ij}} n(x_{i+1/2}) q_1(x_{i+1/2}) \varphi_i^{(m_x)}(x_{i+1/2}) \varphi_j^{(m_y)}(y) - \frac{z_x}{2}[[n(x_{i+1/2})]] \varphi_j^{(m_y)}$$

$$- n(x_{i-1/2}) q_1(x_{i-1/2}) \varphi_i^{(m_x)}(x_{i-1/2}) \varphi_j^{(m_y)}(y) - \frac{z_x}{2}[[n(x_{i-1/2})]] \varphi_j^{(m_y)} \, dy$$

$$\int_{e_{ij}} n^\star q_2 \varphi_i^{(m_x)} \varphi_j^{(m_y)} \Big|_{y_{j-1/2}}^{y_{j+1/2}} \, dx$$

$$= \int_{e_{ij}} n(y_{j+1/2}) q_2(y_{j+1/2}) \varphi_i^{(m_x)}(x) \varphi_j^{(m_y)}(y_{j+1/2}) - \frac{z_y}{2}[[n(y_{j+1/2})]] \varphi_i^{(m_x)}$$

$$- n(y_{j-1/2}) q_2(y_{j-1/2}) \varphi_i^{(m_x)}(x) \varphi_j^{(m_y)}(y_{j-1/2}) - \frac{z_y}{2}[[n(y_{j-1/2})]] \varphi_i^{(m_x)} \, dx$$

where

$$z_x(x_{i-1/2}) = \max\{|\mathbf{q_1}_{ij}(x_{i-1/2}) \varphi_i^{(m_x)}(x_{i-1/2})|, |\mathbf{q_1}_{i-1,j}(x_{i-1/2}) \varphi_i^{(m_x)}(x_{i-1/2})|\},$$

$$z_x(x_{i+1/2}) = \max\{|\mathbf{q_1}_{ij}(x_{i+1/2}) \varphi_i^{(m_x)}(x_{i+1/2})|, |\mathbf{q_1}_{i+1,j}(x_{i+1/2}) \varphi_i^{(m_x)}(x_{i+1/2})|\},$$

$$z_y(y_{j-1/2}) = \max\{|\mathbf{q_2}_{ij}(y_{j-1/2}) \varphi_j^{(m_y)}(y_{j-1/2})|, |\mathbf{q_2}_{i,j-1}(y_{j-1/2}) \varphi_j^{(m_y)}(y_{j-1/2})|\},$$

$$z_y(y_{j+1/2}) = \max\{|\mathbf{q_2}_{ij}(y_{j+1/2}) \varphi_j^{(m_y)}(y_{j+1/2})|, |\mathbf{q_2}_{i,j+1}(y_{j+1/2}) \varphi_j^{(m_y)}(y_{j+1/2})|\},$$

and the jumps are

$$[[n(x_{i-1/2})]] = n_{ij}(x_{i-1/2}) - n_{i-1,j}(x_{i-1/2}),$$

$$[[n(x_{i+1/2})]] = n_{i+1,j}(x_{i+1/2}) - n_{i,j}(x_{i+1/2}),$$

$$[[n(y_{j-1/2})]] = n_{ij}(x_{j-1/2}) - n_{i,j-1}(x_{j-1/2}),$$

$$[[n(y_{j+1/2})]] = n_{i,j+1}(x_{j+1/2}) - n_{i,j}(x_{j+1/2}).$$

These flux terms are respectively written as

$$\int_{e_{ij}} n^\star q_1 \varphi_i^{(m_x)} \varphi_j^{(m_y)} \Big|_{x_{i-1/2}}^{x_{i+1/2}} \, dy = \mathbf{fA_{x}}_{ij}\mathbf{n}_{ij} + \mathbf{fB_{x}}_{ij}\mathbf{n}_{i+1,j} - \mathbf{fC_{x}}_{ij}\mathbf{n}_{i-1,j} - \mathbf{fD_{x}}_{ij}, \qquad (4.131)$$

$$\int_{e_{ij}} n^\star q_2 \varphi_i^{(m_x)} \varphi_j^{(m_y)} \Big|_{y_{j-1/2}}^{y_{j+1/2}} \, dx = \mathbf{fA_{y}}_{ij}\mathbf{n}_{ij} + \mathbf{fB_{y}}_{ij}\mathbf{n}_{i,j+1} - \mathbf{fC_{y}}_{ij}\mathbf{n}_{i,j-1} - \mathbf{fD_{y}}_{ij}, \qquad (4.132)$$

As we determined the mass and stiffness matrices, (4.121)-(4.122), for the two dimensional case, we also need to determine new matrices for $\mathbf{V_1}$, $\mathbf{V_2}$ and $\mathbf{V_3}$ which we used to determine the discontinuous Galerkin approximation in the one dimensional case. These matrices are determined using Gauss Legendre quadrature with the points and weights from Table 4.1 in

both the $x-$ as the $y-$direction and are given by

$$
\begin{aligned}
\mathbf{V_1}_{ij,ml} &\approx \sum_{u=1}^{6}\sum_{v=1}^{6} \chi_1 P_{l_x}(r_u)P_{l_y}(s_v)\left[q_1(x,y)\frac{dP_{m_x}(r_u)}{dr}P_{m_y}(s_v)\frac{\Delta y}{2}\right.\\
&\left.+ q_2(x,y)\, P_{m_x}(r_u)\frac{dP_{m_y}(s_v)}{ds}\frac{\Delta x}{2}\right] w_u w_v,
\end{aligned}
\tag{4.133}
$$

$$
\begin{aligned}
\mathbf{V_2}_{ij,ml} &\approx \sum_{u=1}^{6}\sum_{v=1}^{6}\frac{\Delta x}{2}\frac{\Delta y}{2}P_{l_x}(r_u)P_{l_y}(s_v)P_{m_x}(r_u)P_{m_y}(s_v)\left[\alpha_1 H\left(c(x,y)-\hat{c}\right)c(x,y)\right.\\
&\left.-\beta_2\rho(x,y)\right] w_u w_v,
\end{aligned}
\tag{4.134}
$$

$$
\mathbf{V_3}_{ij,m} \approx \sum_{u=i}^{6}\sum_{v=1}^{6}\frac{\Delta x}{2}\frac{\Delta y}{2}\alpha_0\rho(x,y)\,c(x,y)\,P_{m_x}(r_u)P_{m_x}(s_v)w_v,
\tag{4.135}
$$

where $x = x_i + \frac{\Delta x}{2}r_u$ and $y = y_j + \frac{\Delta y}{2}s_v$, ij refers to the considered element e_{ij} and ml denotes the order of the polynomials, so m_x, m_y, l_x and l_y, r_u and s_v are the internal points for the quadrature and w_u and w_v are the corresponding weights. Note that these weights are not the vector $\mathbf{w}$ from our model.

Using the matrices from Eq. (4.121)-(4.123), the flux relations (4.126) and (4.127), as well as (4.131) and (4.132), with the matrices (4.133)-(4.135) the approximations to the solutions can be found by

$$
\begin{aligned}
\mathbf{M}\frac{\partial \mathbf{n}_{ij}}{\partial t} &= D_2(\mathbf{A_x}-\mathbf{S_x})\mathbf{w_1}_{ij}+D_2\mathbf{B_x}\mathbf{w_1}_{i+1,j}-D_2\mathbf{C_x}\mathbf{w_1}_{i-1,j}\\
&+ D_2(\mathbf{A_y}-\mathbf{S_y})\mathbf{w_2}_{ij}+D_2\mathbf{B_y}\mathbf{w_2}_{i,j+1}-D_2\mathbf{C_y}\mathbf{w_2}_{i,j-1}+(\mathbf{V_1}_{ij}+\mathbf{V_2}_{ij})\mathbf{n}_{ij}+\mathbf{V_3}_{ij}\\
&-\chi_1\left[\mathbf{fA_x}_{ij}\mathbf{n}_{ij}+\mathbf{fB_x}_{ij}\mathbf{n}_{i+1,j}-\mathbf{fC_x}_{ij}\mathbf{n}_{i-1,j}-\mathbf{fD_x}_{ij}\right.\\
&\left.+\mathbf{fA_y}_{ij}\mathbf{n}_{ij}+\mathbf{fB_y}_{ij}\mathbf{n}_{i,j+1}-\mathbf{fC_y}_{ij}\mathbf{n}_{i,j-1}-\mathbf{fD_y}_{ij}\right],
\end{aligned}
\tag{4.136}
$$

$$
\mathbf{M}\mathbf{w_1}_{ij} = (\mathbf{A_x}-\mathbf{S_x})\mathbf{n}_{ij}+\mathbf{B_x}\mathbf{n}_{i+1,j}-\mathbf{C_x}\mathbf{n}_{i-1,j},
\tag{4.137}
$$

$$
\mathbf{M}\mathbf{w_2}_{ij} = (\mathbf{A_y}-\mathbf{S_y})\mathbf{n}_{ij}+\mathbf{B_y}\mathbf{n}_{i,j+1}-\mathbf{C_y}\mathbf{n}_{i,j-1},
\tag{4.138}
$$

Here we also integrate in time using the third order version of the total variation dimishing Runga-Kutta method given in Eq. (4.59).

Vessel density

Finally splitting Eq. (2.10), using $\mathbf{u} = \nabla\rho$, gives

$$
\frac{\partial \rho}{\partial t} = \epsilon\nabla\cdot u - \gamma(\rho-\rho_{eq})+(\mu_1\nabla n - \chi_2 n\nabla c)\cdot\frac{\bar{\mathbf{x}}}{\|\bar{\mathbf{x}}\|},
$$

$$
u = \nabla\rho,
$$

where we have initial condition (2.11) and boundary conditions (2.12). The solution will be approximated as in Eq. (4.116) where $\rho_{ij}^{(l_x,l_y)}$ are coefficients.

With this initial condition we obtain the initial coefficients by applying Eq. (4.31) for the two dimensional problem.

Just as for the capillary tip density, we do not show the weak formulation and its derivation. They can be found the using the same derivation as for the concentration TG-β. After we have determined the mass matrix, the stiffness matrices and the matrices for the flux terms we need to determine the new vectors $\mathbf{g_1}$, $\mathbf{g_2}$ and $\mathbf{g_3}$ instead of the ones we use in Eq. (4.78)-(4.80). This is done using Gauss-Legendre quadrature, with the points and weights from Table 4.1, in both the $x-$ and the $y-$direction.

$$\mathbf{g_1}_{ij,m} = \frac{\Delta x}{2}\frac{\Delta y}{2}\int_{-1}^{1}\int_{-1}^{1}\gamma\rho_{eq}P_{m_x}P_{m_y}drds,$$

$$\rightarrow \ \mathbf{g_1}_{ij} = \frac{\Delta x}{2}\frac{\Delta y}{2}\gamma\rho_{eq}\begin{pmatrix}4\\0\\\vdots\\0\end{pmatrix}, \tag{4.139}$$

$$\mathbf{g_2}_{ij,m} \approx \mu_1\frac{\Delta x}{2}\frac{\Delta y}{2}\sum_{u=1}^{6}\sum_{v=1}^{6}\frac{\left(w_1\left(x,y\right)\cdot x + w_2\left(x,y\right)\cdot y\right)P_{m_x}(r_u)P_{m_y}(s_v)w_uw_v}{\sqrt{x^2+y^2}}, \tag{4.140}$$

$$\mathbf{g_3}_{ij,m} \approx \chi_2\frac{\Delta x}{2}\frac{\Delta y}{2}\sum_{u=1}^{6}\sum_{v=1}^{6}n\left(x,y\right)\left(q_1\left(x,y\right)\cdot x + q_2\left(x,y\right)\cdot y\right)P_{m_x}(r_u)P_{m_y}(s_v)w_uw_v, \tag{4.141}$$

where $x = x_i + \frac{\Delta x}{2}r_u$, $y = y_j + \frac{\Delta y}{2}s_v$, ij refers to the considered element e_{ij} and m denotes the order of the polynomials, so m_x and m_y, r_u and s_v are the internal points for the quadrature and w_u and w_v are the corresponding weights. Further we define

$$\mathbf{g}_{ij} = \mathbf{g_1}_{ij} + \mathbf{g_2}_{ij} - \mathbf{g_3}_{ij}. \tag{4.142}$$

Using the mass matrix and stiffness matrices in Eq. (4.121)-(4.123), the flux parts in relations (4.127) and (4.126) and the vectors as in identities (4.139)-(4.141) we obtain the following approximation to the solution:

$$\mathbf{M}\frac{\partial\rho_{ij}}{\partial t} = \epsilon(\mathbf{A_x} - \mathbf{S_x})\mathbf{u_1}_{ij} + \epsilon\mathbf{B_x}\mathbf{u_1}_{i+1,j} - \epsilon\mathbf{C_x}\mathbf{u_1}_{i-1,j}$$

$$+ \epsilon(\mathbf{A_y} - \mathbf{S_y})\mathbf{u_2}_{ij} + \epsilon\mathbf{B_y}\mathbf{u_2}_{i,j+1} - \epsilon\mathbf{C_y}\mathbf{u_2}_{i,j-1} - \gamma\mathbf{M}\rho_{ij} + \mathbf{g}_{ij}, \tag{4.143}$$

$$\mathbf{M}\mathbf{u_1}_{ij} = (\mathbf{A_x} - \mathbf{S_x})\rho_{ij} + \mathbf{B_x}\rho_{i+1,j} - \mathbf{C_x}\rho_{i-1,j}, \tag{4.144}$$

$$\mathbf{M}\mathbf{u_2}_{ij} = (\mathbf{A_y} - \mathbf{S_y})\rho_{ij} + \mathbf{B_y}\rho_{i,j+1} - \mathbf{C_y}\rho_{i,j-1}, \tag{4.145}$$

Just as before, we integrate in time using the third order version of the total variation dimishing Runga-Kutta method described in Eq. (4.59).

Numerical simulations

The simulations in this subsection are for the two dimensional problem using the discontinuous Galerkin method with square elements. The wound we used also has a square shape.

Because the discontinuous Galerkin method for a two dimensional problem with many elements (100 elements) is a very expensive method, and because the implementation is very recent, we only show some results after a short period in time. Hence the simulations are shown just after the injection of the stem cells.

(a) View 1   (b) View 2
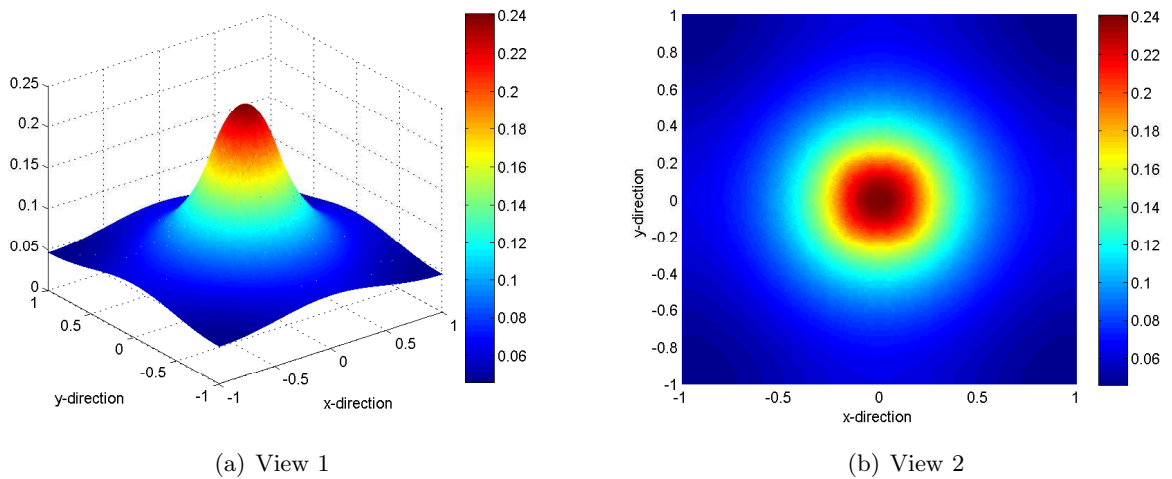
Figure 4.21: *Concentration TG-β for a square shaped wound after t = 0.5.*

In Figure 4.21 the concentration of TG-β is plotted. From Figure 4.21(b) it is clear that the behaviour of the attractant is different for a rectangular shaped wound than for a circular wound as in Chapter 4.4.1.

(a) View 1   (b) View 2
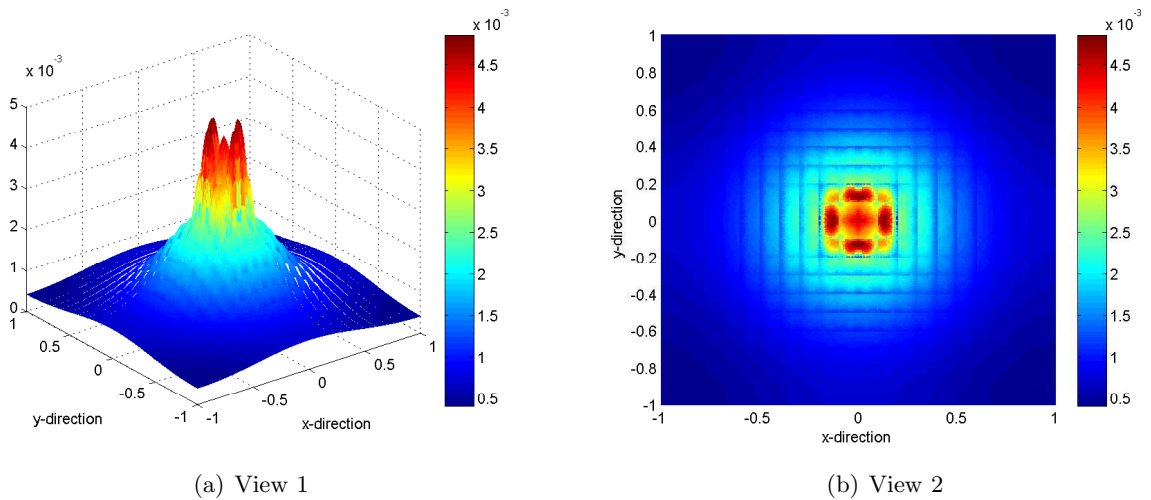
Figure 4.22: *Capillary tip density for a square shaped wound after t = 0.5.*

Figures 4.22 and 4.23 show at first sight some strange minima/maxima. These phenomena are related with the fact that our wound has a rectangular shape and that the length over which transport from the external boundary takes place changes over the wound edge.

First the capillary tip density in Figure 4.22. As we have seen in simulations in for example Chapter 4.3 the capillary tip density starts to increase on the boundary of the wound after a short time. This happens axially symmetric since the wound was circular. Now the wound is rectangular and the points on the boundary where the distance to the center of the wound is the smallest, are the first points where the capillary tip density starts to increase. These are the points of the boundary on the $x-$ and $y-$axis. Therefore, after a short time the maxima

(a) View 1   (b) View 2
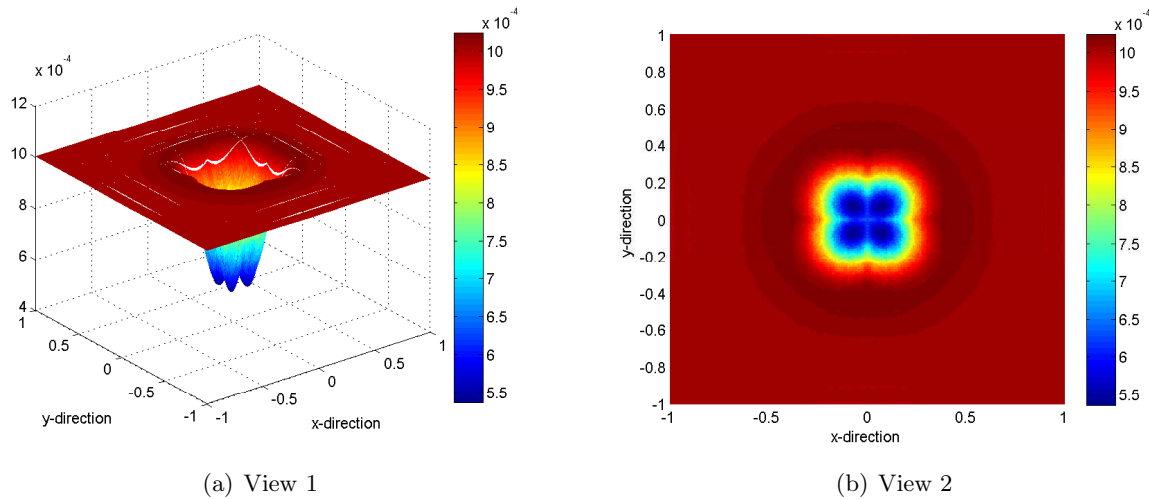
Figure 4.23: *Vessel density for a square shaped wound after* $t = 0.5$.

in the capillary tip density are from the center of the wound to the points of the boundary of the wound on the $x-$ and $y-$axis. The minima on the wound egde are located on the $y = \pm x$ rays/lines.

We see the same phenomenom for the vessel density in Figure 4.23. From the simulations of Chapter 4.3 we know that the vessel density starts to increase on the boundary of the wound since that is the first location where the attractant the vessels and the tips meets. For a rectangular wound this means that the attractant meets vessels and tips at the corner points after meeting of the attractant with the vessels and tips at the other points of the boundary. This occurs due to the fact that the distance from the center to a corner is longer than any other distance from the center to a point on the boundary of the wound. This means that the vessel density on the corner points has increased less than at other points on the boundary after the short time $t = 0.5$. This gives the four minima for the vessel density that are shown in Figure 4.23.

Note that these simulations are done after a relative short time $t = 0.5$ so the biological process has just started. Further, we have only used approximations up to order $k = 2$. Because this a relative low order, we have some big discontinuities between the different solutions on the boundaries of the elements. To get better approximations, we should use at least Legendre polynomials up to order $k = 3$.

How expensive is this method? At each time we needed to determine the nine coefficients per element (there are 100 elements) corresponding to the nine combinations of polynomials. We needed to do this for all six equations (the concentration TG-β, the capillary tip density, the vessel density and the three equations caused by the splitting of the diffusion terms). Because we used RK3-TVD for the time integration we did this whole calculation three times per time step. And with a time step of $\Delta t = 0.0001$ we did this for all 5000 times to come at $t = 0.5$, which is the time of the simulations plotted in the figures above. In Matlab, one iteration takes approximately 83 seconds. Therefore all the 5000 time steps take together approximately 4.83 days. Since this is still just a very short time, we see that it is very expensive.

Chapter 5

Influence of the shape of the wound

In the previous chapters we have looked at numerical simulations for wounds with a circular and a rectangular shape. The simulations for the circular shaped wounds where done using the finite element method and the discontinuous Galerkin method with polar coordinates. Where the last method was shown to be very accurate. The simulations for the rectangular wound where done using the discontinuous Galerkin method.

In this chapter we illustrate what the influence of the shape of the wound is with respect to the time before the equilibrium vessel density inside the original wound has settled in. In order to do this we consider a circular shaped wound and several elliptic wounds, where the wounds have the same initial area. The circular and elliptic wounds we consider are graphically illustrated in Figure 5.1 where the outer circle illustrates the total tissue we observe.
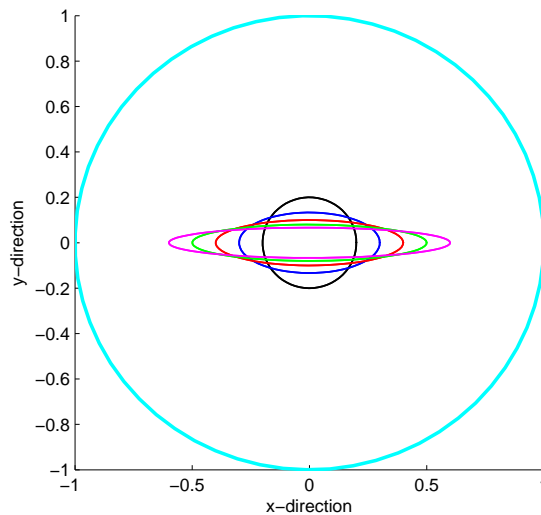
Figure 5.1: *Circular and elliptic wounds.*

For each of these wounds we determine the 'Shape Index' (SI) by

$$\text{SI}(\Omega) = \frac{4\pi \text{A}(\Omega)}{\text{l}^2(\Omega)}, \tag{5.1}$$

$$\tag{5.2}$$

where A(Ω) represents the area of the wound and l(Ω) the circumference. Note that SI(Ω) = 1 corresponds to a circle.

As mentioned, the discontinuous Galerkin method using polar coordinates gives very accurate approximations, but the method is very expensive. Therefore, we use the finite element method for these simualtions. For each different wound we monitor the vessel density in the center of the wound in time. The time at which the vessel density drops below $\rho_{eq} + \epsilon$, with a small ϵ, is time τ.
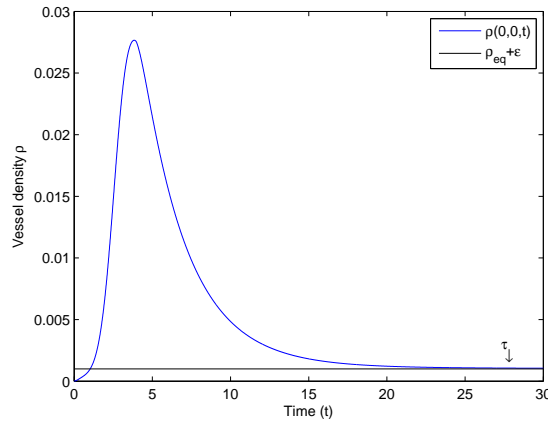
Figure 5.2: *Vessel density in the center of an elliptic wound with $\rho_{eq} = 1 \cdot 10^{-3}$ and epsilon = $6.5 \cdot 10^{-5}$.*

In Figure 5.2 the vessel density is shown in the center of an elliptic wound. This figure illustrates that the vessel density in this center starts in zero, then grows above the equilibrium value and finally converge towards the equilibrium value. The moment that the equilibrium value has settled in ($\rho \leq \rho_{eq} + \epsilon$), is marked with τ in the figure.
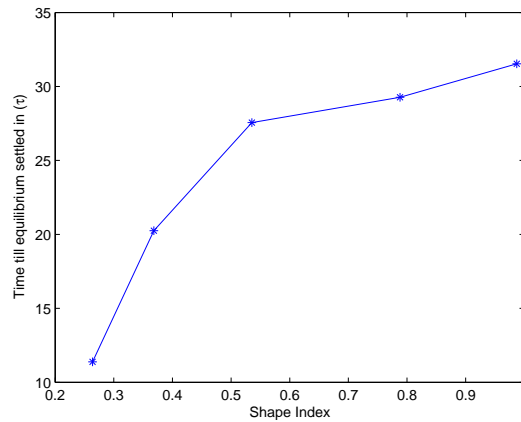
Figure 5.3: *τ values for the wounds from Figure 5.1.*

Knowing the SI and the computed value τ for all the different wound shapes from Figure 5.1, Figure 5.3 is constructed. This figure shows us that with a lower SI, the equilibrium vessel density settles in faster. This means that a network of vessels settles in faster, in the wound.

Hence all of the observed wounds obtain a network of vessels in the wound. But with the formula given in Eq. (5.1), we conclude that the wound is healed earlier if its initial shape index is small, or in other words a "long" wound heals faster than a circular one. In particular, an initial shape index of approximately 0.33 increases the healing rate by about a factor two with respect to a wound with shape index 1.

Chapter 6

Discussion and recommendations

After researching our angiogenesis model, using various techniques, we came to many conclusions. The conclusions concern both the main question and the preferred numerical method.

For all findings, one should keep in mind that all the biological parameters are fixed. The only parameter of significance is m_0 which represents the number of stem cells that is injected.

The main question is:

> "How many stem cells should be injected when aiming at avoiding the formation of scar tissue?"

For this question, the most important finding was done in Chapter 3, where we illustrated with Figure 3.4 that there is a minimal amount of stem cells necessary for the characteristics of the capillary tip density to reach the center of the wound. This means that we need a minimal number of stem cells in order to obtain a network of blood vessels in our 'original' wound.

In Figure 3.5 we see that for different numbers of stem cells the time needed before the network of blood vessels has settled in. Keep in mind that the number of stem cells, $m(\mathbf{x}, t)$, with $\mathbf{x} = \begin{pmatrix} x \\ y \end{pmatrix}$, is dimensionless. Hence, as mentioned in Chapter 6 this will probably be in the order of millions of cells. The dimension for time t is s^{-1} in the model, but it is not certain that it is the real dimension.

To determine the number of stem cells that should be injected, the value of stem cell density and time should be weighted. This means that a decision has to be made: Do we have enough time to allow a relatively low number of stem cells to be injected, or should we implement a relative high number of stem cells, which is probably more expensive.

With the parameters from Table D.2, we know from Figure 3.4 and Figure 3.5 that injecting eight (perhaps million) stem cells is sufficient to obtain succesfull results. Injecting more stem cells will only make the process faster such that we have the desired capillary network sooner.

To obtain the equation for the characteristics of the capillary tip density, some simplifications have been made. Hence in order to observe the 'real' model we need numerical techniques.

6.1 The mathematical model

Initial conditions

For the different equations from our model introduced in Chapter 2 we have relatively simple initial conditions. One may ask if these initial conditions reflect reality.

For the concentration TG-β we have the initial condition

$$c(\mathbf{x}, 0) = 0,$$

for all $\mathbf{x} = \begin{pmatrix} x \\ y \end{pmatrix}$ in our domain Ω. This indicates that we assume that TG$-\beta$ is not an endogenous substance. If it is, this initial condition should be reconsidered.

The initial condition for the capillary tip density and the vessel density are respectively given by

$$n(\mathbf{x}, 0) = 0,$$
$$\rho(\mathbf{x}, 0) = \begin{cases} 0, & \mathbf{x} \in \Omega_w, \\ \rho_{eq}, & \mathbf{x} \in \Omega \backslash \Omega_w, \end{cases}$$

(6.1)

for all $\mathbf{x}$ in our domain Ω. This can be interpreted as that there was initially a closed network of blood vessels without any loose tips and that the part of this network at the position of the wound was cut off during the heart attack.

First, is it fair to state that there is an equilibrium vessel density in a normal situation? This means that at each time, an equal amount of vessels/capillaries branched off and formed (new) loops. This can be possible, where vessels only branch off due to a change in hormones.

Secondly, if there is an equilibrium vessel density, does this mean that the capillary tip density should be equal to zero? The capillary tip density can only be zero if no new tips are branched off, which means that there is just a closed network of blood vessels where no vessels branch off or form loops.

These are questions that must be asked to obtain initial conditons that are biologically more practical. For example, if it is fair to state that there is an equilibrium vessel density, where at each time an equal amount of vessels branched off and formed loops, capillary tips constantly keep branching off and forming loops such that the initial condition for the capillary tip density cannot be equal to zero.

Single injection of stem cells

An important simplification is about the number of stem cells that is injected. For our model we assume that we have a single injection and that the stem cells are immediately well spread among the wound after the injection.

To improve the angiogenesis process one can think of injecting stem cells on a more regular base such that for a longer period more TG$-\beta$ can be produced. In order to be sure that this improves the angiogenesis process such that in the wound a network of blood vessels is settled in faster, numerical simulations for this should be performed.

If simulations show that a injecting stem cells on a more regular base does improve the process, we still need to know if this is clinically possible.

Parameter values

In the model from Chapter 2 we mentioned a lot of different parameters, each representing a biological process. For most simulations we used the parameter values from Table D.2. These

parameters are based on parameter values from literature about the role of angiogenesis in tumor growth [2].

Apart from the fact that these parameter values can be different for each patient, we need the best possible estimate for these parameters in order to get the most realistic simulations.

In collaboration with doctors the best possible estimate for these parameters should be found. Unfortunately, it was not feasible to do this in this project.

Parameter dimensions

In Chapter 2 we assigned dimensions to all parameters.

For the time t we state that it is in seconds. If we consider Figure 3.5, which tells us how much time we need to obtain a network of blood vessels in the 'original' wound for all different injected numbers of stem cells, it appears that we only need seconds in order to obtain a network of blood vessels. Of course this is not realistic. So a better dimension for time t needs to be found.

Our number of stem cells, given by $m(\mathbf{x}, t)$ is dimensionless at the moment. Considering Figure 3.5 again, makes it look like we only need, for example, eight stem cells in order to obtain a network of blood vessles in our 'original' wound. This is a normalized problem, so in reality this will probably be in the order of millions of stem cells. In order to determine this, collaboration with doctors is needed.

The snail trail

The equation for the vessel density, given in Eq. (2.10) contains the snail trail which moves towards the center of the wound, which is located at $(0, 0)$ in this study.

It is possible that there are several damaged parts in the heart after a heart attack. Lets call them $\Omega_{w_1}, \Omega_{w_2}, ..., \Omega_{w_n}$. Then we have to apply our model to this set of wounds, since the healing of wound Ω_i is influenced by the presence of the other wounds. In that case we cannot have the simplified equation for the vessel density as in Eq. (2.10) since we cannot define the origin as the center of a wound. The snail trail term should be adapted.

Several possible adjustments should be considered. A possibility is to introduce a distance function $\Phi = \Phi(\mathbf{x}, t)$, illustrated in Figure 6.1 for a randomly shaped wound.
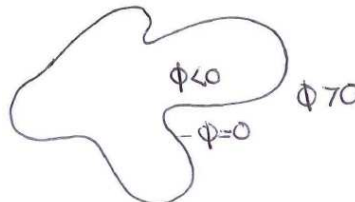

Figure 6.1: *Distance function for a randomly shaped wound.*

Hence the distance function gives the distance between the capillary tip and the boundary of the wound. Then $\nabla \Phi$ should be present in the snail trail and the vessels will move towards the nearest wound. This distance function can also be used if wound healing is modeled as a moving boundary problem.

6.2   Numerical Methods

Choosing a method

To construct a numerical method which is applicable to the model from Chapter 2, we have to consider different aspects.

First, the method should be able to handle complicated geometries since wounds can have any possible shape. Both the finite element method and the discontinous Galerkin method are eligible. Since the discontinous Galerkin method is more expensive, we first applied the finite element method. This method, treated in Section 4.1, gave some good results.

Secondly, the method should be able to handle hyperbolic or convection-dominated problems. Because if it turns out that the chemotaxis term has more influence than has been assumed, the degree of hyperbolicity of the problem will increase. In Section 4.2 the convection term has been made larger by assigning a higher value for the chemotaxis constant χ_1. Unfortunately, we conclude from the results of Figure 4.6 that the finite element method is not suitable anymore while the discontinous Galerkin method is.

Since the discontinuous Galerkin method meets both requirements we wanted to implement this method for the two dimensional model. Before we could do this, we needed to learn how to implement this for the one dimensional model and build our knowledge from there. We already started with this in the literary study.

During the literature study we applied this method to a relative simple advection equation in one dimension with different kinds of boundary conditions. We have introduced a limiter to prevent the appearance of wiggles.

In this report we first described the discontinuous Galerkin method applied to the one dimensional model. This is done in order to practice more with the method and to show some advantages of this method in comparison to the finite element method. This is also done in Section 4.2 where we showed that the discontinuous Galerin method satisfies the second requirement.

Subsequently, we used it to construct the approximations to the two dimensional model. The discontinuous Galerkin method was found to be a very complex and expensive method. Therefore, we only came so far that we can give approximation to situations with a two dimensional circular wound (using polar coordinates) and to situations with a rectangular shaped wound using rectangular elements.

Why is the discontinuous Galerkin method so expensive?

This is due to several facts. First, the discontinuous Galerkin method had many degrees of freedom which makes the method very expensive. Think of N, the number of elements and $p + 1$ the number of basis functions per element. The higher the order of the Legendre Polynomials, the more accurate the approximation is, however, also the more expensive the method is. Secondly, we used the so called Local discontinous Galerkin method, which is an extension of the discontinuous Galerkin method with Runga-Kutta time integration for purely hyperbolic or convection-diffusion systems. This results into the high-order accuracy and easy handling of complicated geometries. Basically, it means splitting the diffusion term such that we obtain a second equation for each equation of our model. The more equations to solve, the more expensive the method becomes. Finally, we use the central flux which uses a stencil of five elements instead of an upwind or downwind flux which uses a stencil of only three elements. We do this because the central flux is the only one that gives good results. The disadvantage is again that it is more expensive.

Is the discontinuous Galerkin method good to use for application?

We found a method which can handle the complicated geometries and the relative high hyperbolicity of the model. The only problem is that the method is very expensive, hence the question whether the discontinuous Galerkin method is suitable to use for application is quite legitimate. The long computation times make the method unattractive at the moment. Hence maybe in the (near) future, when the method has been improved and the computers are way faster, that discontinuous Galerkin can be used for quick application.

6.3 Improving the approximations using the numerical techniques

Finite element method with SUPG

During the literature study [5] we tried to improve the finite element approximations for our convection dominated problem, in only one dimension. At that moment only some basic streamline upwind Petrov-Galerkin method, abbreviated by SUPG, was implemented and it seemed like it did not improve the simulations. Because we only implemented some basic SUPG we cannot exclude SUPG as one of the options to improve the approximations yet. So for further research, the option to improve the approximations using the finite element with SUPG should be reconsidered.

Convergence of the discontinuous Galerkin method

In Section 4.3.3 we determined the order of the discontinuous Galerkin method combined with time integrating method RK3-TVD, by observing the advection equation.

Initially, we wanted to determine the order of the method using our model. Since we do not have an exact solution to our complete model we needed a different method to find the order than used in Section 4.3.3. Therefore, we defined the following norm:

$$Q_h = \sqrt{||c_h||^2 + ||n_h||^2 + ||\rho_h||^2}.$$

This norm will be calculated using Richardson extrapolation. We have

$$Q = Q_h + Kh^2,$$
$$Q = Q_{2h} + K(2h)^2,$$
$$Q = Q_{4h} + K(4h)^2,$$

such that

$$\frac{Q_{4h} - Q_{2h}}{Q_{2h} - Q_h} = 2^p, \tag{6.2}$$

where p denotes the order of the method.

Determining the order for our model with this method does not give any logical results. This is probably due to two things: First, the vessel density has a discontinuous initial condition and the number of stem cells function is discontinuous. Therefore, the model contains several discontinuities as an input. And secondly, the diffusion terms are splitted such that the order of the equations is as low as possible. We have not proved that these factors are the main reason that we cannot find the order, so this should be researched in order to be sure.

Hence, because we did not find a logical order for the method with our model, we analyzed the advection equation whose exact solution is known.

Improving the two dimensional discontinuous Galerkin approximations

In Chapter 4.4.3 we did some simulations using the discontinuous Galerkin method for our model with a square shaped wound. This is a very expensive method so the simulations that we have done are only after $t = 0.5$ where the biological proces had just started. In these simulations we already see some differences with respect to the simulations for a circular wound. In order to draw some more and better conclusions about the healing of a square wound the simulation should run for a longer time. Also, we have only used Legendre polynomials up to order 2. To get a better approximation we need at least an approximation that uses Legendre polynomials up to order 3.

In order to tell more about the healing of a rectangularly shaped wound the simulation should run for a rectangular wound since we have only done it for a square wound. The same Matlab code can be used for this.

Discontinuous Galerkin method with limiting

While determining the approximations to the solution of the equations in the model, in one and in two dimensions, using the discontinuous Galerkin method, we did not use a limiter of any kind. It was not necessary since no wiggles appeared. However, it is worth investigating whether there exist a limiter that improves the approximation. We do have to keep in mind, that implementing a limiter makes this method even more expensive than it already is.

Various wound shapes for the discontinuous Galerkin method

In this study we determined approximations for our two dimensional model with the discontinuous Galerkin method. This was only done for circular and rectangular wounds. In order to determine the approximations for randomly shaped wounds we need to work with triangular elements.

During the last few months we have implemented the discontinuous Galerkin method using triangular elements. Because it is relatively complicated to implement, it is very sensitive to making errors. Trying to find the errors in our implementation we noticed that this method was too expensive to track down the errors. Therefore, we changed to using rectangular elements with the limitations that it is only applicable to rectangular wounds.

Hence, in order to apply the discontinuous Galerkin method to all kind of two dimensional wound shapes, triangular elements should be implemented.

Chapter 7

Conclusions

We developed a model for angiogenesis under the injection of stem cells onto the damaged part of the heart after an infarction. The model is based on reaction-transport equations with a certain degree of hyperbolicity due to chemotaxis as an important mechanism for cell migration.

Using the method of characteristics, we are able to quickly estimate the efficiency of treatment with respect to biological parameters like the number of stem cells injected.

The method, which is based on a "snail trail" formalism, was originally set up in one dimension. One of the challenges in this research was to construct a more-dimensional counterpart of the equations.

Furthermore, we succesfully implemented finite element and discontinuous Galerkin techniques to solve the system of partial differential equations. It is concluded that the discontinuous Galerkin method is very accurate, however the method, in particular in more dimensions, suffers from large computation times, which makes the method still unattractive.

Appendix A

Approximation to solution

The solution to Eq. (2.3) can be approximated by the solution to Eq. (3.2). We prove this in this appendix.

We consider the operator L given by

$$Lu = -D_1\nabla \cdot \nabla(u) + \lambda u,$$

and let $\{\mu_j\}_{j\geq 0}$ be the eigenvalues of L with respective eigenfunctions $\varphi_j(x,y)$.

Further, we consider two problems

- (P_1) $\begin{cases} u_t + Lu = m_0 e^{-\alpha t}\mathbb{1}_{\Omega_1}, & (x,y) \in \Omega, t > 0, \\ u(x,y,0) = 0, \frac{\partial u}{\partial n} = 0, & (x,y) \in \partial\Omega, \end{cases}$

- (P_2) $\begin{cases} L\tilde{u} = m_0 e^{-\alpha t}\mathbb{1}_{\Omega_1}, & (x,y) \in \Omega, \\ \frac{\partial \tilde{u}}{\partial n} = 0, & (x,y) \in \partial\Omega, \end{cases}$

where

$$\mathbb{1}_{\Omega_1}(x,y) = \begin{cases} 1, & (x,y) \in \Omega_1 \subset \Omega, \\ 0, & (x,y) \in \Omega\backslash\Omega_1. \end{cases}$$

Due to the orthogonality of $\{\varphi_j\}_{j\geq 0}$, the set is a basis for $\mathrm{L}^2(\Omega)$. Then, since $\mathbb{1}_{\Omega_1} \subset \mathrm{L}^2$, $\forall \epsilon > 0$, $\exists N > 0$, $\{d_j\}_{j\geq N}$ such that

$$\|\mathbb{1}_{\Omega_1} - \sum_{j=0}^{\tilde{N}} d_j\varphi_j(x,y)\|_{\mathrm{L}^2(\Omega)} < \epsilon, \ \forall \tilde{N} > N.$$

In other words

$$\lim_{n\to\infty} \|\mathbb{1}_{\Omega_1} - \sum_{j=1}^{n} d_j\varphi_j\|_{\mathrm{L}^2(\Omega)} = 0.$$

Since

$$\tilde{u} \in \mathrm{C}^2(\Omega) \cap \mathrm{C}^1(\bar{\Omega}), \ \bar{\Omega} = \Omega \cup \partial\Omega,$$

and

$$u \in \mathrm{L}^2([0,T]; \mathrm{C}^2(\Omega) \cap \mathrm{C}^1(\bar{\Omega})),$$

we can write

$$\tilde{u}(x,y,t) = \sum_{j=1}^{n} \tilde{c}_j(t)\varphi_j(x,y),$$

$$u(x,y,t) = \sum_{j=1}^{n} c_j(t)\varphi_j(x,y),$$

77

both for $n \to \infty$.

Then with using L is self-adjoint (positive definite) we know $\{\varphi_j\}$ is orthogonal. Let us take $\{\varphi_j\}$ orthonormal, i.e.

$$\int_\Omega \varphi_i \varphi_j \ d\Omega = \delta_{ij}.$$

Using the orthonormality and

$$\mathrm{L}u = \mathrm{L}\sum_j c_j \varphi_j = \sum_j c_j \mu_j \varphi_j,$$

we obtain from problem (P_2)

$$\mu_j \tilde{c}_j(t) = m_0 e^{-\alpha t} d_j,$$
$$\tilde{c}_j(t) = \frac{m_0 d_j}{\mu_j} e^{-\alpha t}. \tag{A.1}$$

Further, we get from problem (P_1)

$$c_j' + \mu_j c_j = m_0 e^{-\alpha t} d_j, \ \ c_j(0) = 0.$$

Then, we get

$$[c_j e^{\mu_j t}]' = m_0 e^{(\mu_j - \alpha)t} d_j,$$
$$c_j = e^{-\mu_j t} m_0 d_j \int_0^t e^{(\mu_j - \alpha)s} ds.$$

Hence

$$c_j(t) = m_0 d_j e^{-\mu_j t} \frac{e^{(\mu_j - \alpha)t} - 1}{\mu_j - \alpha} = m_0 d_j \frac{e^{-\alpha t} - e^{-\mu_j t}}{\mu_j - \alpha}. \tag{A.2}$$

Furthermore, combining (A.1) and (A.2) we consider

$$\frac{c_j(t)}{\tilde{c}_j(t)} = \frac{e^{-\alpha t} - e^{-\mu_j t}}{e^{-\alpha t}} \frac{\mu_j}{\mu_j - \alpha} = (1 - e^{(\alpha - \mu_j)t}) \frac{1}{1 - \frac{\alpha}{\mu_j}} = (1 - e^{-\mu_j(1 - \frac{\alpha}{\mu_j})t}) \frac{1}{1 - \frac{\alpha}{\mu_j}}.$$

From this we know that

$$\lim_{\mu_j \to \infty} \frac{c_j(t)}{\tilde{c}_j(t)} = 1.$$

Hence

$$\lim_{\mu_j \to 0} u(x, y, t) = \tilde{u}(x, y, t), \ \ (x, y) \in \Omega.$$

Appendix B

Number of moles TG-β

The number of moles of TG-β is equal to the concentraion TG-β integrated over the domain. Taking the integral of Eq. (2.3) and substituting (3.1) we obtain

$$\frac{d}{dt} \int_\Omega c \; d\Omega - D_1 \int_\Omega \nabla \cdot \nabla c \; d\Omega + \lambda \int_\Omega c \; d\Omega = \alpha m_0 e^{-\beta_1 t} A(\Omega_w). \tag{B.1}$$

Since we have

$$\int_\Omega \nabla \cdot \nabla c \; d\Omega = \int_{\partial\Omega} \frac{\partial c}{\partial \hat{n}} \; d\Gamma = 0,$$

due to our boundary conditions, Eq. (B.1) simplifies to

$$\frac{d}{dt} \int_\Omega c \; d\Omega + \lambda \int_\Omega c \; d\Omega = \alpha m_0 e^{-\beta_1 t} A(\Omega_w). \tag{B.2}$$

Substituting the mean $\bar{c}(t) = \frac{\int_\Omega c \; d\Omega}{\int_\Omega d\Omega}$, Eq. (B.2) becomes

$$\frac{d\bar{c}}{dt} A(\Omega) + \lambda \bar{c} A(\Omega) = \alpha m_0 e^{-\beta_1 t} A(\Omega_w). \tag{B.3}$$

Multiplying (B.3) with $e^{\lambda t}$ and using

$$e^{\lambda t} \frac{d\bar{c}}{dt} + \lambda e^{\lambda t} \bar{c} = \frac{d}{dt}(e^{\lambda t} \bar{c}),$$

we obtain

$$\frac{d}{dt}(e^{\lambda t} \bar{c}) = \alpha m_0 e^{(\lambda - \beta_1)t} \frac{A(\omega_w)}{A(\Omega)}, \tag{B.4}$$

which we integrate to find for $\lambda \neq \beta_1$:

$$\bar{c}(t) = \bar{c}_0 e^{-\lambda t} + \frac{\alpha m_0}{\lambda - \beta_1} e^{-\lambda t} (e^{(\lambda - \beta_1)t} - 1) \frac{A(\Omega_w)}{A(\Omega)},$$

$$= \bar{c}_0 e^{-\lambda t} + \frac{\alpha m_0}{\lambda - \beta_1} (e^{-\beta_1 t} - e^{-\lambda t}) \frac{A(\Omega_w)}{A(\Omega)}, \tag{B.5}$$

and for $\lambda = \beta_1$:

$$\bar{c}(t) = \bar{c}_0 e^{-\lambda t} + \alpha m_0 e^{-\lambda t} \frac{A(\Omega_w)}{A(\Omega)}. \tag{B.6}$$

Appendix C

Calculations for the movement of the characteristics

C.1 Integral of the hyperbolic sine

Integral 1

$$\int \frac{1}{\sinh(x)} dx = 2 \int \frac{1}{e^x - e^{-x}} dx$$

$$= 2 \int \frac{e^x}{e^{2x} - 1} dx$$

$$\stackrel{u = e^x}{=} 2 \int \frac{1}{u^2 - 1} du$$

$$= 2 \int \frac{A}{u+1} + \frac{B}{u-1} du. \tag{C.1}$$

To determine A and B we get

$$A(u - 1) + B(u + 1) = 1,$$
$$(A + B)u + B - A = 1,$$
$$\Rightarrow \ A + B = 0 \ \Rightarrow \ A = -B,$$
$$\Rightarrow \ B + B = 1 \ \Rightarrow \ B = 1/2 \ \Rightarrow \ A = -1/2. \tag{C.2}$$

With A and B from (C.2), Equation (C.1) becomes

$$\int \frac{1}{\sinh(x)} dx = 2 \int \frac{1/2}{u-1} - \frac{1/2}{u+1} du = \int \frac{1}{u-1} - \frac{1}{u+1} du$$

$$= \ln(u - 1) - \ln(u + 1) = \ln\left(\frac{u-1}{u+1}\right) = \ln\left(\frac{e^x - 1}{e^x + 1}\right)$$

$$= \ln\left(\tanh\left(\frac{x}{2}\right)\right). \tag{C.3}$$

Analogously, the solution for

$$\int \frac{1}{\sinh(\gamma x)} dx,$$

is given by

$$\int \frac{1}{\sinh(\gamma x)} dx = \frac{1}{\gamma} \int \frac{1}{\sinh(y)} dy = \frac{1}{\gamma} \ln\left(\tanh\left(\frac{y}{2}\right)\right)$$

$$= \frac{1}{\gamma} \ln\left(\tanh\left(\frac{\gamma x}{2}\right)\right). \tag{C.4}$$

Integral 2

$$
\begin{aligned}
\int \frac{1}{A\sinh(y) - B\cosh(y)}dy &= 2\int \frac{1}{A(e^y - e^{-y}) - B(e^y + e^{-y})}dy \\
&= 2\int \frac{1}{(A - B)e^y - (A + B)e^{-y}}dy \\
&= 2\int \frac{e^y}{(A - B)e^{2y} - (A + B)}dy \\
&= \frac{2}{A - B}\int \frac{e^y}{e^{2y} - \frac{A+B}{A-B}}dy \overset{u=e^y}{=} \frac{2}{A - B}\int \frac{1}{u^2 - \frac{A+B}{A-B}}du. \\
&\overset{z=\frac{A+B}{A-B}}{=} \frac{2}{A - B}\int \frac{\alpha}{u + \sqrt{z}} + \frac{\beta}{u - \sqrt{z}}du
\end{aligned}
$$

To determine α and β we get

$$
\begin{aligned}
&\alpha(u - 1) + \beta(u + 1) = 1, \\
&(\alpha + \beta)\beta - \alpha = 1, \\
&\Rightarrow \ \alpha + \beta = 0 \ \Rightarrow \ \alpha = -\beta, \\
&\Rightarrow \ \beta + \beta = 1 \ \Rightarrow \ \beta = \frac{1}{2\sqrt{z}} \ \Rightarrow \ \alpha = -\frac{1}{2\sqrt{z}}.
\end{aligned}
\tag{C.5}
$$

Substituting this solution, we obtain

$$
\begin{aligned}
\frac{2}{A - B}\int \frac{\alpha}{u + \sqrt{z}} + \frac{\beta}{u - \sqrt{z}}du &= \frac{2}{A - B}\int \frac{\frac{1}{2\sqrt{z}}}{u - \sqrt{z}} - \frac{\frac{1}{2\sqrt{z}}}{u + \sqrt{z}}du \\
&= \frac{1}{\sqrt{A^2 - B^2}}\left[\ln\left(u - \sqrt{z}\right) - \ln\left(u + \sqrt{z}\right)\right].
\end{aligned}
$$

Redo the substitutions that were made, we obtain

$$
\int \frac{1}{A\sinh(y) - B\cosh(y)}dy = \frac{1}{\sqrt{A^2 - B^2}}\ln\left(\frac{e^y - \sqrt{\frac{A+B}{A-B}}}{e^y + \sqrt{\frac{A+B}{A-B}}}\right).
$$

Integral 3

$$
\int \frac{dv}{\gamma\sinh(v) + \sinh(v - w)} = \frac{1}{\gamma}\int \frac{dv}{\sinh(v) + \frac{1}{\gamma}\sinh(v - w)},
$$

where we gonna substitute $A = \frac{1}{\gamma}e^{-w}$ and $B = \frac{1}{\gamma}e^{w}$ to obtain

$$
\begin{aligned}
\frac{1}{\gamma}\int \frac{dv}{\sinh(v) + \frac{1}{\gamma}\sinh(v-w)} &= \frac{2}{\gamma}\int \frac{dv}{(e^v - e^{-v}) + \frac{1}{\gamma}(e^{v-w} - e^{-(v-w)})} \\
&= \frac{2}{\gamma}\int \frac{1}{(e^v - e^{-v}) + Ae^v - Be^{-v}}dv \\
&= \frac{2}{\gamma}\int \frac{1}{e^v(A+1) - e^{-v}(B+1)}dv \\
&= \frac{2}{\gamma}\int \frac{e^v}{e^{2v}(A+1) - (B+1)}dv \\
&\overset{u=e^v}{=} \frac{2}{\gamma}\int \frac{1}{u^2(A+1) - (B+1)}du \\
&= \frac{2}{\gamma}\frac{1}{A+1}\int \frac{1}{u^2 - \frac{B+1}{A+1}}du,
\end{aligned}
$$

which equals, using (C.5),

$$
\begin{aligned}
\frac{1}{\gamma}\int \frac{dv}{\sinh(v) + \frac{1}{\gamma}\sinh(v-w)} &= \frac{2}{\gamma}\frac{1}{A+1}\int \frac{-\frac{1}{2}\sqrt{\frac{A+1}{B+1}}}{u + \sqrt{\frac{B+1}{A+1}}} + \frac{\frac{1}{2}\sqrt{\frac{A+1}{B+1}}}{u - \sqrt{\frac{B+1}{A+1}}}du \\
&= \frac{1}{\gamma}\frac{1}{A+1}\int \frac{-\sqrt{\frac{A+1}{B+1}}}{u + \sqrt{\frac{B+1}{A+1}}} + \frac{\sqrt{\frac{A+1}{B+1}}}{u - \sqrt{\frac{B+1}{A+1}}}du \\
&= \frac{1}{\gamma}\frac{1}{\sqrt{(A+1)(B+1)}}\int \frac{1}{u - \frac{B+1}{A+1}} - \frac{1}{u + \sqrt{\frac{B+1}{A+1}}}du \\
&= \frac{1}{\gamma}\frac{1}{\sqrt{AB + A + B + 1}}\ln\left(\frac{u - \sqrt{\frac{B+1}{A+1}}}{u + \sqrt{\frac{B+1}{A+1}}}\right) \\
&= \frac{1}{\gamma}\frac{1}{\sqrt{AB + A + B + 1}}\ln\left(\frac{e^v - \sqrt{\frac{B+1}{A+1}}}{e^v + \sqrt{\frac{B+1}{A+1}}}\right). \quad \text{(C.6)}
\end{aligned}
$$

C.2 Rewriting some terms

We know that

$$
\sinh\left(\sqrt{\tilde{\lambda}}(1-\delta)\right) = \sinh\left(\sqrt{\tilde{\lambda}}x\right)\cosh\left(\sqrt{\tilde{\lambda}}\delta\right) - \cosh\left(\sqrt{\tilde{\lambda}}x\right)\sinh\left(\sqrt{\tilde{\lambda}}\delta\right),
$$

such that

$$
-\frac{\sinh\left(\sqrt{\tilde{\lambda}}(1-\delta)\right)}{\sinh\left(\sqrt{\tilde{\lambda}}\right)} + \cosh\left(\sqrt{\tilde{\lambda}}\delta\right)
$$

$$
= \frac{-\sinh\left(\sqrt{\tilde{\lambda}}\right)\cosh\left(\sqrt{\tilde{\lambda}}\delta\right) + \cosh\left(\sqrt{\tilde{\lambda}}\right)\sinh\left(\sqrt{\tilde{\lambda}}\delta\right)}{\sinh\left(\sqrt{\tilde{\lambda}}\right)} + \cosh\left(\sqrt{\tilde{\lambda}}\delta\right)
$$

$$
= \frac{\cosh\left(\sqrt{\tilde{\lambda}}\right)\sinh\left(\sqrt{\tilde{\lambda}}\delta\right)}{\sinh\left(\sqrt{\tilde{\lambda}}\right)} = \frac{\sinh\left(\sqrt{\tilde{\lambda}}\delta\right)}{\tanh\left(\sqrt{\tilde{\lambda}}\right)}.
$$

C.3   Movement of the characteristics

First we determine the location of the front as $x_0 < \delta$ and therefore $t > \tau$. In order to do this, we use (3.3) and (3.4). We obtain

$$
\frac{dx}{dt} = -\frac{\alpha m_0}{\lambda}\chi_1\sqrt{\tilde{\lambda}}e^{-\beta_1 t}\frac{\sinh\left(\sqrt{\tilde{\lambda}}(1-\delta)\right)}{\sinh\left(\sqrt{\tilde{\lambda}}\right)}\sinh\left(\sqrt{\tilde{\lambda}}x\right).
$$

Using Seperation of Variables this reduces to

$$
\int_{x_0}^{x}\frac{1}{\sinh\left(\sqrt{\tilde{\lambda}}\bar{x}\right)}\,d\bar{x} = -\frac{\alpha m_0}{\lambda}\chi_1\sqrt{\tilde{\lambda}}\frac{\sinh\left(\sqrt{\tilde{\lambda}}(1-\delta)\right)}{\sinh\left(\sqrt{\tilde{\lambda}}\right)}\int_{\tau}^{t}e^{-\beta_1\bar{t}}\,d\bar{t}.
$$

Using Appendix C.1 on the left hand side, the solution is given as

$$
\frac{1}{\sqrt{\tilde{\lambda}}}\ln\left(\tanh\left(\frac{\sqrt{\tilde{\lambda}}x}{2}\right)\right)\Bigg|_{x_0}^{x} = \frac{\alpha m_0}{\lambda\beta_1}\chi_1\sqrt{\tilde{\lambda}}\frac{\sinh\left(\sqrt{\tilde{\lambda}}(1-\delta)\right)}{\sinh\left(\sqrt{\tilde{\lambda}}\right)}(e^{-\beta_1 t} - e^{-\beta_1\tau}),
$$

such that

$$
x(t) = \frac{2}{\sqrt{\tilde{\lambda}}}\mathrm{arctanh}\Bigg[\tanh\left(\frac{\sqrt{\tilde{\lambda}}x_0}{2}\right)
$$

$$
\cdot\exp\left(\frac{\alpha m_0}{\lambda\beta_1}\chi_1\tilde{\lambda}\frac{\sinh\left(\sqrt{\tilde{\lambda}}(1-\delta)\right)}{\sinh\left(\sqrt{\tilde{\lambda}}\right)}(e^{-\beta_1 t} - e^{-\beta_1\tau})\right)\Bigg],
$$

for $x_0 < \delta$, $t > \tau$.

We do the same when $x_0 \geq \delta$ and therefore $t \leq \tau$ when using (3.3) and (3.5) and obtain

$$
\frac{dx}{dt} = -\frac{\alpha m_0}{\lambda}\chi_1\sqrt{\tilde{\lambda}}\sinh\left(\sqrt{\tilde{\lambda}}\delta\right)e^{-\beta_1 t}\left[\cosh\left(\sqrt{\tilde{\lambda}}x\right) - \frac{\sinh\left(\sqrt{\tilde{\lambda}}x\right)}{\tanh\left(\sqrt{\tilde{\lambda}}\right)}\right].
$$

Using Seperation of Variables this reduces to

$$\int_{x_0}^{x} \frac{1}{\cosh\left(\sqrt{\tilde{\lambda}}x\right) - \dfrac{\sinh\left(\sqrt{\tilde{\lambda}}\bar{x}\right)}{\tanh\left(\sqrt{\tilde{\lambda}}\right)}} \, d\bar{x} = -\frac{\alpha m_0}{\lambda}\chi_1\sqrt{\tilde{\lambda}}\sinh\left(\sqrt{\tilde{\lambda}}\delta\right)\int_0^t e^{-\beta_1\bar{t}} \, d\bar{t}.$$

Substituting $A = \dfrac{-1}{\tanh\left(\sqrt{\tilde{\lambda}}\right)}$ and $B = -1$ and using Appendix C.1 on the left hand side, the solution is given as

$$\frac{-1}{\sqrt{\tilde{\lambda}}}\frac{1}{\sqrt{A^2-B^2}}\ln\left(\frac{e^{\sqrt{\tilde{\lambda}}\bar{x}} - \sqrt{\frac{A+B}{A-B}}}{e^{\sqrt{\tilde{\lambda}}\bar{x}} + \sqrt{\frac{A+B}{A-B}}}\right)\Bigg|_{x_0}^{x} = \underbrace{\frac{\alpha m_0}{\lambda\beta_1}\chi_1\sqrt{\tilde{\lambda}}\sinh\left(\sqrt{\tilde{\lambda}}\delta\right)\left(e^{-\beta_1 t} - 1\right)}_{\psi_1(t)},$$

such that

$$\frac{e^{\sqrt{\tilde{\lambda}}x} - \sqrt{\frac{A+B}{A-B}}}{e^{\sqrt{\tilde{\lambda}}x} + \sqrt{\frac{A+B}{A-B}}} = \exp\underbrace{\left[\ln\left(\frac{e^{\sqrt{\tilde{\lambda}}x_0} - \sqrt{\frac{A+B}{A-B}}}{e^{\sqrt{\tilde{\lambda}}x_0} + \sqrt{\frac{A+B}{A-B}}}\right) - \sqrt{\tilde{\lambda}}\sqrt{A^2-B^2}\psi_1(t)\right]}_{\psi_2(t)},$$

$$\Rightarrow x(t) = \frac{1}{\sqrt{\tilde{\lambda}}}\ln\left(\sqrt{\frac{A+B}{A-B}}\cdot\frac{1+\psi_2(t)}{1-\psi_2(t)}\right), \tag{C.7}$$

for $x_0 \geq \delta$, $t \leq \tau$.

Appendix D

Parameter values for simulations

D.1   Parameters for the movement of the characteristics

Name	Value	Description
Ω_w	0.2	Distance to core of the 'wound' in the heart
m_0	2	Initial density of stem cells
β_1	0.5	Decay of stem cells
D_1	1	Diffusion coefficient for TG$-\beta$
α	3	Growth of TG$-\beta$
λ	1	Decay of TG$-\beta$
χ_1	0.4	Attraction of TG$-\beta$

Table D.1: *Parameter values used for the movement of the characteristics of the capillary tip density.*

D.2   Parameters for many simulations

Name	Value	Description
Ω_w	0.2	Distance to core of the 'wound' in the heart
m_0	2	Initial density of stem cells, in million stem cells
β_1	0.5	Decay of stem cells
D_1	1	Diffusion coefficient for TG-beta
α	3	Growth of TG-beta
λ	1	Decay of TG-beta
χ_1	0.4	Attraction of TG-beta
D_2	0.001	Diffusion coefficient for the capillary tips
α_0	50	Growth of tip density due to primary angiogenesis
α_1	10	Growth of tip density due to secondary angiogenesis
$\hat{c}$	0.2	Threshold of concentration TG-beta
β_2	50	Decay of tip density due to anastomoses
ϵ	0.01	Diffusion coefficient for vessels
γ	0.25	Decay of blood vessels
ρ_{eq}	0.001	Equilibrium value of vessel density
μ_1	0.001	Growth/decay of vessel density influenced by growth/decay in tip density
χ_2	0.4	Growth/decay of vessel density influenced by the number of tips due to growth/decay in concentration TG-beta

Table D.2: *Values of the coefficients in our model* [2].

D.3 Changes and additions in the parameters for the comparison between discontinuous Galerkin and the finite element method

	finite element method	1 dimensional discontinuous galerkin	2 dimensional discontiunous galerkin using polar coordinates
Δt	0.1	0.0001	0.0001
$\Delta x (= \Delta y)$	0.1	0.1	0.1
max order basisfunctions	-	3	3
χ_1	4	4	4
D_2	0.0001	0.0001	0.0001

Table D.3: *Changes and additions in the parameters for the comparison between discontinuous Galerking and the finite element method.*

D.4 Changes in the paramters for the simulations of the two dimensional model using discontinuous galerkin and polar coordinates

Name	Value	Description
D_2	0.1	Diffusion coefficient for the capillary tips
$\hat{c}$	0.1	Threshold of concentration TG-beta

Table D.4: *Changes in the parameters from Table D.2 for the simulations of the two dimension model using discontinuous Galerkin and polar coordinates.*

Bibliography

[1] Kendall Atkinson and Weimin Han, *Theoretical Numerical Analysis* Springer 2005

[2] H. M. Byrne and M. A. J. Chaplain, *Explicit Solutions of a Simplified Model of Capillary Sprout Growth During Tumor Angiogenesis* School of Mathematical Sciences, University of Bath. Claverton Down, Bath BA2 7AY, U.K. 1995

[3] Bernardo Cockburn *An Introduction to the Discontinuous Galerkin Method for Convection-Dominated Problems*

[4] L.Y.D. Crapts, *A mathematical model for angiogenesis around a tumour* Bachelor of Science thesis, Delft Technical University, June 2010

[5] L.Y.D. Crapts, *Modeling an angiogenesis treatment after a myocardial infarction* Literature study for Master of Science thesis, Delft Technical University, March 2012

[6] Jennifer A. Flegg, Helen M. Byrne, D.L. Sean McElwain, *Mathematical Model of Hyperbaric Oxygen Therapy Applied to Chronic Diabetic Wounds* Bulletin of Mathematical Biology (2010) 72: 1867-1891

[7] Jan S. Hesthaven, *Nodal Discontinuous Galerkin Methods* Springer 2008

[8] Randall J. Leveque, *Finite Volume Methods for Hyperbolic Problems* Cambridge Texts in Applied Mathematics. Cambridge University Press, New York, sixth edition, 2002

[9] J. van Kan, A. Segal, and F. Vermolen, *Numerical Methods in Scientific Computation* VSSD, 2008

[10] Sophia A. Maggelakis, *A mathematical model of tissue replacement during epidermal wound healing* Applied Mathematical Modelling 27 (2003) 189196

[11] Sophia A. Maggelakis, *Modeling the role of angiogenesis in epidermal wound healing* Discrete and continuous dynamical systems-series B, Volume 4, Number 1, February 2004

[12] Henri Paillere, *Multidimensional upwind residual distribution schemes for the euler and navier-stokes equations on unstructured meshes*

[13] F.J. Vermolen and A. Gefen, *Wound Healing: MultiScale Modeling*

[14] Jianxian Qiu and Chi-Wang Shu, *RungeKutta discontinuous Galerkin method using Weno limiters* SIAM J. SCI. COMPUT. Vol. 26, No. 3, pp. 907929, 2005 Society for Industrial and Applied Mathematics